RESERVOIR AND SURFACE FACILITIES COUPLED THROUGH PARTIALLY AND FULLY IMPLICIT APPROACHES

A Thesis

by

MENGDI GAO

Submitted to the Office of Graduate and Professional Studies of
Texas A&M University
in partial fulfillment of the requirements for the degree of

MASTER OF SCIENCE

Chair of Committee,	Eduardo Gildin
Committee Members,	Ding Zhu
	Yalchin Efendiev
Head of Department,	Daniel Hill

December 2014

Major Subject: Petroleum Engineering

ABSTRACT

During oil production, the change of production states could cause the change of pressure losses through the production facilities, and consequently result in the variations of well-boundary-conditions in time. In the de-coupled reservoir simulators, the well boundary condition (i.e. bottom hole pressure) is estimated and fixed. Therefore, when performing simulations for production prediction, the de-coupled reservoir simulator would fail to predict the behaviors of the well boundary conditions during production. In this case, a simulator that involves the effects of surface facilities is necessary when perform production prediction . The implementation of partially implicit coupling method has faced the issues due to their inaccuracies and instabilities for complex cases. In this case, the fully implicit coupling is demanded for such complex. This research explores the concept and implementation of fully coupling method.

This study focuses on investigating the effects of coupling surface and subsurface model on production forecast. This production prediction is performed under simple constraints (i.e. surface production and injection pressures) and various surface facilities. The results from running the coupled model showed that the bottom hole pressures of producers are affected by both the gas-oil ratio (GOR) and water cut. Other surface facility fittings (i.e. chock or valves) and more complex reservoir description are considered in this project as well.

DEDICATION

To my family and friends

ACKNOWLEDGEMENTS

I take this opportunity to express my profound gratitude and deep regards to my committee chair, Dr. Gildin and my committee members, Dr. Zhu and Dr. Efendiev for their exemplary guidance, monitoring and constant encouragement throughout the course of this thesis. The blessing, help and guidance given by them shall carry me a long way in the journey of life on which I am about to embark.

I also take this opportunity to express a deep sense of gratitude to my friends and colleagues and the department faculty and staff for the cordial support, valuable information and guidance, which helped me in completing this task through various stages.

Lastly, I thank almighty, my parents and my cousin for their constant encouragement, without which this assignment would not be possible.

NOMENCLATURE

A	Cross-section Area
B_w	Water Formation Volume Factor
B_o	Oil Formation Volume Factor
B_g	Gas Formation Volume Factor
D	Tubing/Pipe Diameter
f_n	Non-Slip Friction Factor
f	Friction factor
g	Gravitational Acceleration
J	Jacobian Matrix
$J^{(p)}$	Jacobian Matrix at p^{th} Newton iteration
k	Apparent Permeability
k_rw	Relative Permeability to Water
k_ro	Relative Permeability to Oil
k_rw	Relative Permeability to Gas
k_x	Permeability in X-Direction
k_y	Permeability in Y-Direction
k_z	Permeability in Z-Direction
p_w	Water Phase Pressure
p_o	Oil Phase Pressure
p_g	Gas Phase Pressure
p_{cow}	Oil-Water Capillary Pressure
p_{cgo}	Gas-Oil Capillary Pressure
p_b	Bubble Point Pressure

p_{wf}	Bottom Hole Flowing Pressure
$\tilde{q_w}$	Mass Flow Rate of Water Phase
$\tilde{q_o}$	Mass Flow Rate of Oil Phase
$\tilde{q_g}$	Mass Flow Rate of Gas Phase
q_w^*	Volume Flow Rate of Water Phase
q_o^*	Volume Flow Rate of Oil Phase
q_g^*	Volume Flow Rate of Gas Phase
R_{res}	Residual Vector of Subsurface Governing Equations
R_{tub}	Residual Vector of Tubing Governing Equations
R_{pipe}	Residual Vector of Surface Pipe Governing Equations
R_{rw}	Residual Vector of Water Conservation Equation in Reservoir Domain
R_{ro}	Residual Vector of Oil Conservation Equation in Reservoir Domain
R_{rg}	Residual Vector of Gas Conservation Equation in Reservoir Domain
R_c	Residual Vector of Closing Equation in Reservoir Domain
R_{Ww}	Residual Vector of Water Flow Equation at Bottom Hole
R_{Wo}	Residual Vector of Oil Flow Equation in Bottom Hole
R_{Wg}	Residual Vector of Gas Flow Equation in Bottom Hole
R_{BHP}	Residual Vector of Pressure Equation in Bottom Hole
R_{tw}	Residual Vector of Water flow Equation in Tubing Domain
R_{to}	Residual Vector of Oil flow Equation in Tubing Domain
R_{tg}	Residual Vector of Gas flow Equation in Tubing Domain
R_{tp}	Residual Vector of Energy Conservation Equation in Tubing Domain
R_{pw}	Residual Vector of Water flow Equation in Surface Pipe Domain
R_{po}	Residual Vector of Oil flow Equation in Surface Pipe Domain
R_{pg}	Residual Vector of Gas flow Equation in Surface Pipe Domain

R_{pp}	Residual Vector of Energy Conservation Equation in Surface Pipe Domain
R_{bc}	Residual Vector of Boundary Condition Equation
R_s	Solution Gas Oil Ratio
r_o	Equivalent Gridblock Radius
r_w	Wellbore Radius
S_w	Water Phase Saturation
S_o	Oil Phase Saturation
S_g	Gas Phase Saturation
t	Time
U^{n+1}	Unknown Vector for Next Timestep
U^{n+1*}	Updated Unknown Vector for Next Timestep
u_{sl}	Superficial Velocity of Liquid
u_m	Superficial Velocity of Gas-Liquid Mixture
WI	Well Index
x	Distance in X-Direction of Cartesian Coordinate
y	Distance in Y-Direction of Cartesian Coordinate
z	Distance in Z-Direction of Cartesian Coordinate
y_l	Liquid Holdup
y_g	Gas Holdup
i, j, k	Subscript Specifying the Properties at Location (i, j, k)
$i+\frac{1}{2}, j, k$	Subscript Specifying the Averaged Properties of Location (i, j, k) and (i+1, j, k)
$i, j+\frac{1}{2}, k$	Subscript Specifying the Averaged Properties of Location (i, j, k) and (i, j+1, k)

$i, j, k + \frac{1}{2}$	Subscript Specifying the Averaged Properties of Location (i, j, k) and (i, j, k+1)
$i - \frac{1}{2}, j, k$	Subscript Specifying the Averaged Properties of Location (i, j, k) and (i-1, j, k)
$i, j - \frac{1}{2}, k$	Subscript Specifying the Averaged Properties of Location (i, j, k) and (i, j-1, k)
$i, j, k - \frac{1}{2}$	Subscript Specifying the Averaged Properties of Location (i, j, k) and (i, j, k-1)
n	Superscript Indicating the Properties at Current Timestep
$n + 1$	Superscript Indicating the Properties at Next Timestep
∂x	Solution Vector of Newton Linearization
ρ_w	Water Density
ρ_o	Oil Density
ρ_g	Gas Density
ρ_L	Density of Liquid in Tubing/Pipe segment
μ_w	Water Phase Viscosity
μ_o	Oil Phase Viscosity
μ_g	Gas Phase Viscosity
ϕ	Porosity
λ_l	Non-Slip Liquid Holdup
λ_w	Water Phase Transmissibility
λ_o	Oil Phase Transmissibility
λ_g	Gas Phase Transmissibility
γ_w	Water Phase Hydrostatic Gradient
γ_o	Oil Phase Hydrostatic Gradient

γ_g Gas Phase Hydrostatic Gradient

θ Inclination Angle

TABLE OF CONTENTS

Page

LIST OF FIGURES

FIGURE Page

LIST OF TABLES

TABLE Page

1. INTRODUCTION

During the life cycle of oil production, pressure losses caused by the surface production system could result in a significant impact on the well productivity, especially for offshore or deep reservoirs. When performing simulations for production prediction and field management, it is then, necessary to implement an integrated modeling approach, which couples the reservoir with several surface networks. The integrated model can be realized by applying the coupling methods, in which the surface model and subsurface model are linked by exchanging control parameters (such as flowing pressure and flow rate of each phase) at the coupling point (e.g bottom hole).

Based on the time-step convergence criteria and coupling level, several coupling mechanisms can be used to integrate surface and subsurface models. In general, they can be classified as explicit, partially implicit and fully implicit. If the obtained solution is only dependent on the convergence of the reservoir equations, and the coupling is operated at time-step level, then the method is explicit; the partially implicit is similar to explicit, the only difference is that the partially implicit coupling is performed at the Newton iteration-step level. And if the convergence of both reservoir and surface facility equations is required, then the coupling is called fully implicit, as it yields completely implicit solutions.

For explicit and partially implicit coupling, the reservoir and surface facilities are treated as two different domains. As the workflow of explicit coupling relies on exchanging the boundary parameters at timestep level, this method may exhibit inaccuracies due to the fact that the boundary conditions are calculated with the reservoir state at the beginning of the time-step, which cannot represent the Inflow Performance Relationships (IPR) at the end of the time-step. Partially implicit cou-

pling differs from explicit coupling for it exchanging the IPR at Newton iteration level, which avoids the issues of explicit coupling. However, the partially implicit method may have unstable issues due the iterative oscillations caused by the significant change of reservoir state, which can result in a reduced convergence rate for partially implicit method.

Differing from the partially coupling (i.e. explicit and partially implicit coupling), fully implicit coupling method treats the reservoir and surface facility as one domain, where the equations of reservoir and surface facility are solved simultaneously at each Newton iteration. Furthermore, the treatment of surface facility convergence is the same as that applied to the de-coupled reservoir simulator. When constructing the coupled model, the state vectors of both the surface and subsurface will be considered, and the corresponding equations of the surface facilities (e.g. chokes, valves and pipelines) are required to be solved as well. Also, the boundary constraints will be moving from bottom hole to the surface downstream/upstream, and the global system of equations will include the reservoir, surface facilities. Since all the equations are solved at the same level, the surface facility equations will be converged within the accuracy of their linearization as well as the reservoir equations.

This study will focus on the coupled surface and subsurface model with the respect to fully implicit coupling mechanism. After developing the fully implicit coupling model, the impact of surface facility settings on production prediction and the efficiency of the fully coupling will be investigated. Consequently, the importance of applying coupled model and the feasibility of fully coupling method can be stated for further engineering of the reservoir field development.

1.1 Objectives

When production is controlled by the surface facilities, it is in generally necessary to include the facilities in a full-field model. Thus, the objective of this study is to construct a fully coupled model and investigate the impact and efficiency of coupling algorithm to realistic reservoir models. In this study, the results from fully coupled and non-coupled model will be compared. Furthermore, the computational costs of various facilities' settings will be investigated. The main task to achieve this objective is to construct a fully coupled model with programming software (i.e. MATLAB®). Also, the partially implicit coupled powered by commercial software (i.e. INTERSECT and PIPESIM) will be utilized to test the correctness of our fully coupled model.

We aim at providing recommendation regarding the usages of the coupling mechanisms and computational efforts associated with their implementation. In order to do that, the additional surface fittings and surface controlling constraints will be added into the fully coupled model, in order to predict how the otherwise specified boundary conditions vary in time. And the computational cost of each simulation run will be stated as well, to demonstrate the efficiency of performing our fully coupled model.

1.2 Surface and Subsurface Model Coupling Methods

there are various types of coupling methods applied to surface/subsurface coupled model. Generally, these methods can be classified as three types: explicit, partially implicit and fully implicit coupling.

1.2.1 Explicit coupling method

For the explicit coupling method, the surface and subsurface are treated as two different domains and the boundary constraint for subsurface (i.e. reservoir) model is applied explicitly at time-step level. At the beginning of each time-step, the surface model is performed to calculate the bottom hole pressure (BHP) with the production rate that obtained from previous time-step, the BHP is then passed to the reservoir model as the boundary condition, and the reservoir equations are solved with this boundary condition.

1.2.2 Partially implicit coupling method

Same as explicit coupling, the surface and subsurface are treated differently in partially implicit coupling method, but the network system is balanced at every Newton-iteration in each time-step. This method can generate a more accurate solution than explicit coupling. However, the computational speed of implicit coupling is limited by the time-step size due to its instability occurring when using large time-step. Also, when the coupling simulations are performed with some commercial reservoir simulator, the feasibility of implicit coupling is challenged by the compatibility of these commercial reservoir simulator to network simulator. The principles of implicit and explicit are very similar, as their solution are obtained based the convergence of reservoir equations.

1.2.3 Fully implicit coupling method

Distinguished from partially coupling (i.e. explicit and implicit coupling), the fully coupling is trying to get the solution based on the convergence of both the reservoir and network equations. The nodes of network system are treated as extended grid blocks of the reservoir domain. Thus, the equations of network (i.e. mass

conservation and momentum conservation) is included in the global equation system and solved at the Newton-iteration level. Since both the reservoir and network systems are included in the coupled system, the compatibility issue can be avoided by implementing fully coupling method. Also, the fully implicit coupling can generate stable solutions. In conventional reservoir model, the system equations are generally linearized and solved with Newton Raphson method which involves the partial derivatives of each residual to every unknown variables (such form of derivatives is called Jacobian matrix). The general structure of Newton linearization ($\partial X = J^{-1}R$) is shown as:

$$[\ \partial x\ ] = [\ A\ ]^{-1}[\ R\ ]$$

Where, the R represents the vector of Residual, while A represents the sub-matrix of Jacobian matrix, and the ∂x represents the solution of vector of Newton linearization of the reservoir equations.

The Newton linearization structure of fully coupled model is similar to that of conventional reservoir model. But the Jacobian matrix will have a different form due to the additional network system. In this research, the network system will be further broken down into multi-segment (i.e. vertical tubing) part and the surface network (i.e. surface pipe) module. Thus, the general Jacobian form of coupled reservoir and network can be expressed as:

$$\begin{bmatrix} \partial X_{res} \\ \partial X_{wb} \\ \partial X_{pip} \end{bmatrix} = \begin{bmatrix} A_{res/res} & A_{res/wb} & A_{res/pip} \\ A_{wb/res} & A_{wb/wb} & A_{wb/pip} \\ A_{pip/res} & A_{pip/wb} & A_{pip/pip} \end{bmatrix}^{-1} \begin{bmatrix} R_{res} \\ R_{wb} \\ R_{pip} \end{bmatrix}$$

Where, the R_{res}, R_{wb} and R_{pip} represent the residual of each domain (i.e. reservoir, wellbores and surface pipes). Each element in Jacobian matrix represents a deriva-

tive of a residual vector to a variable vector, for instance, $A_{res/wb}$ represents the derivative of residual of reservoir equations to the variable vector of multi-segment part (i.e. $\frac{\partial R_{res}}{\partial X_{wb}}$). The vector ∂X_{res}, ∂X_{wb} and ∂X_{pip} represent the solution vectors of corresponding domains. The Newton linearization will be performed at each Newton iteration until the convergences of governing equations occur; In this research, we study these coupling mechanisms and show how one can access the convergence criteria for different domains.

1.3 Literature Review

In this section, the development of model coupling will be briefly reviewed. The evolution of model coupling can be generally classified as two groups: advanced well modeling and surface/subsurface coupling.

The advanced well modeling has extended the reservoir simulation to a simulation process that considers the flow performance in tubing strings. In this case, the boundary conditions for reservoir model will be effected by the involvement of tubing strings, regardless of the surface facility. The advanced well modeling has an advantage over conventional reservoir model in production prediction, because the reservoir boundary conditions (production rate or bottom hole flowing pressure) are usually known for the production prediction case. Thus, it is necessary to move the boundary constraints to a position where the constraints can be controlled. However, the advance well modeling is only applicable for the case with simple surface network constraints, since it fails to represent the production network. When the system involves a complex surface network, the need for a complete surface/subsurface coupled model becomes necessary.

Many authors have described and implemented the surface/subsurface model in

their simulation workflows. Some of these published works are reviewed here.

1.3.1 Advanced well models

In the past years, the implementation of intelligent completion resulted in complex wellbore configurations, and accurately modeling such complexity causes the requirement of a detailed representation of wellbore composition, rate and pressure rather than estimated pressure/rate constraints in the conventional reservoir simulation approach.

Holmes et al.[1,2] presented an implicit three-phases black-oil model with an implicitly coupled wellbore, which is known as advanced well model. The wellbore system includes four primary variables (i.e. total flow rate, fractional flows of water and gas, and pressures) in each segment. The global system equations also contains the phase mass balances and a hydraulic relationship (i.e. the pressure loss caused by gravity, friction and kinetic energy) for each segment. In this system, the equations for pressure at the bottom hole was replaced with the boundary condition constraints, which could be a rate constraints, a bottom-hole flowing pressure constraints and the tubing-head pressure constraints.

More recent, Stone et al.[3] published a more comprehensive model which includes the compositional and thermal applications. In the work of Stone's, a multi-segment and multi-branching wellbore model is fully coupled to a commercial reservoir simulator. The enhancement of this study is to introduce the energy flow terms into the equations system which can represent the heat loss along the wellbore segment due to conduction. As a result, a more accurate volume factor of phases can be predicted. However, the works described above failed to present a complete surface facility, both of these systems terminating at tubing-head are unable to represent a system that includes the surface pipelines/ or a more complex surface network.

1.3.2 Surface and subsurface coupled models

Because of the limitation of the advanced well models mentioned above, several authors have presented methods that simulate the reservoir and the surface facilities simultaneously. These methods are known as surface/subsurface coupled models. An early surface/subsurface coupled model was presented within the work of Dempsey[4]. This model only simulates a gas/water system, using time-step level explicit coupling. Since the Hagedorn-Brown[5] correlation is used for calculating the pressure drop through the well tubing, the system can only work for vertical or near-vertical tubing settings.

Startzman et al.[6], then extended Dempsey's work to a three dimensional black-oil offshore model coupled with a more complex surface facility. The author implicitly coupled the surface/subsurface model at the time-step level, and used the same correlations as Dempsey. Other authors[7-8] also presented coupling works involving different production strategies, such as gas-lift et al.

Schiozer et al.[9] presented an novel technique that improves the efficiency of the coupling method. The authors applied a preconditioner at the beginning of each time-step, which could provide an estimation of the boundary conditions of the reservoir at the new time-step. This technique could increase the equilibrating rate of well/surface on the first Newton iteration. However, the authors only applied this new technique to a partially implicit coupled method. Yet the fully coupled method was concluded as inefficient when applied to complex cases.

Byer et al.[10] then extended the application of preconditioner to a fully coupled model. Rather than using the explicit preconditioning method of Schiozer, a coarse-grid solution was obtained before each Newton iteration to give an accurate estimation of the reservoir boundary conditions. It is stated that the application of the

preconditioning method could reduce the CPU time for certain cases. However, it is difficult to determine the practicality of this model, as it used a homogeneous no-slip model for calculating the frictional pressure drop. Although the improved efficiency was concluded in this work, the CPU time shown in the results are still forbidden as compared with no coupling methods.

Coat et al.[11] developed a comprehensively fully coupled model that involved the idea of preconditioning. In this model, the equations of the network are solved simultaneously with the ones of the reservoir. The difference of this model from the previous works is that it is assumed the network is in steady-state, which avoids the limitation of transient models in which the time-step size is constrained by the change of wellbore conditions. Another aspect of this model is that its convergence is based on reservoir domain, although it had the prior resolution of network/preconditioning, it still needed a continuous active constraints to obtain an accurate solutions for network. Also, it is difficult to conclude the impact of network on production from the results provided, since it focused on discussing the efficiency of this fully coupled model.

Guyaguler et al.[12] proposed a time-step level explicit coupling method. This method calculated the Inflow Performance Relationships (IPRs) with the near-well subdomain at the beginning of each coupling period. The IPRs was then set on the network node coupled to well and used to obtain the rate constraints for reservoir model. This method substantially reduced the balancing errors and oscillations found in the previous approaches. However, a noticeable inaccuracy could occur when applying a large coupling period, and the computational cost may increase when using small coupling period.

Several authors[13-16] presented the coupled model that integrated the commercial network simulator with some commercial subsurface simulators by using the inter-

active field management (FM). Hepgular et al.[17] tried to explicitly couple a network simulator to the commercial software−ECLIPESE with Parallel Virtual Machine (PVM) interface.

Guyaguler et al.[18] integrated the commercial software−PIPESIM with reservoir simulator aiming to solve the real-world case. And the field management that carries out the predictive scenarios was introduced in this article. In Guyaguler's paper, he also mention that a next-generation simulator is able to couple the separate surface and subsurface domains with field-management controller (INTERSECT[19]). However, details of using the field-management of INTERSECT was not shown in his paper.

In this chapter, the fundamental concept of coupling surface and subsurface was introduced. Generally, the coupling methods are classified as explicit, partially implicit and fully implicit based on the convergence criteria and coupling level. Also, the development and current status of implementation of coupled model in oil industry was shown, it is concluded that the partially implicit coupling method is implemented in most practical case, and fully implicit coupling method is currently not applied into the commercial simulators.

2. SURFACE AND SUBSURFACE MODELING MECHANISM

In this chapter, the fundamental formulations and numerical methods that used in surface/subsurface modeling will be presented. The black oil multiphase reservoir model will be employed as the subsurface model, where three phases (i.e. water, oil and gas) fluid flow behavior in porous media will be investigated. The multiphase flow behavior presented in this chapter is based on the textbook by Ertekin et al.[20]. The equations of the network system will also be shown in this section, and the multiphase flow correlations that used in these equation are based on the textbook by Economides et al.[21].

2.1 Reservoir Multiphase Modeling

This section considers the black oil model for describing the hydrocarbon equilibrium in porous media. The formulation of the governing equations that describe this model include the mass conservation relationship and Darcy's law. Finite difference volume approximate procedures are then used for pressure and saturation equations.

In reservoir simulation, the subsurface domain is generally divided into many grid blocks of small size. Each grid block is treated as a porous medium that has its own properties (i.e. porosity ϕ, permeability k, saturation of phases S). The water, oil and gas phases can flow through the porous media, and consequently perturb the properties of the media. The phases flow is generally driven by the pressure differences in between the grid blocks. In black oil model, the densities (i.e. ρ_w, ρ_o and ρ_g) and viscosity (μ_w, μ_o and μ_g) of phases are used as secondary variables in the mass conservation equations.

The fundamental phases equation is based on the concept of material mass bal-

ance where the mass of fluid accumulation in porous media equals to the difference between mass of inflow stream and mass of outflow stream, which is shown as:

$$Mass_{inflow} - Mass_{outflow} = Mass_{accumulation} \tag{2.1}$$

Generally, the fluid flow in porous media obey Darcy's law, thus the left hand side (LHS) of Equation 2.1. can be represented by Darcy's equation, which will give generalized mass balance in porous media as:

$$Mass Flux's\ term = Accumulation\ term + Sink/Source\ term \tag{2.2}$$

Applying the material mass balance and Darcy's law to phases will yield the phases flow equations that is used to describe the states of flow in porous media. In black oil system, the hydrocarbon components are divided into gas component and oil component, and there is no mass transfer occurs between the water phase and the other two phases (i.e. oil and gas). Since there has mass interchange in between the oil and gas phases, the mass is not conserved within each phase, but the total mass of each hydrocarbon component has to be conserved. The partial differential equations of water, oil and gas flow are shown respectively as:

$$\nabla[\frac{\rho_w k_{rw} k}{\mu_w}(\nabla p_w - \rho_w g \nabla z)] = \frac{\partial(\rho_w \phi S_w)}{\partial t} + \widetilde{q_w}. \tag{2.3}$$

$$\nabla[\frac{\rho_o k_{ro} k}{\mu_o}(\nabla p_o - \rho_o g \nabla z)] = \frac{\partial(\rho_o \phi S_o)}{\partial t} + \widetilde{q_o}. \tag{2.4}$$

$$\nabla[\frac{\rho_{Go} k_{ro} k}{\mu_{Go}}(\nabla p_o - \rho_o g \nabla z) + \frac{\rho_g k_{rg} k}{\mu_g}(\nabla p_g - \rho_g g \nabla z)] = \frac{\partial((\rho_{Go} S_o + \rho_g S_g)\phi)}{\partial t} + \widetilde{q_g}. \tag{2.5}$$

For gas equation (2.5), the ρ_{Go} indicates the partial density of the gas component in oil phase. The right hand side of equations (2.3-2.5) is the accumulation term and external sink/source term ($\widetilde{q}$). The LHS is the flux term derived from Darcy's equation.

In the porous media, the three phases will jointly fill the void space and the phases pressure is connected by capillary pressures, which are given by the equations:

$$S_w + S_o + S_g = 1 \tag{2.6}$$

$$P_{cow} = P_o - P_w, \quad P_{cgo} = P_g - Po. \tag{2.7}$$

The water-gas capillary pressure can be given as:

$$P_{cgw} = P_{cgo} - P_{cow}. \tag{2.8}$$

Since mass of each hydrocarbon component is not conserved, the dissolved gas-oil ratio, R_S is used to determine the mass fractions of oil and gas components in the oil phases. The R_S is the volume of gas (at the standard conditions) dissolved in a unit volume of stock tank oil at a specific pressure. The R_S is given as:

$$R_S = \frac{V_{Gs}}{V_{Os}} \tag{2.9}$$

where,

$$V_O = \frac{W_O}{\rho_O} \quad and \quad V_G = \frac{W_G}{\rho_G}. \tag{2.10}$$

where, the W_O and W_G represent the weights of the oil and gas components, respectively. Then the R_S becomes

$$R_S = \frac{W_G \rho_O}{W_O \rho_G}. \tag{2.11}$$

In addition, the formation volume factor, B is considered in the phases equation. B is the defined as the ratio of the volume of one phase measured at reservoir condition to the volume of this phase measured at standard condition:

$$B = \frac{V_{res}}{V_s} \tag{2.12}$$

Since $V = W/\rho$, the densities for water and gas become:

$$\rho_w = \frac{\rho_{Ws}}{B_w} \tag{2.13}$$

$$\rho_g = \frac{\rho_{Gs}}{B_g} \tag{2.14}$$

because the oil phase includes oil and gas components, so the densities for oil phase and gas component in oil phase are shown respectively as:

$$\rho_o = \frac{R_S\rho_{Gs} + \rho_{Os}}{B_o} \tag{2.15}$$

$$\rho_{Go} = \frac{R_S\rho_{Gs}}{B_o} \tag{2.16}$$

substituting (2.13, 2.14 and 2.16) to equations (2.3-2.5) yields:

$$\nabla[\frac{\rho_{Ws}k_{rw}k}{\mu_w B_w}(\nabla p_w - \rho_w g\nabla z)] = \frac{\partial}{\partial t}[\frac{\rho_{Ws}\phi S_w}{B_w}] + \widetilde{q_w} \tag{2.17}$$

$$\nabla[\frac{\rho_{Os}k_{ro}k}{\mu_o B_o}(\nabla p_o - \rho_o g\nabla z)] = \frac{\partial}{\partial t}[\frac{\rho_{Os}\phi S_o}{B_o}] + \widetilde{q_o} \tag{2.18}$$

$$\nabla[\frac{\rho_{Gs}R_S k_{ro}k}{\mu_o B_o}(\nabla p_o - \rho_o g\nabla z) + \frac{\rho_{Gs}k_{rg}k}{\mu_g B_g}(\nabla p_g - \rho_g g\nabla z)]$$
$$= \frac{\partial}{\partial t}[\frac{R_S\rho_{Gs}\phi S_o}{B_o} + \frac{\rho_{Gs}\phi S_g}{B_g}] + \widetilde{q_o}R_S + \widetilde{q_g} \tag{2.19}$$

Defining the *Mobility Ratio*, λ as the ratio of effective permeability to phase viscosity and volume factor, then dividing the equations (2.17-2.19) by densities of phases yields the simplified water, oil and gas conservation equations:

$$\nabla[\lambda_w(\nabla p_w - \rho_w g\nabla z)] = \frac{\partial}{\partial t}(\frac{\phi S_w}{B_w}) + q_w^* \tag{2.20}$$

$$\nabla[\lambda_o(\nabla p_o - \rho_o g\nabla z)] = \frac{\partial}{\partial t}(\frac{\phi S_o}{B_o}) + q_o^* \tag{2.21}$$

$$\nabla[R_S\lambda_o(\nabla p_o - \rho_o g\nabla z) + \lambda_g(\nabla p_g - \rho_g g\nabla z)]$$
$$= \frac{\partial}{\partial t}(\frac{R_S\phi S_o}{B_o} + \frac{\phi S_g}{B_g}) + q_o^* R_S + q_g^* \tag{2.22}$$

The differentiation operator, ∇, indicates the action for taking derivative to the space vector in three-dimension Cartesian coordinate (i.e. $\frac{\partial}{\partial x} + \frac{\partial}{\partial y} + \frac{\partial}{\partial y}$). Also, when considering the constraint equations (2.6 and 2.7), the conservation equation for water, oil and gas phases can be rewritten respectively as:

$$\frac{\partial}{\partial x}[\lambda_{wx}(\frac{\partial p_o}{\partial x} - \frac{\partial p_{cow}}{\partial x} - \rho_w g\frac{\partial z}{\partial x})] + \frac{\partial}{\partial y}[\lambda_{wy}(\frac{\partial p_w}{\partial y} - \frac{\partial p_{cow}}{\partial y} - \rho_w g\frac{\partial z}{\partial y})]$$
$$+ \frac{\partial}{\partial z}[\lambda_{wz}(\frac{\partial p_w}{\partial z} - \frac{\partial p_{cow}}{\partial z} - \rho_w g\frac{\partial z}{\partial z})] = \frac{\partial}{\partial t}(\frac{\phi S_w}{B_w}) + q_w^* \tag{2.23}$$

$$\frac{\partial}{\partial x}[\lambda_{ox}(\frac{\partial p_o}{\partial x}-\rho_o g\frac{\partial z}{\partial x})]+\frac{\partial}{\partial y}[\lambda_{oy}(\frac{\partial p_o}{\partial y}-\rho_o g\frac{\partial z}{\partial y})]$$
$$+\frac{\partial}{\partial z}[\lambda_{oz}(\frac{\partial p_o}{\partial z}-\rho_o g\frac{\partial z}{\partial z})]=\frac{\partial}{\partial t}[\frac{\phi(1-S_g-S_w)}{B_o}]+q_o^* \tag{2.24}$$

$$\frac{\partial}{\partial x}[\lambda_{ox}R_S(\frac{\partial p_o}{\partial x}-\rho_o g\frac{\partial z}{\partial x})]+\frac{\partial}{\partial y}[\lambda_{oy}R_S(\frac{\partial p_o}{\partial y}-\rho_o g\frac{\partial z}{\partial y})]$$
$$+\frac{\partial}{\partial z}[\lambda_{oy}R_S(\frac{\partial p_o}{\partial z}-\rho_o g\frac{\partial z}{\partial z})]$$
$$+\frac{\partial}{\partial x}[\lambda_{gx}(\frac{\partial p_g}{\partial x}-\frac{\partial p_{cgo}}{\partial x}-\rho_g g\frac{\partial z}{\partial x})]$$
$$+\frac{\partial}{\partial y}[\lambda_{gy}(\frac{\partial p_g}{\partial y}-\frac{\partial p_{cgo}}{\partial y}-\rho_g g\frac{\partial z}{\partial y})]$$
$$+\frac{\partial}{\partial z}[\lambda_{gz}(\frac{\partial p_g}{\partial z}-\frac{\partial p_{cgo}}{\partial z}-\rho_g g\frac{\partial z}{\partial z})]$$
$$=\frac{\partial}{\partial t}[\frac{R_S\phi(1-S_g-S_w)}{B_o}+\frac{\phi S_g}{B_g}]+R_S q_o^*+q_g^* \tag{2.25}$$

2.1.1 The saturation constraints in reservoir modeling

In black oil model, the gas component can exist in both oil phase and gas phase. When reservoir pressure is higher than the bubble point pressure, the gas component only exists in oil phase, and the reservoir is regarded as undersaturated, and the constraint for this condition is:

$$S_w+S_o=1 \quad , \quad S_g=0 \quad , \quad R_s=0$$

and,

$$p_o > p_b$$

where, p_b indicates the bubble point pressure.

When the reservoir pressure is below bubble point pressure, the gas component starts to vaporize from oil phase, and the free gas phase will present in reservoir condition, when this occurs, the reservoir is regarded as saturated. The constraints for saturated reservoir become:

$$S_w + S_o + S_g = 1 \quad , \quad R_s > 0$$

and,

$$p_o \leq p_b$$

2.1.2 Discretization of conservation equation for water phase

To solve the conservation equations provided above, the block-centered finite difference numerical method is used in this study. First we treat the grid block as a rectangular cube whose faces are parallel to the Cartesian coordinate axes (see Figure 2.1). The centroid of the cube is denoted as (x, y, z), and the lengths of cube in each direction are $\Delta x, \Delta y, \Delta z$.

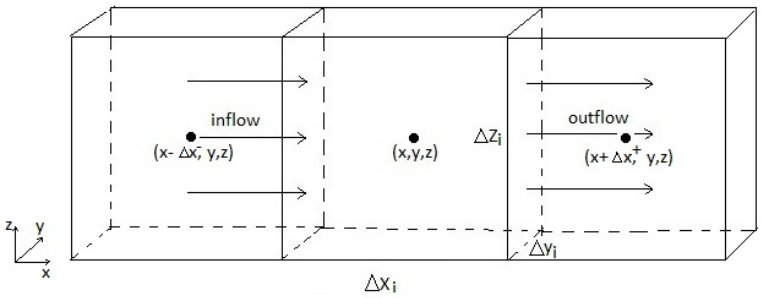

Figure 2.1: Flow across gridblocks in x-direction

Referring to Figure 2.1, the mass flux across the interface in x direction can be expressed as:

$$(\rho u_x)_{x-\frac{\Delta x}{2},y,z} \quad , \quad (\rho u_x)_{x+\frac{\Delta x}{2},y,z} \tag{2.26}$$

And the pressure differences gradient in x direction are:

$$\frac{p_{ox+\Delta x^+,y,z} - p_{ox,y,z}}{\Delta x^+} \quad , \quad \frac{p_{ox-\Delta x^-,y,z} - p_{ox,y,z}}{\Delta x^-} \tag{2.27}$$

Applying concepts in the equations (2.26 and 2.27) to the Darcy's terms in the conservation equations yields the discretization of the phase flux in x, y and z directions for water phase (assuming no potential energy along x, y direction):

$$\begin{aligned} &\frac{\partial}{\partial x}[\lambda_{wx}(\frac{\partial p_o}{\partial x} - \frac{\partial p_{cow}}{\partial x} - \rho_w g \frac{\partial z}{\partial x})] \\ &\doteq \frac{1}{\Delta x_i}(\lambda_{wi+\frac{1}{2},j,k}\frac{p_{oi+1,j,k} - p_{oi,j,k}}{\Delta x_i^+} + \lambda_{wi-\frac{1}{2},j,k}\frac{p_{oi-1,j,k} - p_{oi,j,k}}{\Delta x_i^-}) \end{aligned} \tag{2.28}$$

$$\begin{aligned} &\frac{\partial}{\partial y}[\lambda_{wy}(\frac{\partial p_o}{\partial y} - \frac{\partial p_{cow}}{\partial y} - \rho_w g \frac{\partial z}{\partial y})] \\ &\doteq \frac{1}{\Delta y_i}(\lambda_{wi,j+\frac{1}{2},k}\frac{p_{oi,j+1,k} - p_{oi,j,k}}{\Delta y_i^+} + \lambda_{wi,j-\frac{1}{2},k}\frac{p_{oi,j-1,k} - p_{oi,j,k}}{\Delta y_i^-}) \end{aligned} \tag{2.29}$$

$$\begin{aligned} &\frac{\partial}{\partial z}[\lambda_{wz}(\frac{\partial p_w}{\partial z} - \frac{\partial p_{cow}}{\partial z} - \rho_w g \frac{\partial z}{\partial z})] \\ &\doteq \frac{1}{\Delta z_i}(\lambda_{wi,j,k+\frac{1}{2}}\frac{p_{oi,j,k+1} - p_{oi,j,k}}{\Delta z_i^+} + \lambda_{wi,j,k-\frac{1}{2}}\frac{p_{oi,j,k-1} - p_{oi,j,k}}{\Delta z_i^-} \\ &- \lambda_{wi,j,k+\frac{1}{2}}\gamma_{wi,j,k+\frac{1}{2}}\frac{z_{i,j,k+1} - z_{i,j,k}}{\Delta z_i^+} - \lambda_{wi,j,k-\frac{1}{2}}\gamma_{wi,j,k-\frac{1}{2}}\frac{z_{i,j,k-1} - z_{i,j,k}}{\Delta z_i^-}) \end{aligned} \tag{2.30}$$

where, $\gamma = \rho g$, the (i, j, k) is the coordinate index that indicates the x, y and z

direction respectively. The subscript $(i+1,j,k)$ of water phase pressure, p_w indicates the pressure of the adjacent gridblock in the positive x direction. While $(i-1,j,k)$ indicates the properties of adjacent gridblock in negative x direction. The subscript $(i+\frac{1}{2},j,k)$ indicates the average property at the interface of two adjacent gridblock in positive x direction, and the subscript $(i-\frac{1}{2},j,k)$ indicates the properties at the interface of two adjacent gridblock in negative x direction. Referring to Figure 2.1., the distance between the centroids of middle cube and right cube is expressed as Δx_i^+, while the distance between middle cube and left cube is expressed as Δx_i^-. The same idea of the subscript is applied to y, z directions.

Combining the equations (2.28-2.30) yields the discretization of Darcy's term for water conservation equations:

$$\begin{aligned}
&\frac{\partial}{\partial x}[\lambda_{wx}(\frac{\partial p_o}{\partial x}-\frac{\partial p_{cow}}{\partial x}-\rho_w g\frac{\partial z}{\partial x})]+\frac{\partial}{\partial y}[\lambda_{wy}(\frac{\partial p_o}{\partial y}-\frac{\partial p_{cow}}{\partial y}-\rho_w g\frac{\partial z}{\partial y})]\\
&+\frac{\partial}{\partial z}[\lambda_{wz}(\frac{\partial p_o}{\partial z}-\frac{\partial p_{cow}}{\partial z}-\rho_w g\frac{\partial z}{\partial z})]\\
&\doteq\frac{1}{\Delta x_i}(\lambda_{wi+\frac{1}{2},j,k}\frac{p_{oi+1,j,k}-p_{oi,j,k}}{\Delta x_i^+}+\lambda_{wi-\frac{1}{2},j,k}\frac{p_{oi-1,j,k}-p_{oi,j,k}}{\Delta x_i^-})\\
&\frac{1}{\Delta y_i}(\lambda_{wi,j+\frac{1}{2},k}\frac{p_{oi,j+1,k}-p_{oi,j,k}}{\Delta y_i^+}+\lambda_{wi,j-\frac{1}{2},k}\frac{p_{oi,j-1,k}-p_{oi,j,k}}{\Delta y_i^-})\\
&\frac{1}{\Delta z_i}(\lambda_{wi,j,k+\frac{1}{2}}\frac{p_{oi,j,k+1}-p_{oi,j,k}}{\Delta z_i^+}+\lambda_{wi,j,k-\frac{1}{2}}\frac{p_{oi,j,k-1}-p_{oi,j,k}}{\Delta z_i^-}\\
&-\lambda_{wi,j,k+\frac{1}{2}}\gamma_{wi,j,k+\frac{1}{2}}\frac{z_{i,j,k+1}-z_{i,j,k}}{\Delta z_i^+}-\lambda_{wi,j,k-\frac{1}{2}}\gamma_{wi,j,k-\frac{1}{2}}\frac{z_{i,j,k-1}-z_{i,j,k}}{\Delta z_i^-})
\end{aligned}\tag{2.31}$$

The timescale discretization of accumulation term in water conservation equation is derived based on the textbook by Ertekin[20]:

$$\frac{\partial}{\partial t}(\frac{\phi S_w}{B_w})={S_w}^n({b_w}^{n+1}\phi'+\phi^n{b_w}')\Delta p_w+(\phi^{n+1}{b_w}^{n+1})\Delta S_w \tag{2.32}$$

where, $b_w = \frac{1}{B_w}$, $b'_w = \frac{{b_w}^{n+1} - {b_w}^n}{{p_w}^{n+1} - {p_w}^n}$, $\phi' = \frac{\phi^{n+1} - \phi^n}{{p_w}^{n+1} - {p_w}^n}$, $\Delta p_w = \frac{{p_w}^{n+1} - {p_w}^n}{\Delta t}$ and $\Delta S_w = \frac{{S_w}^{n+1} - {S_w}^n}{\Delta t}$.

The superscript, n indicates the properties at the current time-step, while $n+1$ indicates the properties at the next time-step.

In this research, a simplified vertical wellbore model is used. Therefore, the sink/source term q_w^*, can be derived from Peaceman's equations[20], which is shown in equations (2.33). If the wellbore model involves more complex configurations (e.g. Fracturing), the Peaceman's equations will not be applicable.

$$q_w^* = WI_w({p_w}_{wc}^{n+1} - p_{wf}) \tag{2.33}$$

where, the subscript, wc indicates the gridblocks where the well is placed. While, the well index, WI_w is defined as:

$$WI_w = -\frac{2\pi k_{rw}\sqrt{k_x k_y}h}{\mu_w B_w[ln(\frac{r_0}{r_w}) + s]} \tag{2.34}$$

where, k_x is permeability in x-direction, k_y is permeability in y-direction, h is thickness of gridblock, and r_w is wellbore radius. The equivalent radius, within which the pressure is equal to the well-block pressure at steady-state. The formulation for equivalent wellbore radius is:

$$r_0 = 0.28\frac{\sqrt{[(\frac{k_y}{k_x})^{\frac{1}{2}}(\Delta x)^2] + [(\frac{k_x}{k_y})^{\frac{1}{2}}(\Delta y)^2]}}{(\frac{k_y}{k_x})^{\frac{1}{4}} + (\frac{k_x}{k_y})^{\frac{1}{4}}} \tag{2.35}$$

Combining equations (2.31-2.33) and (2.23) yields the discretization of water conser-

vation equation:

$$\frac{1}{\Delta x_i}(\lambda_{wi+\frac{1}{2},j,k}\frac{p_{oi+1,j,k}-p_{oi,j,k}}{\Delta x_i^+}+\lambda_{wi-\frac{1}{2},j,k}\frac{p_{oi-1,j,k}-p_{oi,j,k}}{\Delta x_i^-})$$
$$\frac{1}{\Delta y_i}(\lambda_{wi,j+\frac{1}{2},k}\frac{p_{oi,j+1,k}-p_{oi,j,k}}{\Delta y_i^+}+\lambda_{wi,j-\frac{1}{2},k}\frac{p_{oi,j-1,k}-p_{oi,j,k}}{\Delta y_i^-})$$
$$\frac{1}{\Delta z_i}(\lambda_{wi,j,k+\frac{1}{2}}\frac{p_{oi,j,k+1}-p_{oi,j,k}}{\Delta z_i^+}+\lambda_{wi,j,k-\frac{1}{2}}\frac{p_{oi,j,k-1}-p_{oi,j,k}}{\Delta z_i^-}$$
$$-\lambda_{wi,j,k+\frac{1}{2}}\gamma_{wi,j,k+\frac{1}{2}}\frac{z_{i,j,k+1}-z_{i,j,k}}{\Delta z_i^+}-\lambda_{wi,j,k-\frac{1}{2}}\gamma_{wi,j,k-\frac{1}{2}}\frac{z_{i,j,k-1}-z_{i,j,k}}{\Delta z_i^-})$$
$$={S_w}^n({b_w}^{n+1}\phi'+\phi^n{b_w}')\Delta p_w+(\phi^{n+1}{b_w}^{n+1})\Delta S_w$$
$$+WI_w(p_{w_{wc}}^{n+1}-p_{wf}) \tag{2.36}$$

2.1.3 Discretization of conservation equation for oil phase

Similarly, the discretization oil flux term can be extended as:

$$\frac{\partial}{\partial x}[\lambda_{ox}(\frac{\partial p_o}{\partial x}-\rho_o g\frac{\partial z}{\partial x})]+\frac{\partial}{\partial y}[\lambda_{oy}(\frac{\partial p_o}{\partial y}-\rho_o g\frac{\partial z}{\partial y})]+\frac{\partial}{\partial z}[\lambda_{oz}(\frac{\partial p_o}{\partial z}-\rho_o g\frac{\partial z}{\partial z})]$$
$$\doteq\frac{1}{\Delta x_i}(\lambda_{oi+\frac{1}{2},j,k}\frac{p_{oi+1,j,k}-p_{oi,j,k}}{\Delta x_i^+}+\lambda_{oi-\frac{1}{2},j,k}\frac{p_{oi-1,j,k}-p_{oi,j,k}}{\Delta x_i^-})$$
$$\frac{1}{\Delta y_i}(\lambda_{oi,j+\frac{1}{2},k}\frac{p_{oi,j+1,k}-p_{oi,j,k}}{\Delta y_i^+}+\lambda_{oi,j-\frac{1}{2},k}\frac{p_{oi,j-1,k}-p_{oi,j,k}}{\Delta y_i^-})$$
$$\frac{1}{\Delta z_i}(\lambda_{oi,j,k+\frac{1}{2}}\frac{p_{oi,j,k+1}-p_{oi,j,k}}{\Delta z_i^+}+\lambda_{oi,j,k-\frac{1}{2}}\frac{p_{oi,j,k-1}-p_{oi,j,k}}{\Delta z_i^-}$$
$$-\lambda_{oi,j,k+\frac{1}{2}}\gamma_{oi,j,k+\frac{1}{2}}\frac{z_{i,j,k+1}-z_{i,j,k}}{\Delta z_i^+}-\lambda_{oi,j,k-\frac{1}{2}}\gamma_{oi,j,k-\frac{1}{2}}\frac{z_{i,j,k-1}-z_{i,j,k}}{\Delta z_i^-}) \tag{2.37}$$

The oil accumulation term on the RHS is expended regarding to the material balance:

$$\frac{\partial}{\partial t}[\frac{\phi(1-S_g-S_w)}{B_o}]=[(1-S_w-S_g)^n({b_o}^{n+1}\phi'+\phi^n b_o'\Delta p_o$$
$$-(\phi b_o)^{n+1}\Delta S_w-(\phi b_o)^{n+1}\Delta S_g] \tag{2.38}$$

where, $b_o = \frac{1}{B_o}$, $b'_o = \frac{{b_o}^{n+1} - {b_o}^n}{{p_o}^{n+1} - {p_o}^n}$, $\phi' = \frac{{\phi_o}^{n+1} - {\phi_o}^n}{{p_o}^{n+1} - {p_o}^n}$, $\Delta p_o = \frac{{p_o}^{n+1} - {p_o}^n}{\Delta t}$, $\Delta S_w = \frac{{S_w}^{n+1} - {S_w}^n}{\Delta t}$ and $\Delta S_g = \frac{{S_g}^{n+1} - {S_g}^n}{\Delta t}$.

The sink/source term for oil phase, q_o* is expended with Peaceman's equation:

$$q_o* = WI_o(p_{o_{wc}}^{n+1} - p_{wf}) \tag{2.39}$$

where,

$$WI_o = -\frac{2\pi k_{ro}\sqrt{k_x k_y}h}{\mu_o B_o[ln(\frac{r_0}{r_w}) + s]} \tag{2.40}$$

Combining the equations (2.37-2.39) and (2.24) yields the discretization formulation for oil phase conservation:

$$\begin{aligned}
&\frac{1}{\Delta x_i}(\lambda_{o_{i+\frac{1}{2},j,k}}\frac{p_{o_{i+1,j,k}} - p_{o_{i,j,k}}}{\Delta x_i^+} + \lambda_{o_{i-\frac{1}{2},j,k}}\frac{p_{o_{i-1,j,k}} - p_{o_{i,j,k}}}{\Delta x_i^-}) \\
&\frac{1}{\Delta y_i}(\lambda_{o_{i,j+\frac{1}{2},k}}\frac{p_{o_{i,j+1,k}} - p_{o_{i,j,k}}}{\Delta y_i^+} + \lambda_{o_{i,j-\frac{1}{2},k}}\frac{p_{o_{i,j-1,k}} - p_{o_{i,j,k}}}{\Delta y_i^-}) \\
&\frac{1}{\Delta z_i}(\lambda_{o_{i,j,k+\frac{1}{2}}}\frac{p_{o_{i,j,k+1}} - p_{o_{i,j,k}}}{\Delta z_i^+} + \lambda_{o_{i,j,k-\frac{1}{2}}}\frac{p_{o_{i,j,k-1}} - p_{o_{i,j,k}}}{\Delta z_i^-} \\
&- \lambda_{o_{i,j,k+\frac{1}{2}}}\gamma_{o_{i,j,k+\frac{1}{2}}}\frac{z_{i,j,k+1} - z_{i,j,k}}{\Delta z_i^+} - \lambda_{o_{i,j,k-\frac{1}{2}}}\gamma_{o_{i,j,k-\frac{1}{2}}}\frac{z_{i,j,k-1} - z_{i,j,k}}{\Delta z_i^-}) \\
&= [(1 - S_w - S_g)^n({b_o}^{n+1}\phi' + \phi^n b'_o)\Delta p_o \\
&- (\phi b_o)^{n+1}\Delta S_w - (\phi b_o)^{n+1}\Delta S_g] + WI_o(p_{o_{wc}}^{n+1} - p_{wf})
\end{aligned} \tag{2.41}$$

2.1.4 Discretization of conservation equation for gas phase

For the discretization of gas conservation, the additional terms that represents the gas components in oil phase are considered, and their formulation in x, y and

z-directions are shown respectively as:

$$\begin{aligned}
&\frac{\partial}{\partial x}[R_s\lambda_{ox}(\frac{\partial p_o}{\partial x}-\gamma_o\frac{\partial z}{\partial x})]\\
&=\frac{1}{\Delta x_i}[(R_s\lambda_o)_{i+\frac{1}{2},j,k}\frac{p_{oi+1,j,k}-p_{oi,j,k}}{\Delta x_i^+}\\
&+(R_s\lambda_o)_{i-\frac{1}{2},j,k}\frac{p_{oi-1,j,k}-p_{oi,j,k}}{\Delta x_i^-}]
\end{aligned}\tag{2.42}$$

$$\begin{aligned}
&\frac{\partial}{\partial y}[R_s\lambda_{oy}(\frac{\partial p_o}{\partial y}-\gamma_o\frac{\partial z}{\partial y})]\\
&=\frac{1}{\Delta y_i}[(R_s\lambda_o)_{i,j+\frac{1}{2},k}\frac{p_{oi,j+1,k}-p_{oi,j,k}}{\Delta y_i^+}\\
&+(R_s\lambda_o)_{i,j-\frac{1}{2},k}\frac{p_{oi,j-1,k}-p_{oi,j,k}}{\Delta y_i^-}]
\end{aligned}\tag{2.43}$$

$$\begin{aligned}
&\frac{\partial}{\partial z}[R_s\lambda_{oz}(\frac{\partial p_o}{\partial z}-\gamma_o\frac{\partial z}{\partial z})]\\
&=\frac{1}{\Delta z_i}[(R_s\lambda_o)_{i,j,k+\frac{1}{2}}\frac{p_{oi,j,k+1}-p_{oi,j,k}}{\Delta z_i^+}\\
&+(R_s\lambda_o)_{i,j,k-\frac{1}{2}}\frac{p_{oi,j,k-1}-p_{oi,j,k}}{\Delta z_i^-}\\
&-(R_s\lambda_o)_{i,j,k+\frac{1}{2}}\gamma_{oi,j,k+\frac{1}{2}}\frac{z_{i,j,k+1}-z_{i,j,k}}{\Delta z_i^+}\\
&-(R_s\lambda_o)_{i,j,k-\frac{1}{2}}\gamma_{oi,j,k-\frac{1}{2}}\frac{z_{i,j,k-1}-z_{i,j,k}}{\Delta z_i^-}]
\end{aligned}\tag{2.44}$$

Then the gas flux term of conservation is expended as:

$$
\begin{aligned}
&\frac{\partial}{\partial x}[\lambda_{ox}R_S(\frac{\partial p_o}{\partial x}-\rho_o g\frac{\partial z}{\partial x})]+\frac{\partial}{\partial y}[\lambda_{oy}R_S(\frac{\partial p_o}{\partial y}-\rho_o g\frac{\partial z}{\partial y})]\\
&+\frac{\partial}{\partial z}[\lambda_{oy}R_S(\frac{\partial p_o}{\partial z}-\rho_o g\frac{\partial z}{\partial z})]\\
&+\frac{\partial}{\partial x}[\lambda_{gx}(\frac{\partial p_g}{\partial x}-\frac{\partial p_{cgo}}{\partial x}-\rho_g g\frac{\partial z}{\partial x})]\\
&+\frac{\partial}{\partial y}[\lambda_{gy}(\frac{\partial p_g}{\partial y}-\frac{\partial p_{cgo}}{\partial y}-\rho_g g\frac{\partial z}{\partial y})]\\
&+\frac{\partial}{\partial z}[\lambda_{gz}(\frac{\partial p_g}{\partial z}-\frac{\partial p_{cgo}}{\partial z}-\rho_g g\frac{\partial z}{\partial z})]\\
&=\frac{1}{\Delta x_i}[(R_s\lambda_o)_{i+\frac{1}{2},j,k}\frac{p_{oi+1,j,k}-p_{oi,j,k}}{\Delta x_i^+}+(R_s\lambda_o)_{i-\frac{1}{2},j,k}\frac{p_{oi-1,j,k}-p_{oi,j,k}}{\Delta x_i^-}]\\
&+\frac{1}{\Delta y_i}[(R_s\lambda_o)_{i,j+\frac{1}{2},k}\frac{p_{oi,j+1,k}-p_{oi,j,k}}{\Delta y_i^+}+(R_s\lambda_o)_{i,j-\frac{1}{2},k}\frac{p_{oi,j-1,k}-p_{oi,j,k}}{\Delta y_i^-}]\\
&+\frac{1}{\Delta z_i}[(R_s\lambda_o)_{i,j,k+\frac{1}{2}}\frac{p_{oi,j,k+1}-p_{oi,j,k}}{\Delta z_i^+}+(R_s\lambda_o)_{i,j,k-\frac{1}{2}}\frac{p_{oi,j,k-1}-p_{oi,j,k}}{\Delta z_i^-}\\
&-(R_s\lambda_o)_{i,j,k+\frac{1}{2}}\gamma_{oi,j,k+\frac{1}{2}}\frac{z_{i,j,k+1}-z_{i,j,k}}{\Delta z_i^+}-(R_s\lambda_o)_{i,j,k-\frac{1}{2}}\gamma_{oi,j,k-\frac{1}{2}}\frac{z_{i,j,k-1}-z_{i,j,k}}{\Delta z_i^-}]\\
&+\frac{1}{\Delta x_i}(\lambda_{g_{i+\frac{1}{2},j,k}}\frac{p_{oi+1,j,k}-p_{oi,j,k}}{\Delta x_i^+}+\lambda_{g_{i-\frac{1}{2},j,k}}\frac{p_{oi-1,j,k}-p_{oi,j,k}}{\Delta x_i^-})\\
&\frac{1}{\Delta y_i}(\lambda_{g_{i,j+\frac{1}{2},k}}\frac{p_{oi,j+1,k}-p_{oi,j,k}}{\Delta y_i^+}+\lambda_{g_{i,j-\frac{1}{2},k}}\frac{p_{oi,j-1,k}-p_{oi,j,k}}{\Delta y_i^-})\\
&\frac{1}{\Delta z_i}(\lambda_{g_{i,j,k+\frac{1}{2}}}\frac{p_{oi,j,k+1}-p_{oi,j,k}}{\Delta z_i^+}+\lambda_{g_{i,j,k-\frac{1}{2}}}\frac{p_{oi,j,k-1}-p_{oi,j,k}}{\Delta z_i^-}\\
&-\lambda_{g_{i,j,k+\frac{1}{2}}}\gamma_{g_{i,j,k+\frac{1}{2}}}\frac{z_{i,j,k+1}-z_{i,j,k}}{\Delta z_i^+}-\lambda_{g_{i,j,k-\frac{1}{2}}}\gamma_{g_{i,j,k-\frac{1}{2}}}\frac{z_{i,j,k-1}-z_{i,j,k}}{\Delta z_i^-})
\end{aligned}
\tag{2.45}
$$

The accumulation term in gas conservation formulation is expended as:

$$\begin{aligned}
&\frac{\partial}{\partial t}[\frac{R_S\phi(1-S_g-S_w)}{B_o}+\frac{\phi S_g}{B_g}] \\
&= \Delta p_o\{(1-S_w-S_g)^n[R_s^n({b_o}^{n+1}\phi'+\phi^n b_o')+R_s'(\phi b_o)^{n+1}] \\
&+ S_g^n({b_g}^{n+1}\phi'+\phi^n b_g')\} \\
&- R_s^{n+1}(b_o\phi)^{n+1}\Delta S_w \\
&+ [(b_g\phi)^{n+1}-R_s^{n+1}(b_o\phi)^{n+1}]\Delta S_g
\end{aligned} \tag{2.46}$$

then, the sink/source term for gas phase can be expended as:

$$R_s q_o * + q_g * = WI_g(p_{g_{i,j,k}}^{n+1}-p_w f)+R_s^{n+1}WI_o(p_{g_{i,j,k}}^{n+1}-p_w f) \tag{2.47}$$

where, the well index for oil, WI_o is already shown in equation (2.48), and the WI_g is:

$$WI_g = -\frac{2\pi k_{rg}\sqrt{k_x k_y}h}{\mu_g B_g[ln(\frac{r_0}{r_w})+s]} \tag{2.48}$$

Finally, combining equations (2.25) and (2.45-2.47) yields the gas conservation equa-

tion:

$$
\begin{aligned}
&\frac{1}{\Delta x_i}[(R_s\lambda_o)_{i+\frac{1}{2},j,k}\frac{p_{oi+1,j,k}-p_{oi,j,k}}{\Delta x_i^+}+(R_s\lambda_o)_{i-\frac{1}{2},j,k}\frac{p_{oi-1,j,k}-p_{oi,j,k}}{\Delta x_i^-}]\\
&+\frac{1}{\Delta y_i}[(R_s\lambda_o)_{i,j+\frac{1}{2},k}\frac{p_{oi,j+1,k}-p_{oi,j,k}}{\Delta y_i^+}+(R_s\lambda_o)_{i,j-\frac{1}{2},k}\frac{p_{oi,j-1,k}-p_{oi,j,k}}{\Delta y_i^-}]\\
&+\frac{1}{\Delta z_i}[(R_s\lambda_o)_{i,j,k+\frac{1}{2}}\frac{p_{oi,j,k+1}-p_{oi,j,k}}{\Delta z_i^+}+(R_s\lambda_o)_{i,j,k-\frac{1}{2}}\frac{p_{oi,j,k-1}-p_{oi,j,k}}{\Delta z_i^-}\\
&-(R_s\lambda_o)_{i,j,k+\frac{1}{2}}\gamma_{oi,j,k+\frac{1}{2}}\frac{z_{i,j,k+1}-z_{i,j,k}}{\Delta z_i^+}-(R_s\lambda_o)_{i,j,k-\frac{1}{2}}\gamma_{oi,j,k-\frac{1}{2}}\frac{z_{i,j,k-1}-z_{i,j,k}}{\Delta z_i^-}]\\
&+\frac{1}{\Delta x_i}(\lambda_{g_{i+\frac{1}{2},j,k}}\frac{p_{oi+1,j,k}-p_{oi,j,k}}{\Delta x_i^+}+\lambda_{g_{i-\frac{1}{2},j,k}}\frac{p_{oi-1,j,k}-p_{oi,j,k}}{\Delta x_i^-})\\
&\frac{1}{\Delta y_i}(\lambda_{g_{i,j+\frac{1}{2},k}}\frac{p_{oi,j+1,k}-p_{oi,j,k}}{\Delta y_i^+}+\lambda_{g_{i,j-\frac{1}{2},k}}\frac{p_{oi,j-1,k}-p_{oi,j,k}}{\Delta y_i^-})\\
&\frac{1}{\Delta z_i}(\lambda_{g_{i,j,k+\frac{1}{2}}}\frac{p_{oi,j,k+1}-p_{oi,j,k}}{\Delta z_i^+}+\lambda_{g_{i,j,k-\frac{1}{2}}}\frac{p_{oi,j,k-1}-p_{oi,j,k}}{\Delta z_i^-}\\
&-\lambda_{g_{i,j,k+\frac{1}{2}}}\gamma_{g_{i,j,k+\frac{1}{2}}}\frac{z_{i,j,k+1}-z_{i,j,k}}{\Delta z_i^+}-\lambda_{g_{i,j,k-\frac{1}{2}}}\gamma_{g_{i,j,k-\frac{1}{2}}}\frac{z_{i,j,k-1}-z_{i,j,k}}{\Delta z_i^-})\\
&=\Delta p_o\{(1-S_w-S_g)^n[R_s^n({b_o}^{n+1}\phi'+\phi^n b_o')+R_s'(\phi b_o)^{n+1}]\\
&+S_g^n({b_g}^{n+1}\phi'+\phi^n b_g')\}\\
&-R_s^{n+1}(b_o\phi)^{n+1}\Delta S_w\\
&+[(b_g\phi)^{n+1}-R_s^{n+1}(b_o\phi)^{n+1}]\Delta S_g\\
&+WI_g({p_g}_{i,j,k}^{n+1}-p_wf)+R_s^{n+1}WI_o({p_g}_{i,j,k}^{n+1}-p_wf)
\end{aligned}
\tag{2.49}
$$

It can be seen that the discretization of the conservation equation for water, oil and gas phase are complete nonlinear equations. Thus, a linearization method is required to solve these governing equations. In this study, the Newton-Raphson method is used to linearize the governing equations. The details of Newton-Raphson will be discussed in the next chapter.

2.2 Network Multiphase Flow Modeling

In black-oil coupled model, the flow in tubing and pipes are generally multiphase flow. The distribution of different phase in tubing and pipe affects the aspects of the multiphase flow, such as holdups of phases and pressure gradient throughout the production system. Thus, it is important to identify the manner where the phases are distributed. The fundamental theories and formulations that used in this study are based the textbook by Economides[21].

The main task of the network modeling is to determine the pressure losses throughout the production system (see Figure 2.2), which is the main task when coupling the surface/subsurface. The distribution of liquid and gas phase has significant impacts on the pressure gradient; and the change of pressure in the tubing/pipe further affects the properties of the fluids, which complicates the production system modeling. In production system, the pressure loss will occur throughout the entire surface facilities, and the general formulation for production system is in the form of:

$$p_{wf} = p_{sep} + \Delta p_v + \Delta p_t + \Delta p_c$$

where, p_{wf} indicates the bottom hole flowing pressure. Δp_v indicates the pressure loss caused by the safety valve restriction. The pressure losses through tubing is indicated by Δp_t. At wellhead, the surface choke is usually used to control the upstream pressure and fluid flow rate, and the pressure loss across the surface choke is indicated by Δp_c. Finally, the flowing pressure at separator is indicates by p_{sep}.

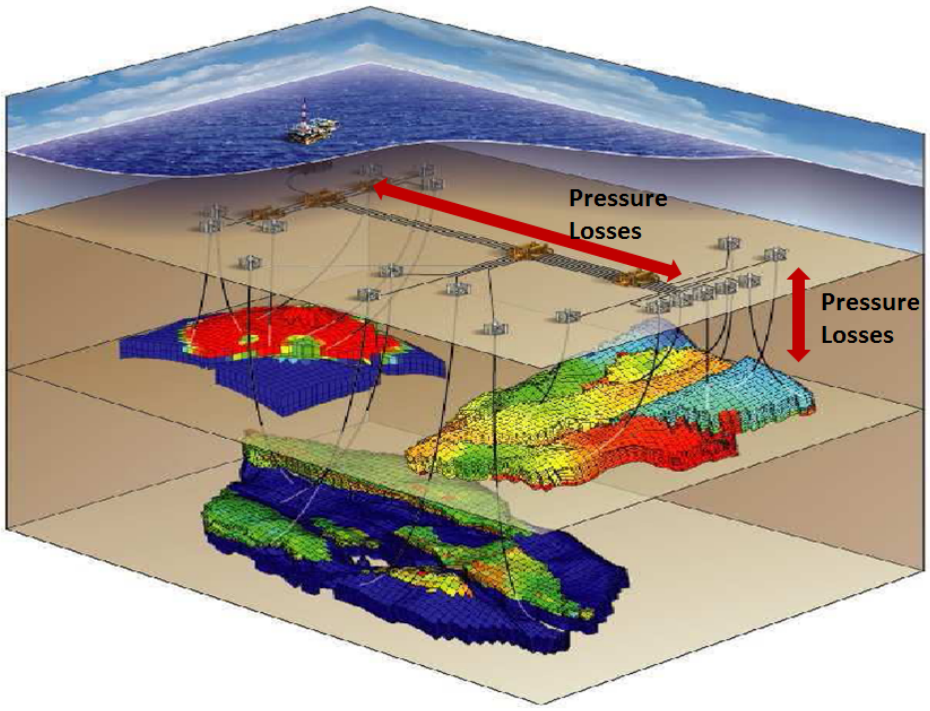

Figure 2.2: Pressure losses in production systems

Usually, the simplified production system does not involve all the surface facilities that is mentioned above. In this study, the pressure loss across tubing, flowline and choke will be investigated.

Similar to the reservoir model, the network modeling is operated based on the concept of material balance. Instead of using gridblocks within reservoir modeling, the tubing and flowline are divide into several segments, where the phases flow has only one direction. In each segment, all the phases flow follow the material:

$$Mass_{inflow} - Mass_{outflow} = Mass_{accumulation}$$

The accumulation is affected by the holdup of each phase. And the partial equations

of liquid and gas flow are shown respectively as:

$$\widetilde{q}_{l_{in}} - \widetilde{q}_{l_{out}} = V_{segment}\frac{\partial}{\partial t}(y_l \rho_l) \tag{2.50}$$

$$(\widetilde{q}_{g_{in}} - \widetilde{q}_{g_{out}}) = V_{segment}\frac{\partial}{\partial t}(y_g \rho_g) \tag{2.51}$$

where, $V_{segment}$ indicates the volume of each segment of tubing or flowline. The parameter, $y_p(p = l, g)$ indicates the *holdup* for each phase. In two-phase or multiphase flow, the lighter phase moves faster than the denser phase. This phenomenon result in that the in-situ volume fraction of denser phase is greater than the input volume fraction of this phase, which is called holdup. In multiphase flow, the liquid holdup is determine by using correlations. Different phases flow correlations are chosen regarding to the inclination of flow. The multiphase correlation used in this study will be discussed late in this section.

2.2.1 Mass conservation for tubing and pipe

Each segment of tubing/pipe is treated as a cylinderical cell, where phases flow has the same direction (see Figure 2.3). The length of each segment is indicated by Δx_i.

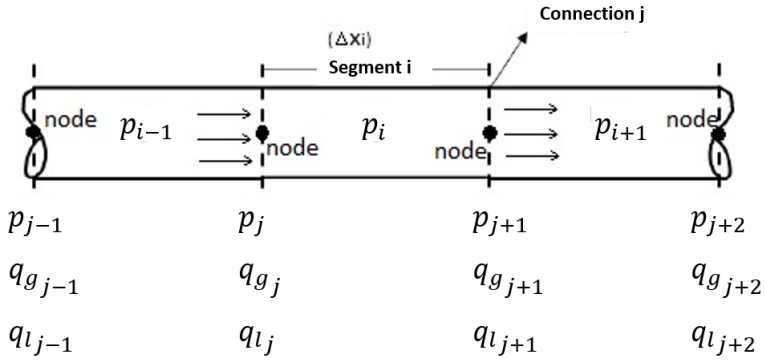

Figure 2.3: Flow across tubing segment

Referring to Figure 2.3. the subscript i indicates the properties of fluid within the segment, while the subscript j indicates the properties of fluid flow at the interface between two adjacent segments. Based on equations (2.50-2.51), the mass conservation equations for water, oil and gas phase are shown respectively as:

$$\widetilde{q_{wj}} - \widetilde{q_{wj+1}} = \Delta x_i A_i \frac{\partial}{\partial t}(y_w \rho_{Ws} b_w)_i \tag{2.52}$$

$$\widetilde{q}_{oj} - \widetilde{q}_{oj+1} = \Delta x_i A_i \frac{\partial}{\partial t}(y_o \rho_{Os} b_o)_i \tag{2.53}$$

$$(\widetilde{q}_{g_j} - \widetilde{q}_{g_{j+1}}) = \Delta x_i A_i \frac{\partial}{\partial t}(y_g \rho_{Gs} b_g + R_s y_o \rho_{Gs} b_o)_i \tag{2.54}$$

where, the mass flow rate $\widetilde{q}$ is the flow rate at surface standard conditions. A_i indicates the cross-section area of segment i. The parameters, phase holdup and volume

factor are calculated with the segment pressure, p_i, where, the segment pressure is the average value of the pressures at segment interfaces ($p_i = \frac{p_j + p_{j+1}}{2}$). Then, taking the time-scale discretization of the RHS of the tubing conservation equations and dividing by density yields:

$$q^*_{wj} - q^*_{wj+1} = \frac{\Delta x_i A_i}{\Delta t}[(y_w b_w)^{n+1}_i - (y_w b_w)^n_i] \tag{2.55}$$

$$q^*_{oj} - q^*_{oj+1} = \frac{\Delta x_i A_i}{\Delta t}[(y_o b_o)^{n+1}_i - (y_o b_o)^n_i] \tag{2.56}$$

$$(q^*_{gj} - q^*_{gj+1}) = \frac{\Delta x_i A_i}{\Delta t}[(y_g b_g)^{n+1}_i - (y_g b_g)^n_i + (R_s y_o b_o)^{n+1}_i - (R_s y_o b_o)^n_i] \tag{2.57}$$

Referring to equations (2.55-2.57), it can be seen that the flow rate change with time within each timestep, which is called transient flows. Since the timestep in transient well model is limited by the time scale where the equations of the wellbore flow are solve with Newton iteration, the computational efficiency will be significantly reduced for transient wellbore flow. In this study, the flow in wellbore and flowline is assumed as steady-state, where flows do not change with time at any location in the well/pipeline system within each timestep, such that:

$$\frac{\Delta x_i A_i}{\Delta t}[(y_w b_w)^{n+1}_i - (y_w b_w)^n_i] \approx 0$$
$$\frac{\Delta x_i A_i}{\Delta t}[(y_o b_o)^{n+1}_i - (y_o b_o)^n_i] \approx 0$$
$$\frac{\Delta x_i A_i}{\Delta t}[(y_g b_g)^{n+1}_i - (y_g b_g)^n_i + (R_s y_o b_o)^{n+1}_i - (R_s y_o b_o)^n_i] \approx 0$$

Applying the steady-state flow into the equations (2.55-2.57) yields the finally for-

mulation for tubing flow conservation:

$$q^*_{wj} - q^*_{wj+1} \approx 0 \tag{2.58}$$

$$q^*_{oj} - q^*_{oj+1} \approx 0 \tag{2.59}$$

$$(q^*_{gj} - q^*_{gj+1}) + R_s(q^*_{oj} - q^*_{oj+1}) \approx 0 \tag{2.60}$$

2.2.2 Momentum conservation for vertical tubing and horizontal pipe

In tubing model, the momentum is conserved in each segment of tubing string, such that the pressure difference between the two interfaces equals to the fluid pressure loss through the segment. Referring to Figure 2.3., the energy conservation for one segment can be expressed as:

$$p_i - p_{i+1} = \Delta p_{PEi} + \Delta p_{f_i} + \Delta p_{acci} \tag{2.61}$$

where, Δp indicate the pressure loss, the subscript, PE indicates that the pressure loss is caused by potential energy, the subscript f indicates the pressure loss caused by friction, and acc stands for the pressure loss due to kinetic energy change. In this study, the pressure drop caused by kinetic energy change is ignored due to the small affect compared to pressure drop caused by potential energy and friction. Thus, the equation (2.61) can be rewritten in pressure gradient form as:

$$\frac{dp}{dz} = (\frac{dp}{dz})_{pe} + (\frac{dp}{dz})_f, \tag{2.62}$$

where, $p_i - p_{i+1} = \Delta x_i \frac{dp}{dz}$. And the potential energy term is calculated with:

$$(\frac{dp}{dz})_{pe} = \frac{g}{g_c}\bar{\rho} sin\theta, \tag{2.63}$$

where, $\theta = \frac{\pi}{2}$ for vertical tubing, and $\theta = 0$ for horizontal pipe. Here $\bar{\rho}$ is the in-situ average density in the tubing segment so that:

$$\bar{\rho} = y_l \rho_l + y_g \rho_g, \tag{2.64}$$

$$y_l = \frac{V_l}{V_{seg}} \quad and \quad y_l + y_g = 1, \tag{2.65}$$

and yl is the liquid holdup that is calculated with tubing flow correlation. In this study, the Modified Hagedorn and Brown[22] correlation is used to determine the liquid holdup for vertical tubing, the liquid holdup is determined with Beggs-Brill[5] correlation. These multiphase flow correlations will be introduced later in this section. The friction term is calculated with:

$$(\frac{dp}{dz})_f = \frac{2f\rho_m u_m^2}{g_c D}, \tag{2.66}$$

where, D is the tubing diameter. And ρ_m is the density of liquid and gas mixture, which is calculated as:

$$\rho_m = \rho_l \lambda_l + \rho_g \lambda_g, \tag{2.67}$$

where, the λ stands for the input fraction of each phase,

$$\lambda_l = \frac{q_l}{q_l + q_g} \quad and \quad \lambda_g = 1 - \lambda_l$$

for mixture velocity u_m:

$$u_m = u_{sl} + u_{sg}, \tag{2.68}$$

where the superficial velocity is

$$u_{sli} = \frac{q_{li}}{A_i} \quad and \quad u_{sg_i} = \frac{q_{g_i}}{A_i},$$

and the volumetric flow q_{li} and q_{g_i} is the in-situ flow at the conditions of segment i. the two phase friction factor f is calculated with

$$f = f_n exp(S), \tag{2.69}$$

where

$$S = \frac{ln(x)}{-0.0523 + 3.182ln(x) - 0.8725[ln(x)]^2 + 0.01853[ln(x)]^4}$$

or

$$S = ln(2.2x - 1.2) \qquad (1 < x < 1.2)$$

and

$$x = \frac{\lambda_l}{{y_l}^2}$$

the no-slip friction factor, f_n is based the tubing/pipe relative roughness, ϵ and Reynolds number, N_{Re}. According to Economides[21], the Chen's equation is used to determine no-slip friction factor when Reynolds number is greater than 2100. While Fanning equation[21] is used for the situation where the Reynolds number is less than

2100.

Chen equation ($N_{Re} > 2100$)

$$\frac{1}{\sqrt{f_n}} = -4log\{\frac{\epsilon}{3.7065} - \frac{5.0452}{N_{Re}}log[\frac{\epsilon^{1.1098}}{2.8257} + (\frac{7.149}{N_{Re}})^{0.8981}]\} \tag{2.70}$$

Fanning eqation ($N_{Re} < 2100$)

$$f_n = \frac{16}{N_{Re}} \tag{2.71}$$

where

$$N_{Re} = \frac{\rho_m u_m D}{\mu_m}$$

and

$$\mu_m = \mu_l \lambda_l + \mu_g \lambda_g$$

Here μ_l is the viscosity of the oil/water mixture regardless of the emulsion effect. Also assuming that no slip occurs between oil and water phases, the viscosity of the liquid mixture is calculated with volume fraction-weighted average as:

$$\mu_l = (\frac{WOR\rho_w}{WOR\rho_w + B_o\rho_o})\mu_w + (\frac{B_o\rho_o}{WOR\rho_w + B_o\rho_o})\mu_o \tag{2.72}$$

2.2.3 Liquid holdup correlation for vertical tubing

Liquid holdup in vertical tubing can be determined with several correlations. In this study, the Modified Hargedorn-Brown[22] correlation is implemented for the multiphase flow in vertical tubing. The modified Hargedorn-Brown correlation is an

empirical two-phase flow correlation based on the original Hagedorn-Brown correlation.

The modification of original correlation uses no-slip holdup when the predicted liquid holdup is less than the no-slip holdup; the Griffith correlation[21] is used for bubble flow in modified Hagedorn-Brown correlation. Bubble flow is the regime where dispersed bubble of gas phase is in continuous liquid phase, it exists when $\lambda_g < L_B$, where

$$L_B = 1.071 - 0.2218(\frac{u_m^2}{D}) \tag{2.73}$$

and L_B has to be great than or equal to 0.13. Once the flow regime is determined to be bubble flow, the Griffith correlation is used to determine the liquid holdup

$$y_l = 1 - \frac{1}{2}[1 + \frac{u_m}{u_s} - \sqrt{(1 + \frac{u_m}{u_s})^2 - 4\frac{u_{sg}}{u_s}}] \tag{2.74}$$

where, u_s is a constant velocity that is equal to 0.24384 m/s. When the flow regime is determined to be the flow regime rather than bubble flow, the original Hagedorn-Brown is used to determine the liquid holdup

$$y_l = \psi\frac{y_l}{\psi} \tag{2.75}$$

and

$$\frac{y_l}{\psi} = (\frac{0.0047 + 1123.32H + 729489.64H^2}{1 + 1097.1566H + 722153.97H^2})^{0.5} \tag{2.76}$$

$$\psi = \frac{1.0886 - 69.9473B + 2334.3497B^2 - 12896.683B^3}{1 - 53.4401B + 1517.9369B^2 - 8419.8115B^3} \tag{2.77}$$

where

$$H = \frac{N_{vl} p^{0.1(CN_L)}}{{N_{vg}}^{0.575} p_a^{0.1} N_D} \tag{2.78}$$

$$B = \frac{N_{vg} N_L^{0.380}}{N_D^{2.14}} \tag{2.79}$$

and

$$CN_L = \frac{0.0019 + 0.0322N_L - 0.6642N_L^2 + 4.9951N_L^3}{1 - 10.0147N_L + 33.8696N_L^2 + 277.2817N_L^3} \tag{2.80}$$

$$N_{vl} = u_{sl} \sqrt[4]{\frac{\rho_l}{g\sigma}} \tag{2.81}$$

$$N_{vg} = \sqrt[4]{\frac{\rho_l}{g\sigma}} \tag{2.82}$$

$$N_D = D\sqrt{\frac{\rho_l g}{\sigma}} \tag{2.83}$$

$$N_L = \mu_l \sqrt[4]{\frac{g}{\rho_l \sigma^3}} \tag{2.84}$$

where, the surface tension σ is defined as the elastic-like force existing in the surface of a body, especially a liquid, tending to minimize the area of the surface, caused by asymmetries in the intermolecular forces between surface molecules.. The SI unit of surface tension is in $\frac{N}{m}$.

The advantage of Hagedorn-Brown correlation is that it is able to calculate the liquid holdup with a set of continuous equations, regardless the identification of the flow regime. However, this correlation is only applicable for vertical or near-vertical tubing/pipe. Thus, other correlation has to be applied to the flow in horizontal pipe.

2.2.4 Liquid holdup correlation for horizontal pipe

The Beggs-Brill correlation is advanced in that the Beggs-Brill correlation is applicable to any flow direction. In this study, the flow regime and liquid holdup determine is based on the Beggs-Brill correlation. Differing from Hagedorn-Brown correlation, the Beggs-Brill correlation involves the regime identification, which complicates the modeling of horizontal pipe. Thus, the Beggs-brill is only recommended for the wellbore or pipe that is not vertical or near vertical.

To introduce the Beggs-Brill correlation, it is necessary to understand the flow regime in horizontal pipe. The flow regime of horizontal flow is shown in Figure 2.4. Generally, the flow regime is classified in to three patterns.

Referring from Figure 2.4. the types of flow regimes are defined as: segregated flows, where the gas and liquid phases are almost separated; intermittent flows, where the gas and liquid phases exist alternatively; and distributed flows, where the one phase is dispersed in another phase.

Based on the flow regime, Beggs and Brill gave a flow regime map that involves the relationship between input liquid holdup, λ_l and Froude number, N_{Fr} (see Figure 2.5). The Froude number is defined as:

$$N_{Fr} = \frac{u_m^2}{gD}$$

In the flow regime map, Beggs and Brill also introduced the *transitionregime* that

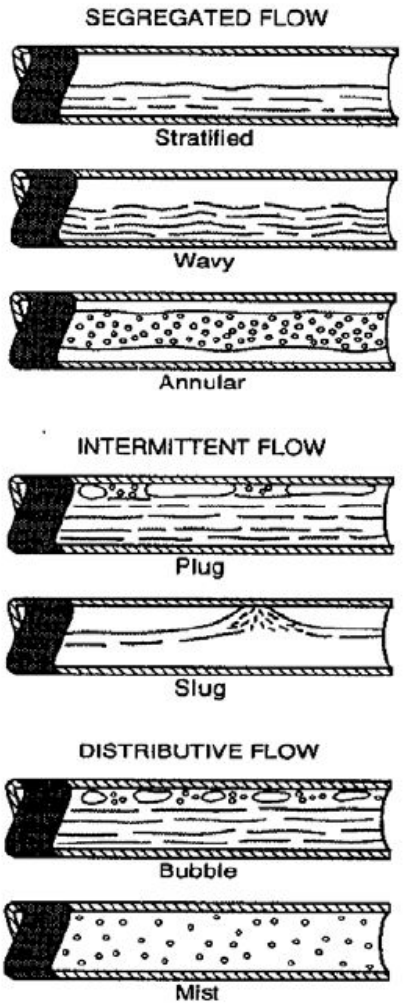

Figure 2.4: Flow regime in horizontal pipe (source: Beggs, H.D.[5])

is the transient state in between intermittent and segregated regime.

Referring to the regime map, it is found that the distributed flow can occur at large N_{Fr}; segregated flows occur at relatively small N_{Fr} and input liquid holdup; while intermittent flows exist at high input liquid holdup. The Beggs-Brill correlation determine the flow regime base the following parameters:

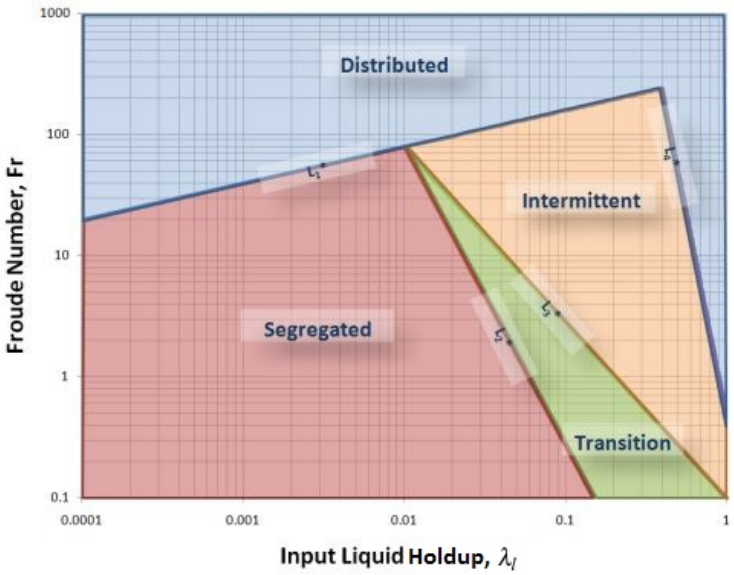

Figure 2.5: Flow regime map (based on Beggs, H.D.[5])

$$N_{Fr} = \frac{u_m^2}{gD} \tag{2.85}$$

$$\lambda_l = \frac{u_{sl}}{u_m} \tag{2.86}$$

$$L_1 = 316\lambda_l^{0.302} \tag{2.87}$$

$$L_2 = 0.0009252\lambda_l^{-2.4684} \tag{2.88}$$

$$L_3 = 0.10\lambda_l^{-1.4516} \tag{2.89}$$

$$L_4 = 0.5\lambda_l^{-6.738} \tag{2.90}$$

Once the parameters are calculated, the flow regime can be determined by using the empirical correlation. The determination of flow regime is shown in Table 2.1.

Table 2.1: Determination of flow regime (base on: Beggs, H.D.[5])

Flow Regime	Flow regime range
Segregated flow	$\lambda_l < 0.01$ and $N_{Fr} < L_1$ or $\lambda_l \geq 0.01$ and $N_{Fr} < L_2$
Transition flow	$\lambda_l \geq 0.01$ and $L_2 < N_{Fr} \leq L_3$
Intermittent flow	$0.01 \leq \lambda_l < 0.4$ and $L_3 < N_{Fr} \leq L_1 or \lambda_l > 0.4$ and $L_3 < N_{Fr} \leq L_4$
Distributed flow	$\lambda_l < 0.4$ and $N_{Fr} \geq L_1$ or $\lambda_l \geq 0.4$ and $N_{Fr} > L_4$

The equation that are used to calculate the liquid holdup are

$$y_l = y_{lo}\psi \tag{2.91}$$

$$y_{lo} = \frac{a\lambda_l^b}{N_{Fr}^c} \tag{2.92}$$

where

$$\psi = 1 + C[sin(1.8\theta) - 0.333sin^3(1.8\theta)] \tag{2.93}$$

where θ is the inclination angle, and

$$C = (1 - \lambda_l) ln(d\lambda_l^e N_{vl}^f N_{Fr}^g) \tag{2.94}$$

If the flow regime is determined as transition flow, the liquid holdup can be calculated with both the segregated and intermittent equations and interpolated using following:

$$y_l = Ay_l(segregated) + By_l(intermittent) \tag{2.95}$$

where

$$A = \frac{L_3 - N_{Fr}}{L_3 - L_2} \tag{2.96}$$

$$B = 1 - A \tag{2.97}$$

The coefficient, a, b, c, d, e, f and g used in correlation equation are based on the flow regime and the value of these holdup coefficients are given in Table 2.2. and Table 2.3.

Table 2.2: Beggs-Brill holdup coefficient (base on: Beggs, H.D.[5])

Flow Regime	a	b	c
Segregated	0.98	0.4846	0.0868
Intermittent	0.845	0.5351	0.0173
Distributed	1.065	0.5824	0.0609

Once the liquid holdup is obtained, the average density and slip friction factor can be calculated and consequently applied to the pressure gradient calculation.

Table 2.3: Beggs-Brill holdup coefficient at inclination (base on: Beggs, H.D.[5])

Flow Regime	d	e	f	g
Segregated uphill	0.011	-3.768	3.539	-1.614
Intermittent uphill	2.96	0.305	-0.4473	0.0978
Distributed uphill	1	0	0	0
All regimes downhill	4.7	-0.3692	0.1244	-0.5056

2.2.5 Flow through choke

The flow rate is generally restricted with a wellhead choke, which is a device providing restriction in flow line. The reason to apply choke in production system could be various, such as prevent gas coning or sand production.

The flow rate across a choke is generally classified as critical and sub-critical flow[21]; the critical exists when the flow reaches sonic velocity in the throat of choke; while the sub-critical flow exists when the flow velocity is less than sonic velocity. Therefore, to predict the flow rate-pressure drop relationship for flow through the choke, the flow state has to be determined first. When multiphase flow is in critical state, the change of downstream pressure at choke does not affect the upstream pressure, while the upstream pressure is only function of liquid flow rate and gas/liquid ratio. In this study, the Ros correlation[21] is used for critical flow, and the pressure drop across the choke for sub-critical flow is calculated with mechanistic correlation[23].

The Ros correlation is an empirical correlation that depends on the producing

gas-liquid ratio and liquid rate

$$p_{up} = \frac{Aq_l(GLR)^B}{D_{64}^C} \tag{2.98}$$

where D_{64} is the choke diameter in 64ths of an inch, and the coefficient A, B and C is given in Table 2.4

Table 2.4: Empirical coefficient for Ros correlation (source from: Economides[21])

A	B	C
17.4	0.5	2.0

The Ros correlation is claimed to be valid for pressure ratio ($p_{downstream}/p_{upstream}$) of 0.7. Therefore, the determination of critical or sub-critical flow is depends on the pressure ratio in this study, such that the critical flow exists when the $0.7p_{upstream} > p_{downstream}$, otherwise, the flow is sub-critical. Additionally, the constraint that upstream pressure is greater than downstream pressure must be set to guarantee the flow through the choke.

For sub-critical flow across the choke, the upstream pressure becomes the function of both the phases flow rates and downstream pressure. The pressure drop across the choke is calculated with mechanistic correlation[23]

$$\Delta p = \lambda_l \Delta p_l + \lambda_g \Delta p_g \tag{2.99}$$

and the liquid and gas phase pressure is given by Bernouili's equation:

$$\Delta p_l = \frac{\rho_n}{c}(\frac{v}{c_{vl}})^2 \tag{2.100}$$

$$\Delta p_g = \frac{\rho_n}{2}(\frac{v}{c_{vg}B_g})^2 \tag{2.101}$$

where the mixture velocity v and no-slip mixture density are calculated with:

$$v = \frac{q}{A_{bean}\rho_n} \tag{2.102}$$

$$\rho_n = \lambda_l\rho_l + \lambda_g\rho_g \tag{2.103}$$

and λ is the phase flowing fraction at upstream pressure.

In this chapter, the fundamental mechanisms and governing equations of reservoir and network model are introduced. The governing equations of both models are mainly based on the material and energy balance. The phase flow correlations (i.e. Hagedorn-Brown and Beggs-Brill) are employed to determine the liquid holdups for flow in pipe.

3. SURFACE AND SUBSURFACE COUPLING MECHANISM

The main reason of coupling surface and subsurface model is to predict an accurate bottom hole pressure when production constraint is at surface facility. In this chapter, different coupling methods are presented, and the advantage and disadvantage of each method is discussed as well.

As this study is to investigate and construct the fully coupling model, this section summarized the detailed aspects of the fully coupling model. In addition, the linearization of the governing equations system is presented in order to understand the concept of the solving system of equations in the fully implicit frame works.

3.1 Partially Coupling Method

As mentioned in chapter one, the partially coupling method involves the explicit coupling and partially implicit methods. These two method treat the reservoir and network models as different domains; and solve the equations in the basis of convergence of the reservoir and surface network equations.

3.1.1 Explicit coupling

For explicit coupling, the coupling process is operated at the time-step level. The well boundary condition (i.e. bottom hole pressure) is calculated with network model at the beginning of each time-step; the reservoir system is then solved with the boundary constraint passed from the network model. The flowchart of the explicit coupling method is shown in Figure 3.1.

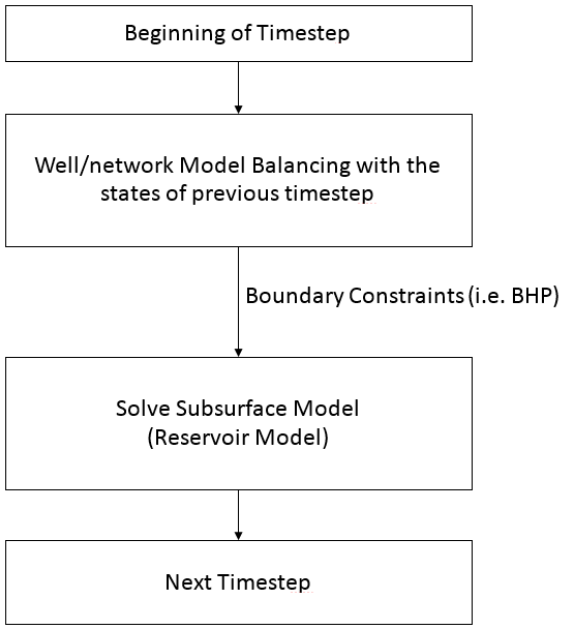

Figure 3.1: Flowchart of explicit coupling method

Referring to Figure 3.1, the surface and subsurface models are only balanced at the beginning of each time-step. Therefore, the explicit coupling required few computational operations. Also since this method treats the reservoir and surface domain explicitly, the explicit coupling can be accomplished by externally coupling independent reservoir and network software. The explicit coupling method is employed in the work of Hepgular et al.[17], where the network and reservoir software are coupled to simulation the overall performance of producing field. However, this method fails to provide an accurate result due to the fact that the state of reservoir state cannot represent the state at the end of each time-step.

3.1.2 Partially implicit coupling

For partially implicit coupling method, the coupling process is operated at the Newton iteration level, and the coupling frequency is varied. The general procedure of partially implicit coupling is:

1. At each Newton iteration, the require for coupling action is determined. If the coupling action is required for current Newton iteration, the surface model is solved with the parameters of previous iteration.

2. Once the surface model is converged, the obtained bottom hole pressure (BHP) is passed to the subsurface model as the boundary constraint.

3. solve the reservoir governing equations with the BHP calculated with surface model.

4. check the convergence of the reservoir equations.

5. once the reservoir model is converged, process to next time-step.

As the partially implicit coupling method balances the surface and subsurface model at Newton iteration level, the computational operations is higher than that of explicit coupling; while the accuracy of the solution is based on the coupling frequency in partially implicit coupling, to this end more coupling or balance frequency operated will result in more accurate results. When the coupling frequency equals to one, such that the balancing of surface and subsurface models is only performed at the first Newton iteration of each time-step, the partially implicit coupling is equivalent to explicit coupling. Similarly to the explicit coupling, the time-step convergence is based on only the reservoir equations. However, because of the balancing performed before solving reservoir equations, the network equations can be converged within

the accuracy of their linearizations if the balancing frequency is appropriate. The flowchart of partially implicit is shown in Figure 3.2. Based on the partially implicit coupling method, Trick[24] coupled a commercial multiphase gas deliverability forecasting program and black-oil reservoir simulator, ECLIPSE 100 at Newton iteration level, and it reported that the coupled model needed sixty minutes to complete one year forecast.

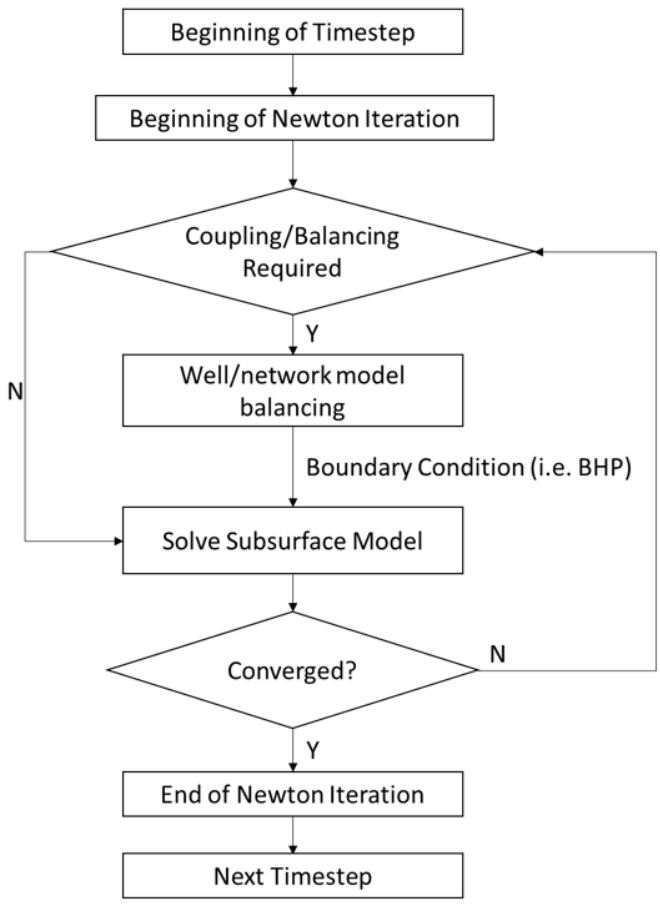

Figure 3.2: Flowchart of partially implicit coupling

3.2 Fully Implicit Coupling Method

Differing from partially implicit coupling, the fully implicit coupling solves the governing equations of surface and subsurface simultaneously at the Newton iteration level. The flowchart of fully implicit coupling is shown in Figure 3.3. In this section, the details of constructing the system of equations and the linearization of the nonlinear equations will be further discussed.

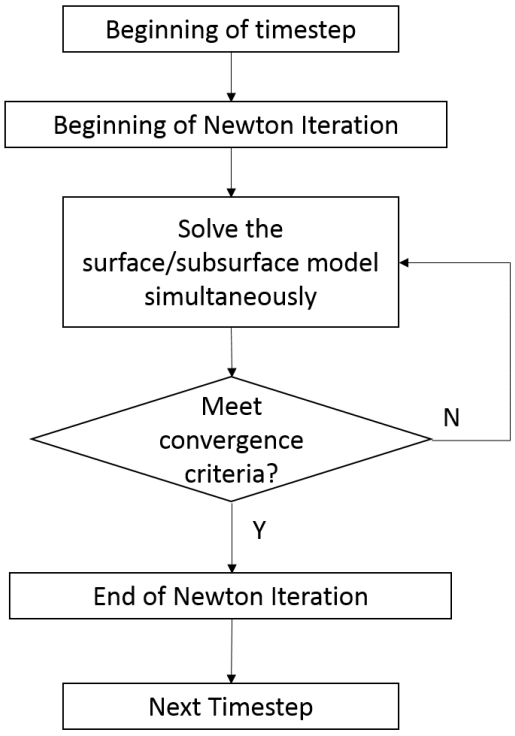

Figure 3.3: Flowchart of fully implicit coupling

3.2.1 Construction of the fully coupling system of equations

In general, the governing equations is contributed by the equations of reservoir, welbore and surface pipe. These equations are connected by exchanging the material and momentum parameters (i.e. phases flow rates or pressures) and making sure these parameters are consistent. Generally, the governing equations are non-linear function, and one needs to linearize them in order to be able to solve for the unknown parameters. To this end, one can represent the non-linear equation in terms of the Residual, R. These residual equations are all based on:

Residual of Discretized Water Conservation Equation

$$\begin{aligned}
R_{rw} =& \frac{1}{\Delta x_i}(\lambda_{wi+\frac{1}{2},j,k}\frac{p_{oi+1,j,k}-p_{oi,j,k}}{\Delta x_i^+} + \lambda_{wi-\frac{1}{2},j,k}\frac{p_{oi-1,j,k}-p_{oi,j,k}}{\Delta x_i^-}) \\
& \frac{1}{\Delta y_i}(\lambda_{wi,j+\frac{1}{2},k}\frac{p_{oi,j+1,k}-p_{oi,j,k}}{\Delta y_i^+} + \lambda_{wi,j-\frac{1}{2},k}\frac{p_{oi,j-1,k}-p_{oi,j,k}}{\Delta y_i^-}) \\
& \frac{1}{\Delta z_i}(\lambda_{wi,j,k+\frac{1}{2}}\frac{p_{oi,j,k+1}-p_{oi,j,k}}{\Delta z_i^+} + \lambda_{wi,j,k-\frac{1}{2}}\frac{p_{oi,j,k-1}-p_{oi,j,k}}{\Delta z_i^-} \\
& - \lambda_{wi,j,k+\frac{1}{2}}\gamma_{wi,j,k+\frac{1}{2}}\frac{z_{i,j,k+1}-z_{i,j,k}}{\Delta z_i^+} - \lambda_{wi,j,k-\frac{1}{2}}\gamma_{wi,j,k-\frac{1}{2}}\frac{z_{i,j,k-1}-z_{i,j,k}}{\Delta z_i^-}) \\
& - {S_w}^n({b_w}^{n+1}\phi' + \phi^n {b_w}') \Delta p_w + (\phi^{n+1}{b_w}^{n+1})\Delta S_w \\
& + q_w^* \qquad (3.1)
\end{aligned}$$

Residual of Discretized Oil Conservation Equation

$$
\begin{aligned}
R_{ro} =& \frac{1}{\Delta x_i}(\lambda_{o i+\frac{1}{2},j,k}\frac{p_{oi+1,j,k}-p_{oi,j,k}}{\Delta x_i^+}+\lambda_{oi-\frac{1}{2},j,k}\frac{p_{oi-1,j,k}-p_{oi,j,k}}{\Delta x_i^-})\\
&\frac{1}{\Delta y_i}(\lambda_{oi,j+\frac{1}{2},k}\frac{p_{oi,j+1,k}-p_{oi,j,k}}{\Delta y_i^+}+\lambda_{oi,j-\frac{1}{2},k}\frac{p_{oi,j-1,k}-p_{oi,j,k}}{\Delta y_i^-})\\
&\frac{1}{\Delta z_i}(\lambda_{oi,j,k+\frac{1}{2}}\frac{p_{oi,j,k+1}-p_{oi,j,k}}{\Delta z_i^+}+\lambda_{oi,j,k-\frac{1}{2}}\frac{p_{oi,j,k-1}-p_{oi,j,k}}{\Delta z_i^-}\\
&-\lambda_{oi,j,k+\frac{1}{2}}\gamma_{oi,j,k+\frac{1}{2}}\frac{z_{i,j,k+1}-z_{i,j,k}}{\Delta z_i^+}-\lambda_{oi,j,k-\frac{1}{2}}\gamma_{oi,j,k-\frac{1}{2}}\frac{z_{i,j,k-1}-z_{i,j,k}}{\Delta z_i^-})\\
&-[(1-S_w-S_g)^n({b_o}^{n+1}\phi'+\phi^n b_o')\Delta p_o\\
&-(\phi b_o)^{n+1}\Delta S_w-(\phi b_o)^{n+1}\Delta S_g]+q_o^*
\end{aligned}
\tag{3.2}
$$

Residual of Discretized Gas Conservation Equation

$$
\begin{aligned}
R_{rg} =& \frac{1}{\Delta x_i}[(R_s\lambda_o)_{i+\frac{1}{2},j,k}\frac{p_{oi+1,j,k}-p_{oi,j,k}}{\Delta x_i^+}+(R_s\lambda_o)_{i-\frac{1}{2},j,k}\frac{p_{oi-1,j,k}-p_{oi,j,k}}{\Delta x_i^-}]\\
&+\frac{1}{\Delta y_i}[(R_s\lambda_o)_{i,j+\frac{1}{2},k}\frac{p_{oi,j+1,k}-p_{oi,j,k}}{\Delta y_i^+}+(R_s\lambda_o)_{i,j-\frac{1}{2},k}\frac{p_{oi,j-1,k}-p_{oi,j,k}}{\Delta y_i^-}]\\
&+\frac{1}{\Delta z_i}[(R_s\lambda_o)_{i,j,k+\frac{1}{2}}\frac{p_{oi,j,k+1}-p_{oi,j,k}}{\Delta z_i^+}+(R_s\lambda_o)_{i,j,k-\frac{1}{2}}\frac{p_{oi,j,k-1}-p_{oi,j,k}}{\Delta z_i^-}\\
&-(R_s\lambda_o)_{i,j,k+\frac{1}{2}}\gamma_{oi,j,k+\frac{1}{2}}\frac{z_{i,j,k+1}-z_{i,j,k}}{\Delta z_i^+}-(R_s\lambda_o)_{i,j,k-\frac{1}{2}}\gamma_{oi,j,k-\frac{1}{2}}\frac{z_{i,j,k-1}-z_{i,j,k}}{\Delta z_i^-}]\\
&+\frac{1}{\Delta x_i}(\lambda_{g i+\frac{1}{2},j,k}\frac{p_{oi+1,j,k}-p_{oi,j,k}}{\Delta x_i^+}+\lambda_{g i-\frac{1}{2},j,k}\frac{p_{oi-1,j,k}-p_{oi,j,k}}{\Delta x_i^-})\\
&\frac{1}{\Delta y_i}(\lambda_{g i,j+\frac{1}{2},k}\frac{p_{oi,j+1,k}-p_{oi,j,k}}{\Delta y_i^+}+\lambda_{g i,j-\frac{1}{2},k}\frac{p_{oi,j-1,k}-p_{oi,j,k}}{\Delta y_i^-})\\
&\frac{1}{\Delta z_i}(\lambda_{g i,j,k+\frac{1}{2}}\frac{p_{oi,j,k+1}-p_{oi,j,k}}{\Delta z_i^+}+\lambda_{g i,j,k-\frac{1}{2}}\frac{p_{oi,j,k-1}-p_{oi,j,k}}{\Delta z_i^-}
\end{aligned}
$$

$$- \lambda_{g_{i,j,k+\frac{1}{2}}} \gamma_{g_{i,j,k+\frac{1}{2}}} \frac{z_{i,j,k+1} - z_{i,j,k}}{\Delta z_i^+} - \lambda_{g_{i,j,k-\frac{1}{2}}} \gamma_{g_{i,j,k-\frac{1}{2}}} \frac{z_{i,j,k-1} - z_{i,j,k}}{\Delta z_i^-})$$
$$- \Delta p_o \{(1 - S_w - S_g)^n [R_s^n ({b_o}^{n+1} \phi' + \phi^n b_o') + R_s' (\phi b_o)^{n+1}]$$
$$+ S_g^n ({b_g}^{n+1} \phi' + \phi^n b_g')\} - R_s^{n+1} (b_o \phi)^{n+1} \Delta S_w + [(b_g \phi)^{n+1} - R_s^{n+1} (b_o \phi)^{n+1}] \Delta S_g$$
$$+ q_g^* \tag{3.3}$$

Residual of Well Water Flow Equation

$$R_{Ww} = q_w^* - WI_w ({p_w}_{wc}^{n+1} - p_{wf}) \tag{3.4}$$

Residual of Well Oil Flow Equation

$$R_{Wo} = q_o^* - WI_o (p_{o_{wc}}^{n+1} - p_{wf}) \tag{3.5}$$

Residual of Well Gas Flow Equation

$$R_{Wg} = q_g^* - R_s^{n+1} WI_o (p_{g_{wc}}^{n+1} - p_{wf}) - WI_g (p_{g_{i,j,k}}^{n+1} - p_w f) \tag{3.6}$$

Residual of Well Bottom Hole Equation

$$R_{BHP} = p_w f - p_{t1} \tag{3.7}$$

where, the p_{t1} is the pressure at the first node in the tubing. In other words, it is assumed that the first node of the tubing is located at the bottom hole.

As mentioned in the second chapter, the network system is considered as steady state, regardless of the changes of phases volumes in time with each segment. Therefore, the phase flow rate of each node is the same. This implies that the flow rate

of each phase equals to the bottom hole phase flow rate, q^* at surface condition. Therefore the residue equations for tubing system are:

Residual of Water Conservation in Tubing

$$R_{tw} = {q_{tw}}_i^{n+1} - q_w^{*\,n+1} \tag{3.8}$$

Residual of Oil Conservation in Tubing

$$R_{to} = {q_{to}}_i^{n+1} - q_o^{*n+1} \tag{3.9}$$

Residual of Gas Conservation in Tubing

$$R_{tg} = {q_{tg}}_i^{n+1} - q_g^{*n+1} \tag{3.10}$$

Residual of Energy Conservation in Tubing

$$R_{tp} = {p_t}_{i+1}^{n+1} - {p_t}_i^{n+1} - \Delta p_{tj}^{n+1} \tag{3.11}$$

where, the index i indicates the properties at node i, while j indicates the properties at segment j. The pressure drop though segment j is calculated with energy conservation equations and Hagedorn-Brown correlation. In addition, the p_{ti} at wellhead is calculated with Ros correlation when the flow is critical across the choke, and the Mechanistic correlation is used when the flow is sub-critical. While the p_t at wellhead equals to the p_p (i.e. pressure at node of surface pipe) at wellhead when there is no choke placed at the wellhead.

The residual equations of surface pipe system is similar to that of tubing system,

which are shown as:

Residual of Water Conservation in Surface pipe

$$R_{pw} = {q_{pw}}_i^{n+1} - q_w^{*\,n+1} \tag{3.12}$$

Residual of Oil Conservation in Surface pipe

$$R_{po} = {q_{po}}_i^{n+1} - q_o^{*n+1} \tag{3.13}$$

Residual of Gas Conservation in Surface pipe

$$R_{pg} = {q_{pg}}_i^{n+1} - q_g^{*n+1} \tag{3.14}$$

Residual of Energy Conservation in Surface pipe

$$R_{pp} = {p_p}_{i+1}^{n+1} - {p_p}_i^{n+1} - \Delta p_{pj}^{n+1} \tag{3.15}$$

Where, the pressure drop through the segment of surface pipe, Δp_{pj} is calculated with momentum conservation equation (2.61) and Beggs-Brill correlation. In this case the pressure at downstream (e.g. separator) point (e.g. separator) equals to the boundary constrain pressure, such that

Residual of Boundary equation

$$R_{bc} = {p_p}_i^{n+1} - p_{constrain} \tag{3.16}$$

3.2.2 Newton-Raphson linearization

Since the fully coupled system equations are nonlinear in terms of the primary unknown vectors, the lineariztion is performed in order to solve the set of governing equations. In this study, the Newton-Raphson method is used to linearize and solve the system equations iteratively. Newton Raphson is a general procedure that can be applied in many diverse situations. When specialized to the problem of locating a zero of a real-valued function of a real variable, it is called *Newton-Raphson iteration*. If we have a function, f whose zeros are to be determined numerically. Then let r be a zero of f and let x be an approximation to r. By Taylor's Theorem:

$$f(r) = f(x+h) = f(x) + hf'(x) + O(h^2) = 0$$

where $h = r - x$. $O(h^2)$ can be ignored if h is small. Therefore, the result is $h = -f(x)/f'(x)$. Thus $x - f(x)/f'(x)$ should be a better approximation to r. Then the general form for Newton's method is:

$$x_{n+1} = x_n - \frac{f(x_n)}{f'(x_n)} \qquad (n \geq 0)$$

In our case, the real-valued function is the residual equations, $R(x)$. The general scheme of Newton-Raphson is shown in the form of flowchart in Figure 3.4.

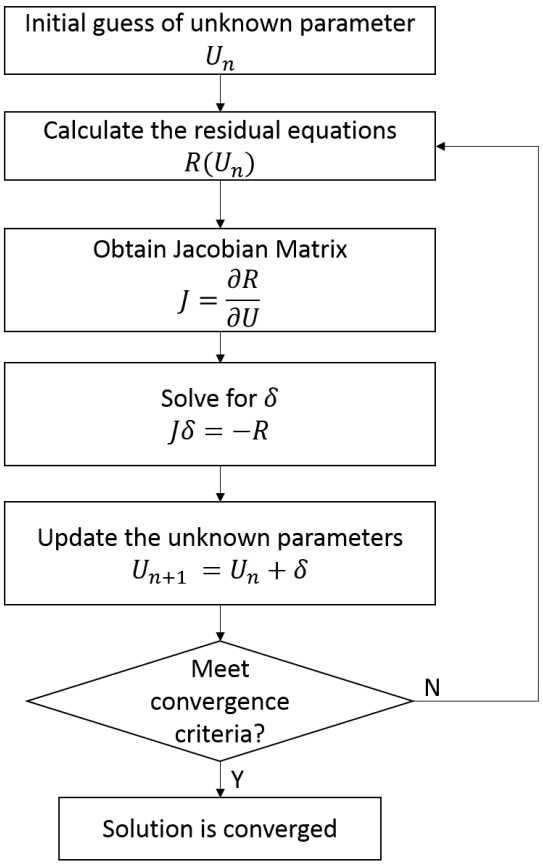

Figure 3.4: Flowchart of Newton-Raphson method

Referring to Figure 3.4, the Jacobian matrix, J is calculated in order to generate the linearized system equations for solving the unknown vectors. To understand the format of Jacobian matrix, the residuals and unknown vectors are defined as:

Residual vectors for reservoir, tubing and surface pipe system

$$R_{res} = (R_{rw}, R_{ro}, R_{rg}, R_c, R_{Ww}, R_{Wo}, R_{Wg}, R_{BHP})^T$$

$$R_{tub} = (R_{tw}, R_{to}, R_{tg}, R_{tp})^T$$

$$R_{pipe} = (R_{pw}, R_{po}, R_{pg}, R_{pp}, R_{bc})^T$$

Unknown vectors for reservoir, tubing and surface pipe system

$$U_{res} = (p_{res}, S_w, S_g, R_s, q_w, q_o, q_g, p_{wf})^T$$
$$U_{tub} = (p_{tub}, q_{tw}, q_{to}, q_{tg})^T$$
$$U_{pipe} = (p_{pipe}, q_{pw}, q_{po}, q_{pg})^T$$

Then the Jacobian matrix can be formed as

$$J = \frac{\partial R}{\partial U} = \begin{bmatrix} \frac{\partial R_{res}}{\partial U_{res}} & \frac{\partial R_{res}}{\partial U_{tub}} & \frac{\partial R_{res}}{\partial U_{pipe}} \\ \frac{\partial R_{tub}}{\partial U_{res}} & \frac{\partial R_{tub}}{\partial U_{tub}} & \frac{\partial R_{tub}}{\partial U_{pipe}} \\ \frac{\partial R_{pipe}}{\partial U_{res}} & \frac{\partial R_{pipe}}{\partial U_{tub}} & \frac{\partial R_{pipe}}{\partial U_{pipe}} \end{bmatrix} \tag{3.17}$$

After obtain the Jacobian of coupled system, the current state/unknown vector is updated with Newton-Raphson iteration, which is shown:

$$\delta U^p = (J^p)^{-1}(-R^p) \tag{3.18}$$

$$U^{p+1} = U^p + \delta U^p \tag{3.19}$$

The Newton Raphson iteration is performed continuously until the residuals of governing equations are converged. The identification of convergence depends on whether the residuals equals to zero. In practical, the iteration will stop when all the norms of residuals are smaller than the set tolerance values, while the tolerance values may vary for different governing equations.

In this chapter, the detailed scheme of each coupling method is presented, and it is found that the convergences of both explicit and partially implicit is based on

the reservoir governing equations, while the convergence of fully implicit coupling is determine in the basis of reservoir and surface facility governing equations. Also, the residual equations of fully coupled system is presented in this chapter; and the linearization of residuals in a form of Jacobian matrix is presented as well. The Newton-Raphson iteration is then introduced in order to explain the process of solving the fully coupled system.

4. EFFECTS OF PARTIALLY IMPLICIT COUPLING FREQUENCY ON PRODUCTION PERFORMANCE

In this chapter, the impacts of coupling frequency on production performance under different reservoir descriptions will be investigated. Here, we couple the commercial reservoir and network simulators in a partially implicit fashion to access the production performance forecast. Consequently, the results and computational costs of the each production performance will be presented.

4.1 Field Management System for Coupling

This section gives a general overview of the field management that is used in this study. The Field Management includes the reservoir and surface models as well as production strategy for coupling the surface/subsurface model. The general process of constructing a partially-implicit coupled model will also be presented.

4.1.1 Surface management

The surface management is realized with the PIPESIM[23] Network model; PIPESIM is a commercial network simulator developed by Schlumberger. In this study, the main task of using PIPESIM is to calculate the pressure drop throughout the surface system and generate the Inflow Performance Relationship (IPR) for coupling purpose.

In the Field Management system, the data of PIPESIM model is input in the "*casenam*.pst" file format. The PST. file contains the keyword that specifies each surface facility (e.g. the tubing, surface flowline and sink). In our case study, both the tubing and pipes have ten nodes, of which the location and temperature is specified.

Since the constructed surface model is isothermal, the temperatures at all nodes is the same as the temperature in the reservoir. The correlations used for calculating the pressure gradient in vertical flow is the modified Hagedorn-Brown, which is shown in the previous chapters. For horizontal flow, the Beggs-Brill correlation is used to calculate the pressure gradient. The vertical or horizontal flow is determined in basis of the inclination angle. To this end, if the inclination angle is greater than forty-five degree, the flow is treated as vertical flow, otherwise, the flow is treated as horizontal flow.

4.1.2 Reservoir management and field management for coupling

The INTERSECT[19] reservoir model is used as the subsurface modeling tool. INTERSECT is the next-generation reservoir simulator developed by Sclumberger. In order to design the scheduling and control of the oilfield production operations, the INTERSECT Field Management is used in this study.

The Field Management system is generated by adding user edits to the file called "*casename* fm edits.ixf"; and it provides a comprehensive framework and set of tools with which to build a working operational model of the oilfield. This model captures all the operational constraints and complex operating logic required to manage the asset. As the model is moved through time, different production strategies may be explored using reservoir simulation workflows. Different predictive scenarios may be evaluated to assist in field development planning, surface facility design, and in the optimization of revenue from the asset. The work-flow of INTERSECT Field Management is shown in Figure 4.1.

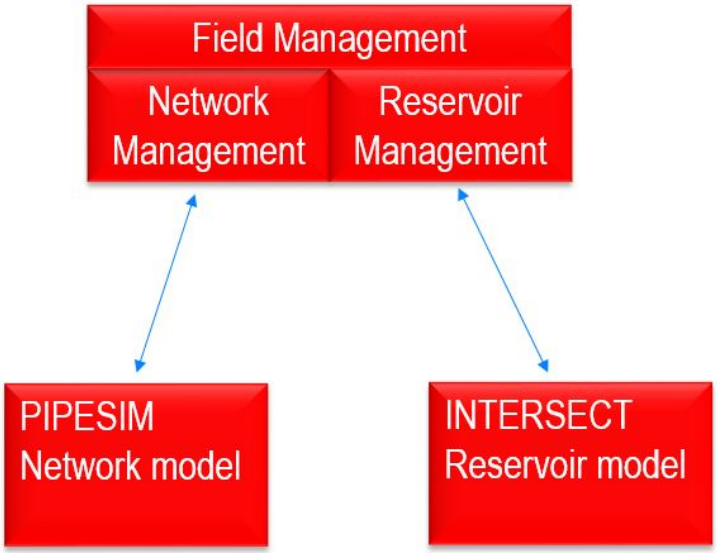

Figure 4.1: Field management workflow

The keyword that used for coupling in INTERSECT[19] Field Management is called "NetworkBalanceAction" (ACT_ NET_ BAL), where the subsurface (i.e. reservoir) model is balanced with the surface network model at the coupling location (the default location is bottom hole). During the balance process, the surface model will calculate the pressure drops throughout the surface network under various flow rate, and consequently generate the Outflow Performance relationship (OPR); whereas the INTERSECT Field Management will generate the Inflow Performance Relationship (IPR). The intersection of the OPR and IPR curve is the solution of balance action, which is then passed to the subsurface model as the boundary constraints (i.e. bottom hole pressures).

Another keyword that used in INTERSECT Field Management is "Coupling-Properties" where the solution scheme (i.e. coupling level and coupling frequency) can be set. The solution scheme involves two approaches, which are *Periodic* and

Iteratively Lagged. In the Periodic solution method, the coupling action is performed once at the beginning of every defined period (e.g. 0, 30, 60 days and so on.), which means the coupled is taken place at the timestep level. The periodic solution method results in a looser coupling, and produces shorter run times.

In the Iteratively Lagged solution method, the coupling action is performed at defined number (N_c) of Newton Iterations within every timestep, the N_c is called coupling frequency. If the reservoir simulator converge within the first N_c iterations, then the strategy will be executed fewer times. While if the more Newton iterations are required for convergence of the reservoir model, then bottom hole pressure targets will be fixed to those determined by the Field Management system for the remainder of the reservoir iterations. These iterations are referred to as non-coupled Newton iterations. An example of Iteratively Lagged solution is displayed in Figure 4.2, where the N_c equals to 3.

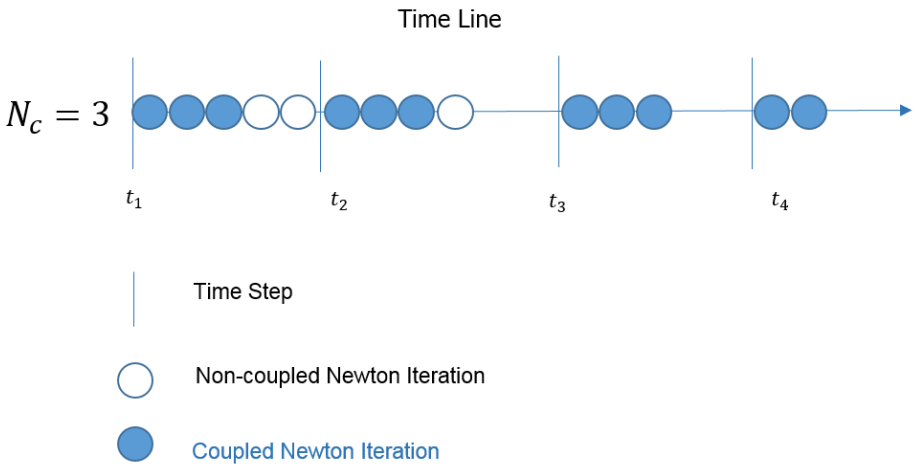

Figure 4.2: Coupling of field management at the reservoir simulator Newton iteration level (source: Adapted from INTERSECT reference manual[19])

Referring to Figure 4.2, the reservoir simulator cannot converge after 3 iterations at time step t_1, therefore the rest iterations are treated as non-coupled. While at time step t_3 the reservoir simulator converged after two iterations, hence the strategy is not set by Field Management after the second iteration.

The advantage of Using INTERSECT Field Management is that it can externally couple the reservoir and network simulator. Other coupling tools (e.g. ECLIPSE network option) usually use the VLP tables obtained from the surface production model in order to generate the IPR. However, this method may fail to couple the surface and subsurface model when the current states of parameters exceed the limitation of the VLP table. Since the Field Management enables the reservoir simulator to couple with the surface production simulator in a seamless fashion, instead of estimating the control constraints with a pre-generated VLP table, the coupling with Field Management is capable to access all the states of parameters during the simulation run. However, the INTERSECT Field Management currently fail to support the injection networks, therefore only the production networks are coupled with the reservoir model in the study of this chapter. The impact of the injection networks on the production performance will be investigated with the fully implicitly coupled model in next chapter.

4.2 Descriptions of Surface and Subsurface Models

This section focuses on the investigation of the effect of the coupling frequency on the production performance under different reservoir descriptions. The coupled model is preformed with the partially implicit coupling method. The descriptions of the reservoir and production properties will be shown below.

4.2.1 Description of reservoir model

In this study, four scenarios are used in order to investigated the impact of coupling frequency (i.e., N_c) on the production performance under different reservoir models. In these scenarios, different reservoir models are coupled with a set of common well/network model. In scenario-1, the well/network model is coupled with a homogeneous permeability reservoir model; In scenario-2, the well/network model is coupled with a homogeneous high-permeability reservoir model; In scenario-3, the well/network model is coupled with a heterogeneous permeability reservoir model; In scenario-4, the well/network model is coupled with unconventional reservoir (i.e. tight sand). The description of different reservoir models used in the four scenarios are displayed in Table 4.1

Table 4.1: Descriptions of reservoir models for investigating the effects of coupling frequency

	Scn-1	Scn-2	Scn-3	Scn-4
$N_x : N_y : N_z$	15:15:3	15:15:3	15:15:3	15:15:3
$\Delta x \times \Delta y \times \Delta z$ (ft)	250×250×10	250×250×10	250×250×10	250×250×10
Permeability (mD)	250	550	100-4000	0.01-0.1
Porosity (%)	20	20	20	20
Initial Pressure (psia)	3000	3000	3000	3000
Reservoir Top Depth (ft)	3000	3000	3000	3000
Initial Water saturation	0.1	0.1	0.1	0.1
Initial Oil Saturation	0.9	0.9	0.9	0.9

Since the permeability maps of the heterogeneous models (Scn-3 and Scn-4) cannot be displayed in the table form, the distribution of the permeability in x-direction of the reservoir is shown in Figure 4.3. The permeability range from 100-4000 mD with a high permeable channel located in the northwest part of the reservoir. And the average of the permeability is around 200 mD, while the ratio of permeability (vertical direction to horizontal direction) is 0.1.

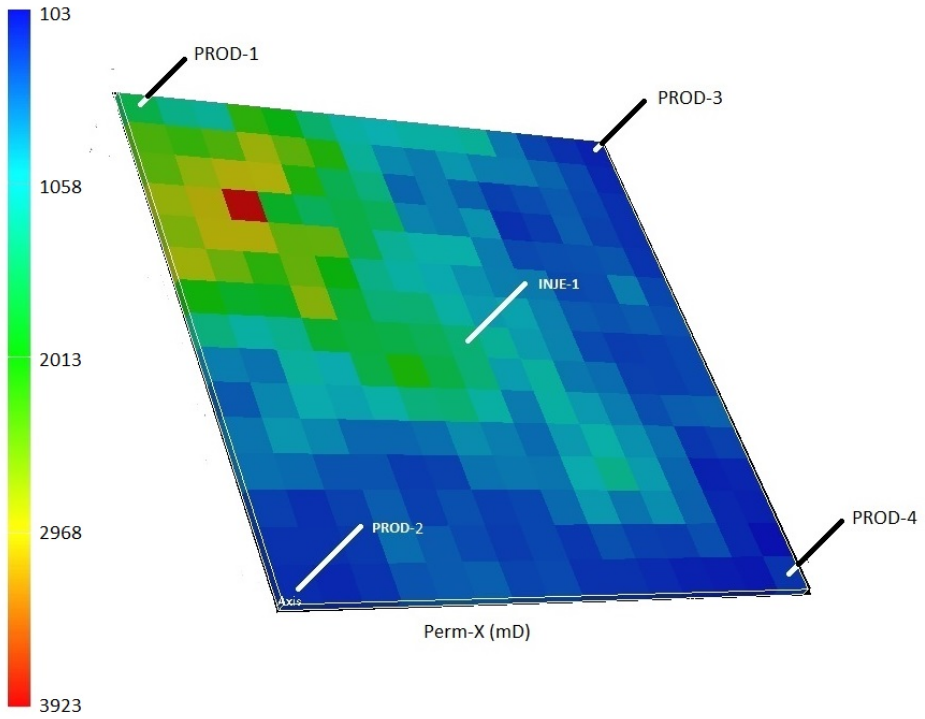

Figure 4.3: Permeability map in x-direction of heterogeneous reservoir model

4.2.2 Description of production model

The production strategy used in this study is five-spot water flooding with one injection well placed in the middle of the reservoir and four producers located at

the corners of the reservoir, and the example of the production system is shown in Figure 4.4. The properties of these four production systems are identical, which are displayed in the Table 4.2. The production network of each producer consists of a horizontal pipeline and a constant pressure separator is set at the end of surface pipeline. Since the injection well is not coupled in this phase of study, the properties of injection well is not provided.

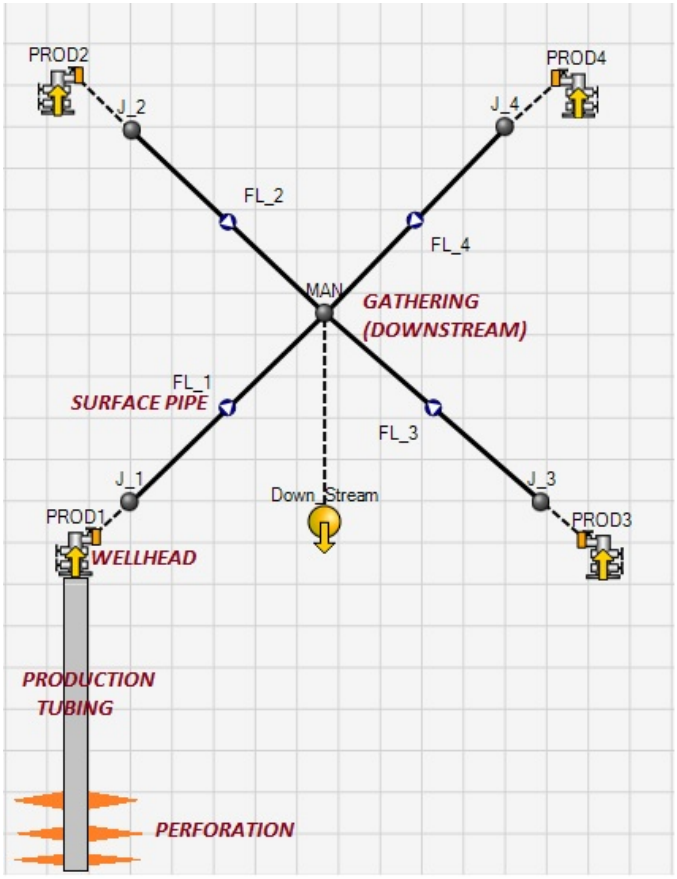

Figure 4.4: Surface facilities of production systems

Table 4.2: Properties of production model

Production System Properties	Value	Unit
Production Tubing ID	3	in
production Tubing Length	3005	ft
Surface Pipe ID	3	in
Downstream Production pressure	300	psia
Bottom Hole pressure of Injection well	3700	psia

4.2.3 Description of fluid properties

The fluid that used in this study is lived-oil, such that there will be three phases to be considered in the coupled the model. The properties of the fluids that used is displayed in the Table 4.3. The oil is saturated at the pressure of 4014.7 *psia*.

Table 4.3: Description of fluid properties

Fluid Properties	Value	Unit
Oil Density	48.33	API
Gas Specific Gravity	0.819	
Water Specific Gravity	1.038	
Solution GOR	1.6	MSCF/STB

4.3 Case Studies on the Effects of Coupling Frequency on Production Performance

In order to investigation the effect of coupling on production performance, each scenario described above is performed with three different coupling frequency ($N_c =$

1, 3, 15).

4.3.1 Case study with scenario-1

In this case study, the predictive results of oil production, gas production and bottom hole pressure under different coupling frequency will be displayed. In homogeneous permeable reservoir, the production states are identical for all four wells, therefore, only the production forecast of PROD-1 is displayed and discussed in the case study of homogeneous reservoir models.

The oil production, gas production, and bottom hole pressure of PROD-1 are shown in Figures 4.5-4.6, where the blue curve, green curve and red curve represent the production profiles under the coupling frequency of 1, 3 and 15, respectively. The total simulation time is 1100 days.

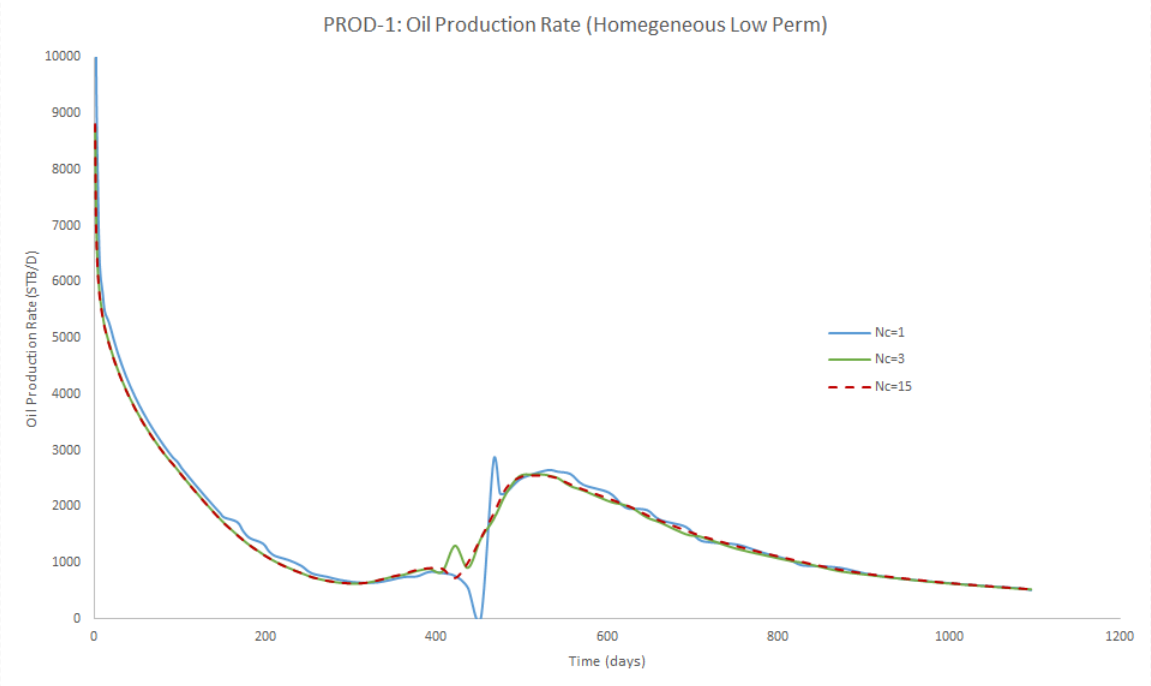

Figure 4.5: Oil production of PROD-1 for Scn-1

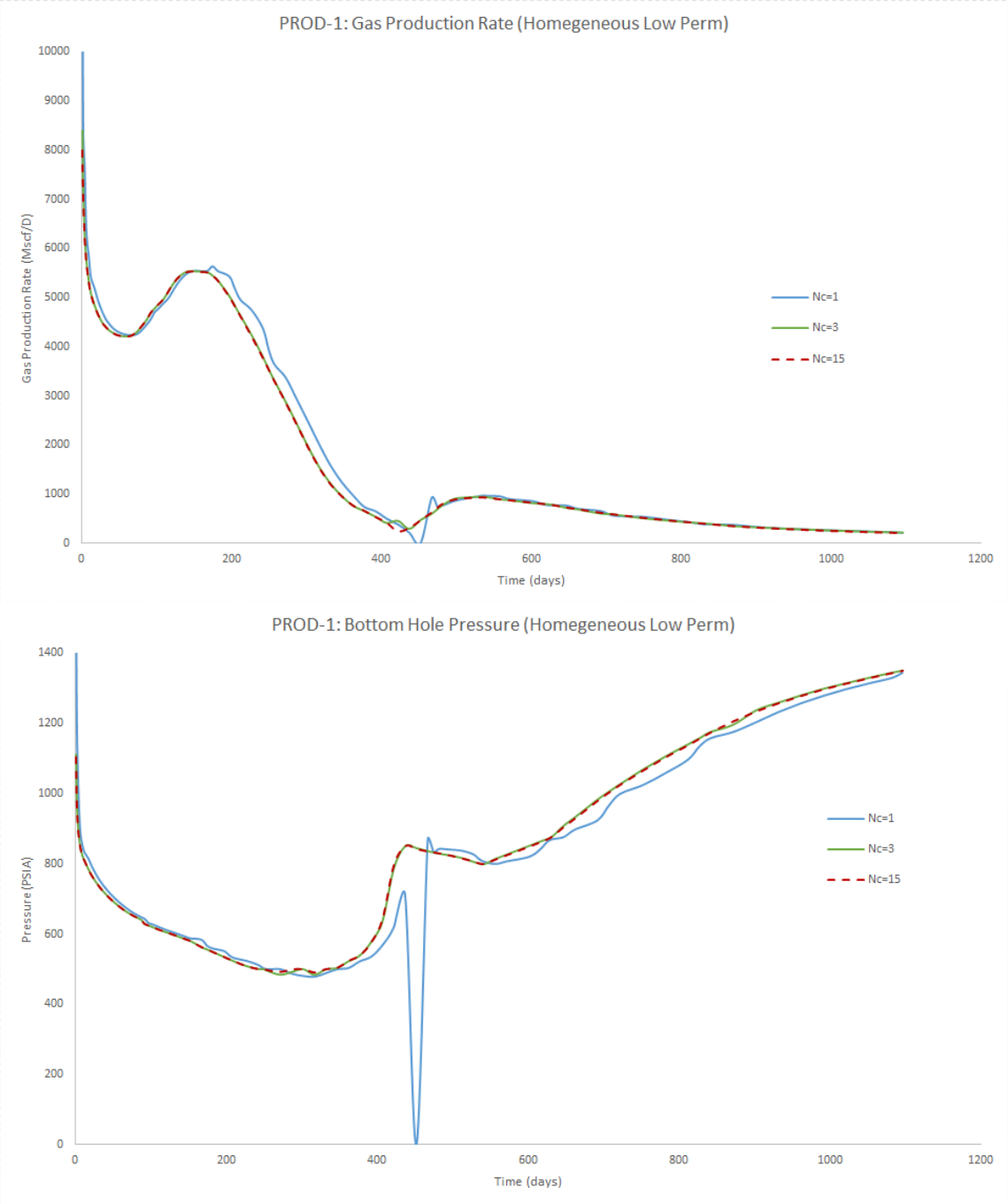

Figure 4.6: Gas production and bottom hole pressure of PROD-1 for Scn-1

Inferred from the results provided above, it can be observed that the difference between the production profiles of Nc=3 and that of Nc=15 is not significant, while the production profile of Nc=1 significantly differs from that of the other two. This differences indicate that the balancing between the reservoir and production model is not complete when the coupling frequency equals to one, and the control parameters (boundary condition) calculated with the production model cannot represent the control parameters at the end of the time-step. In such manner, the results obtained with this coupling frequency will have relative large errors. In addition, an oscillation occurred at the 59^{th} iteration. This can be explained as that the reservoir model failed to obtain the solution within the default iterations by using the boundary conditions passed from well/network model.

4.3.2 Case study with scenario-2

Similar to the Scenario-1, the predictive results of oil production, gas production and bottom hole pressure of Scenario-2 is displayed in Figure 4.7-4.8.

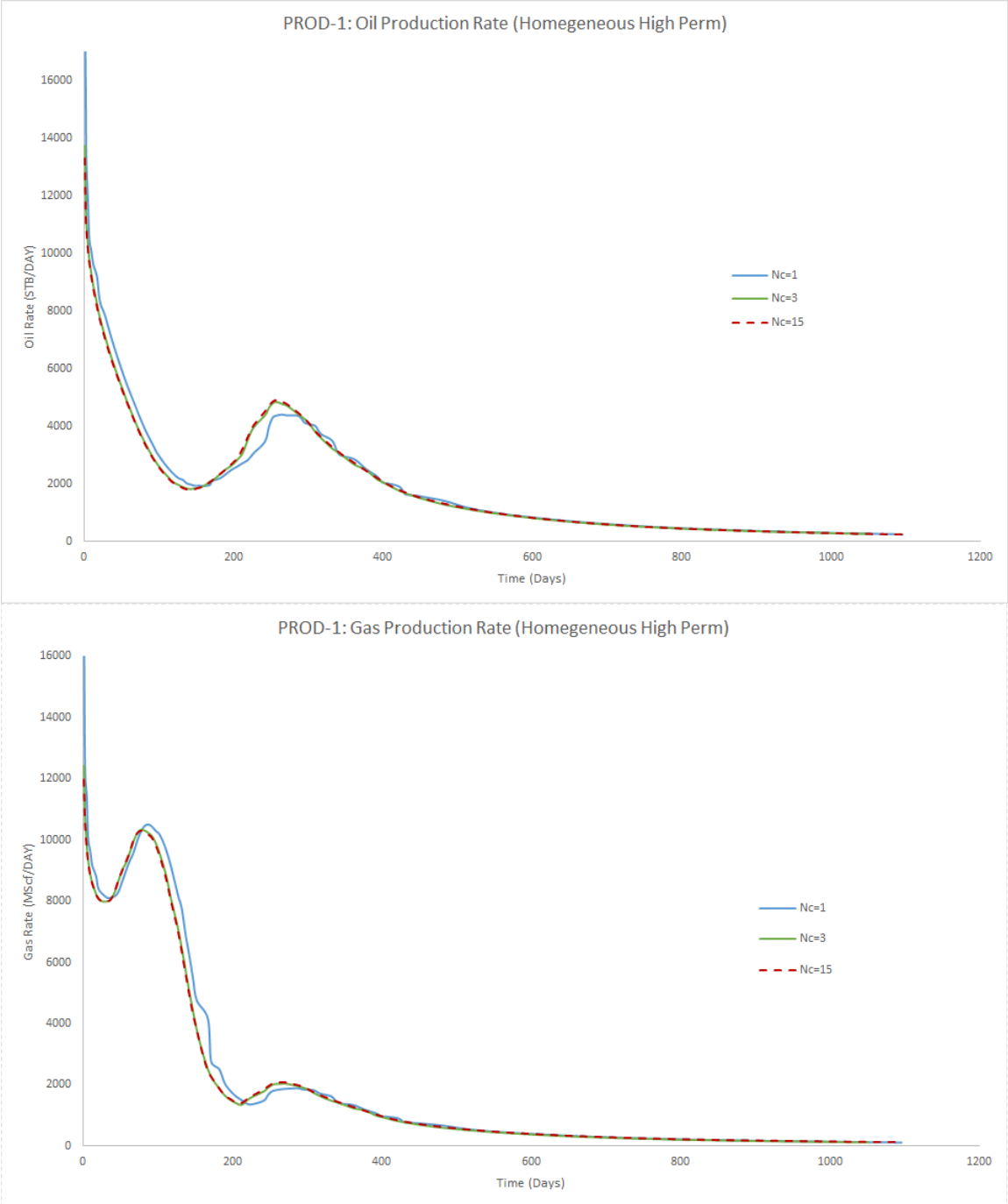

Figure 4.7: Oil and gas production of PROD-1 for Scn-2

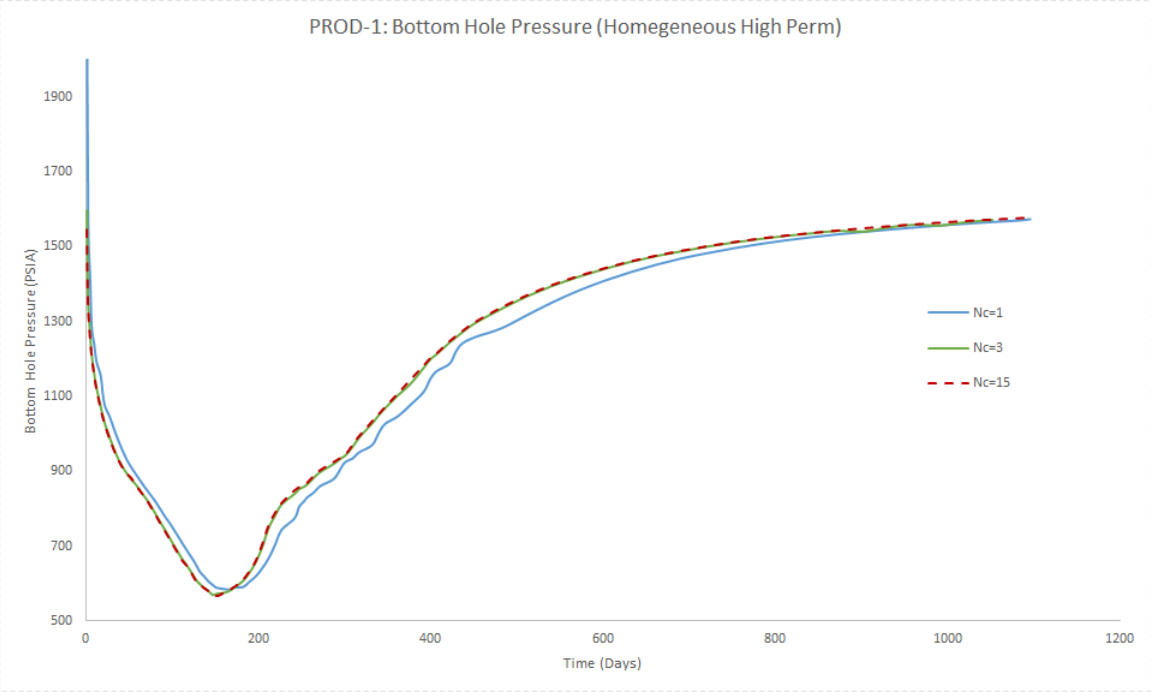

Figure 4.8: Bottom hole pressure of PROD-1 for Scn-2

By observing the results above, we concluded that the difference of production profile between different coupling frequency in high-permeable reservoirs are larger than that in low permeable reservoir, regardless of the oscillation occurred in the case of low-permeable reservoir.

One of the possible reason is that the mobility ratio in high-permeable reservoir is higher than that in the low-permeable reservoir referring to Peaceman's equation (see Equation 2.33). Therefore, the production rate is more sensitive to the change of flowing pressure at bottom hole.

4.3.3 Case study with scenario-3

For the heterogeneous permeability reservoir model, the production profiles of four producers are located at different permeability zone. Referring to Figure 4.3,

it can be observed that PROD-1 is located at the high permeability zone, while the other three producers is placed at the low permeability zones. Similarly to the previous cases, the production profiles for Scenario-3 are shown in Figure 4.9-4.14

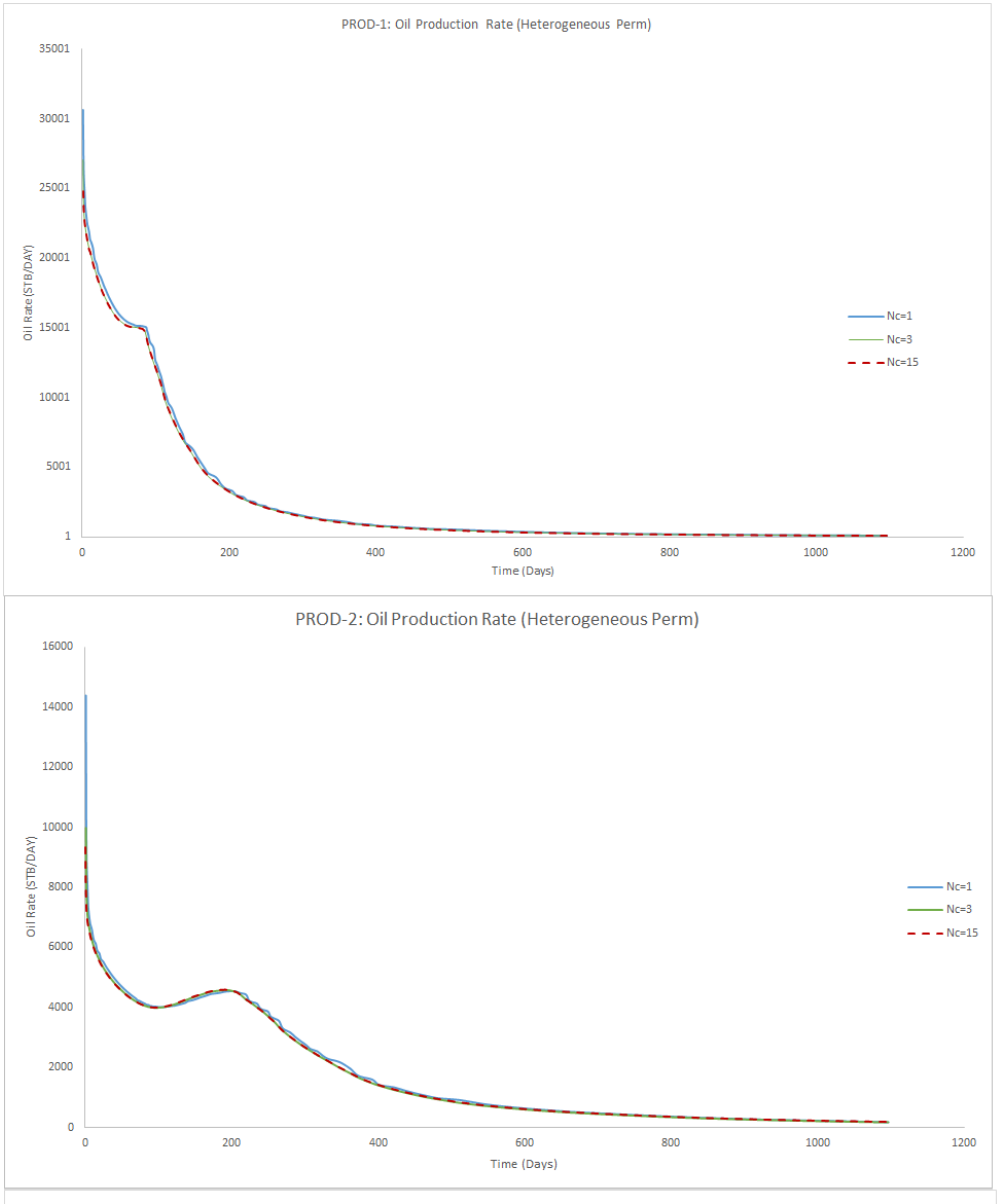

Figure 4.9: Oil production for Scn-3 (PROD-1 and PROD-2)

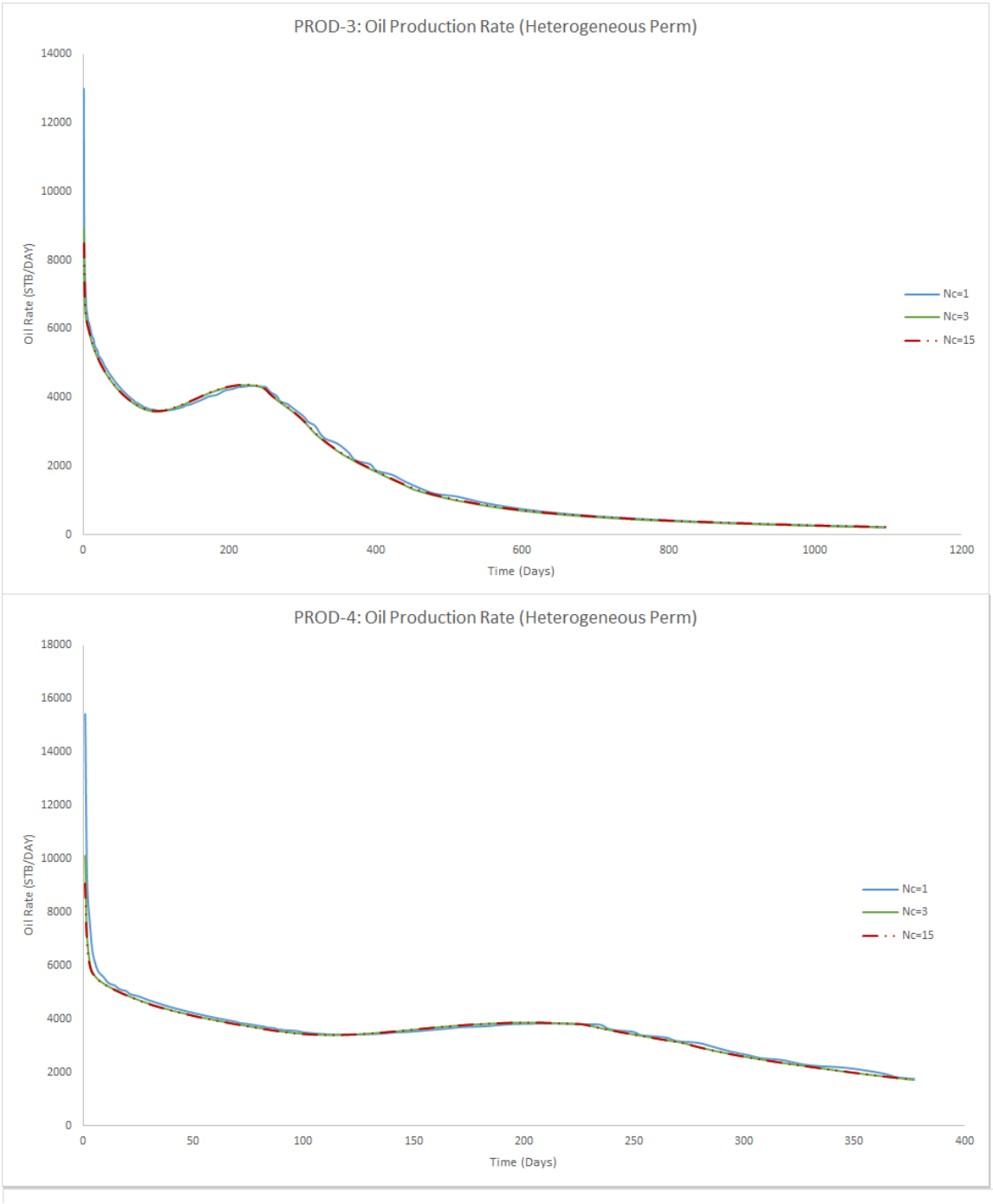

Figure 4.10: Oil production for Scn-3 (PROD-3 and PROD-4)

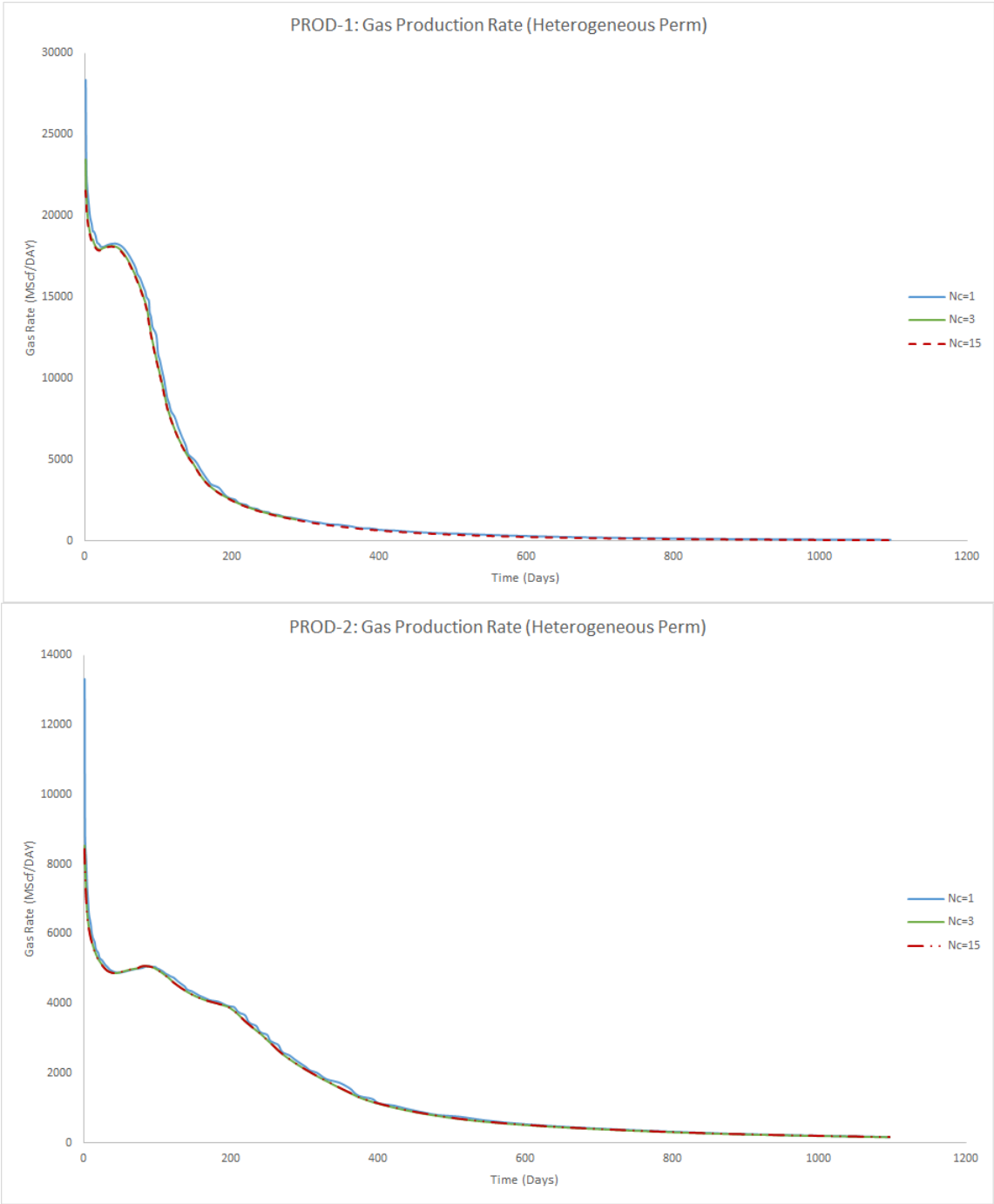

Figure 4.11: Gas production for Scn-3 (PROD-1 and PROD-2)

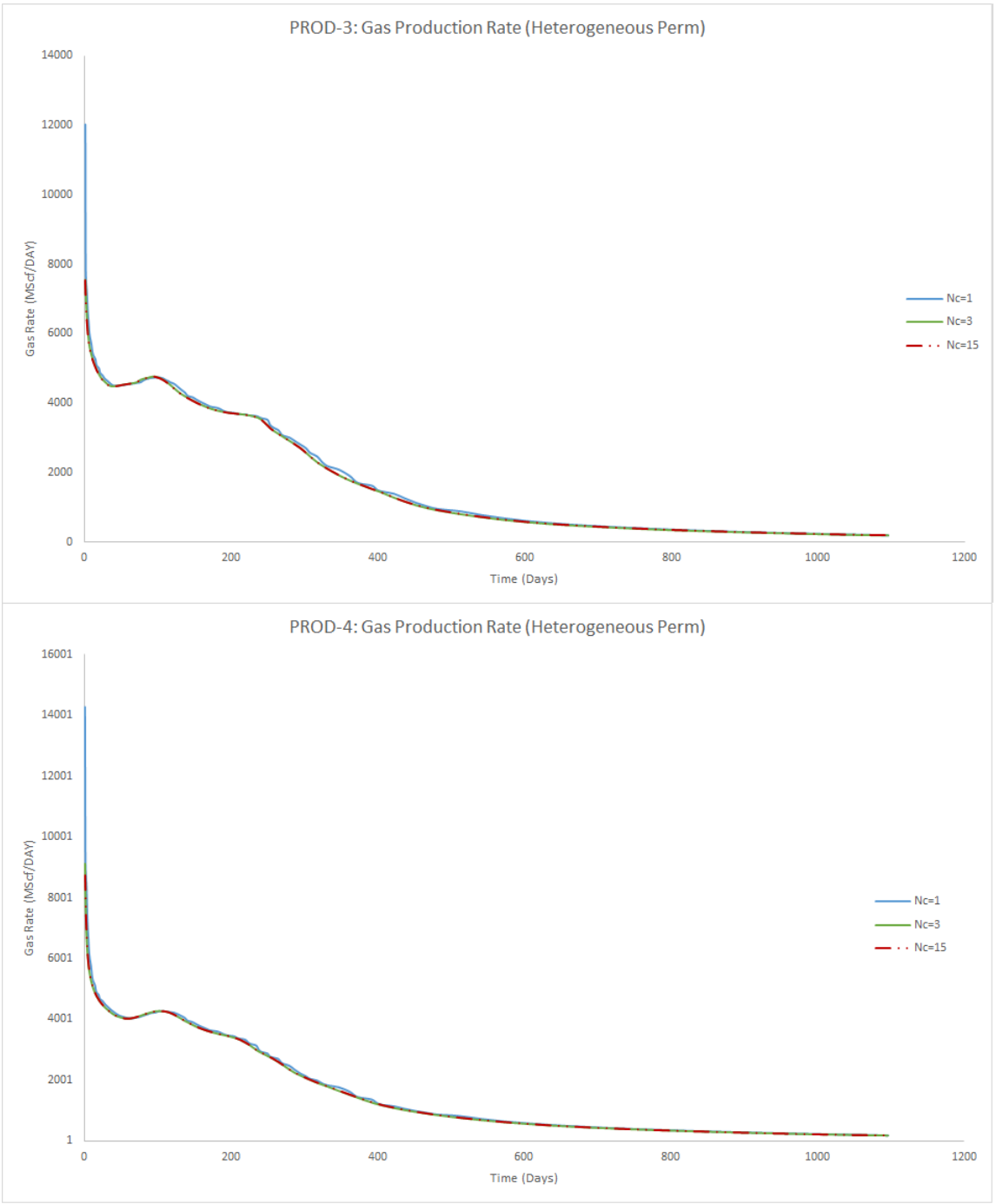

Figure 4.12: Gas production for Scn-3 (PROD-3 and PROD-4)

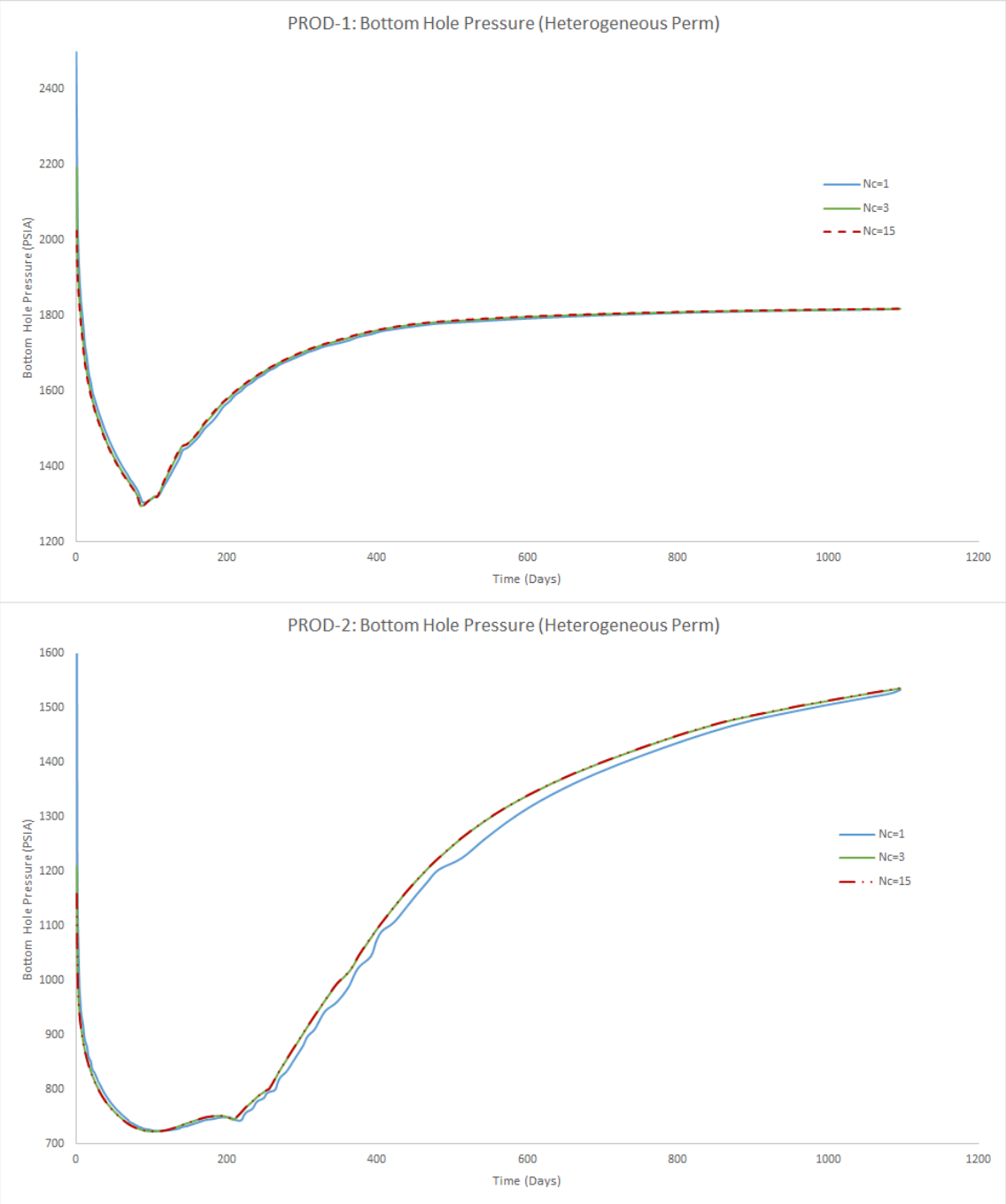

Figure 4.13: Bottom hole pressure for Scn-3 (PROD-1 and PROD-2)

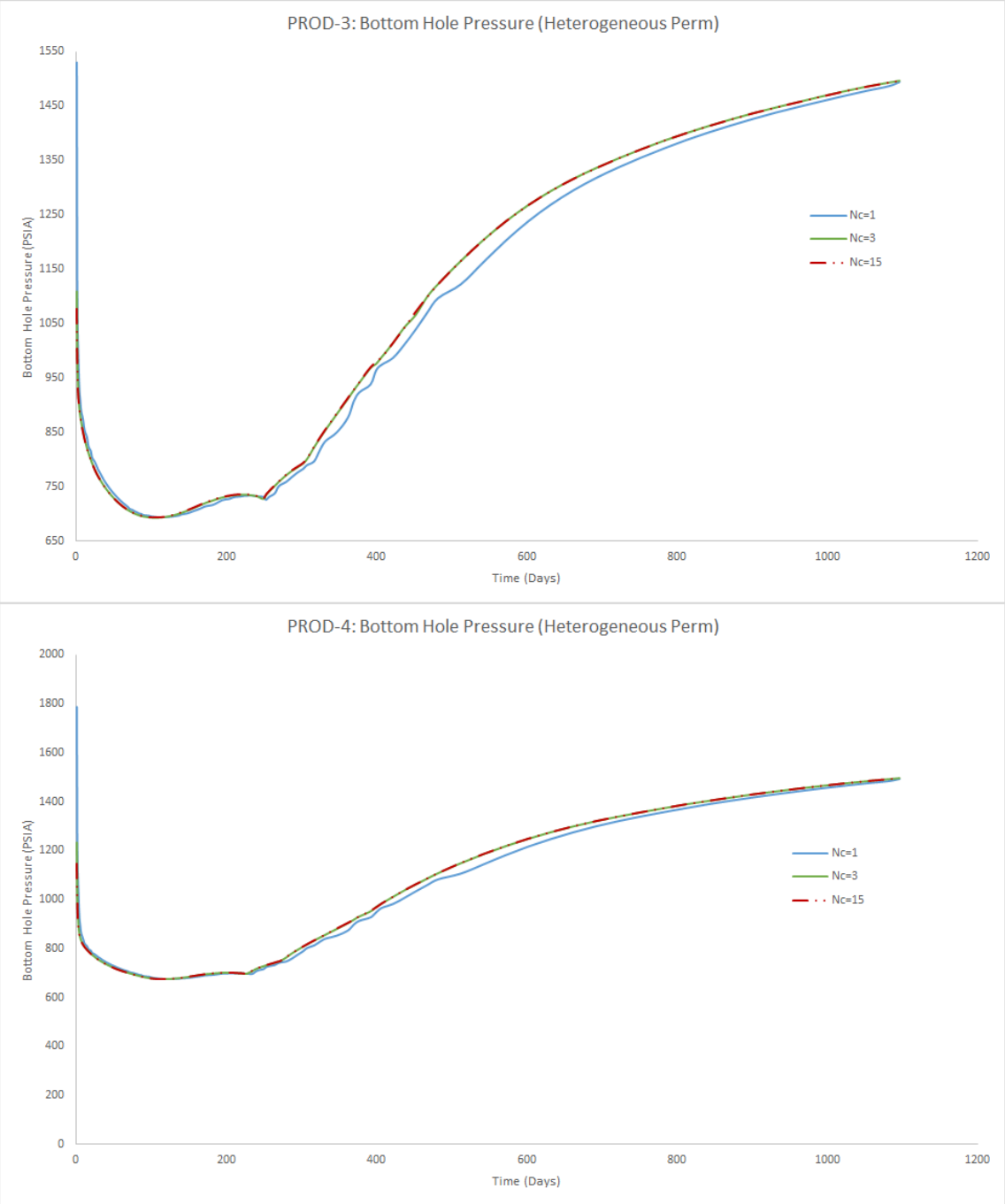

Figure 4.14: Bottom hole pressure for Scn-3 (PROD-3 and PROD-4)

Referring to the results above, it can be seen that the differences in oil and

gas production performance due to the various coupling frequencies are not obvious compared to the production profiles of the homogeneous reservoir. This can be explained as the change of pressure and flow rate in the heterogeneous permeability case is not significant as those in the homogeneous permeability case, therefore, fewer coupling frequency is needed to obtain the accurate parameters at coupling point.

4.3.4 Case study with scenario-4

In general, the permeability of unconventional reservoir is extremely low, which will result in low production rates and relatively stable production behavior.

This case study will investigate the impacts of the coupling frequency on the production performance under unconventional reservoir. The permeability of the unconventional reservoir model ranges from 0.01 to 0.1 mD, and the permeability map is simular to the one of Scn-3. Figure 4.15-4.20 show the production profiles of Scn-4.

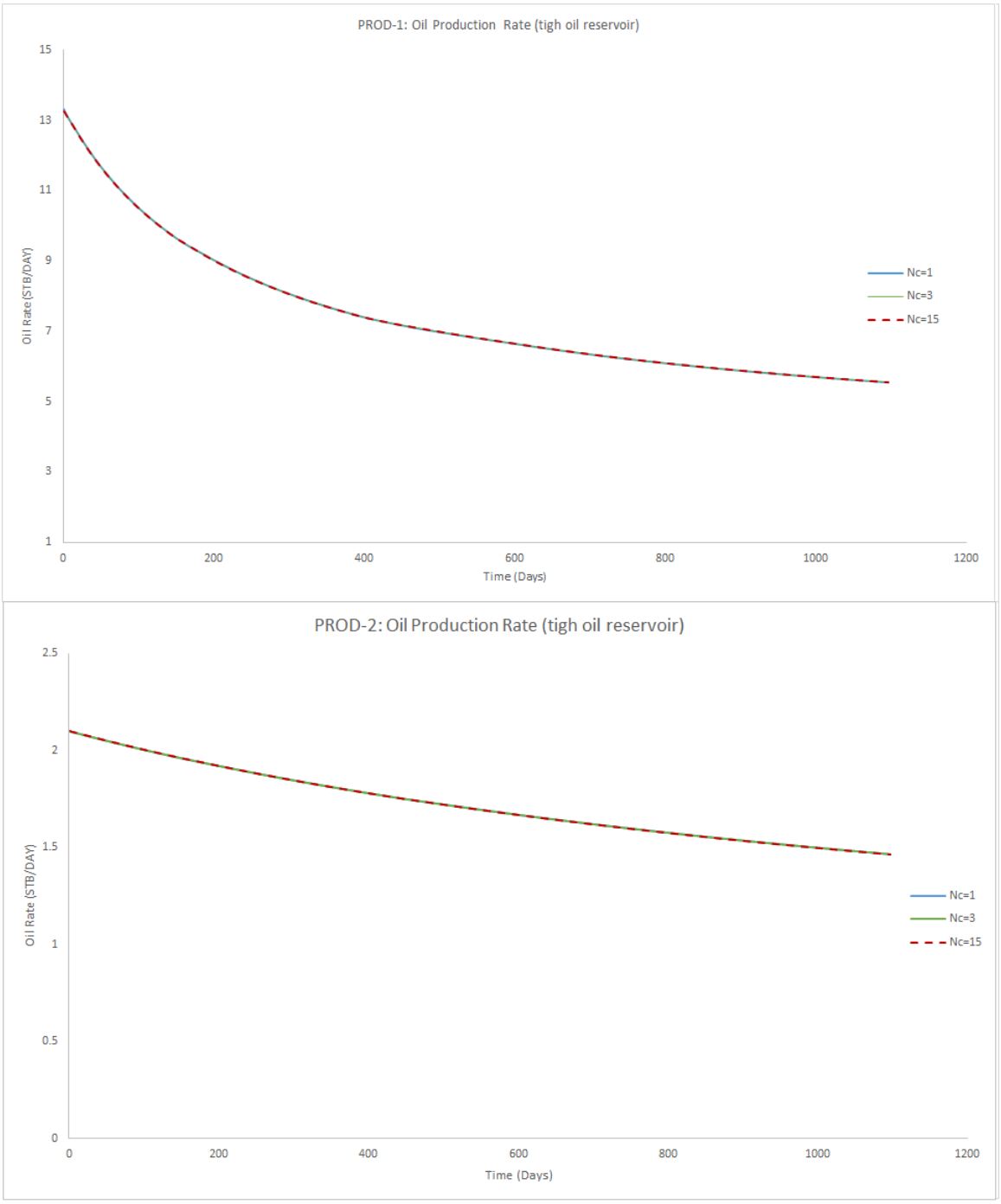

Figure 4.15: Oil production for Scn-4 (PROD-1 and PROD-2)

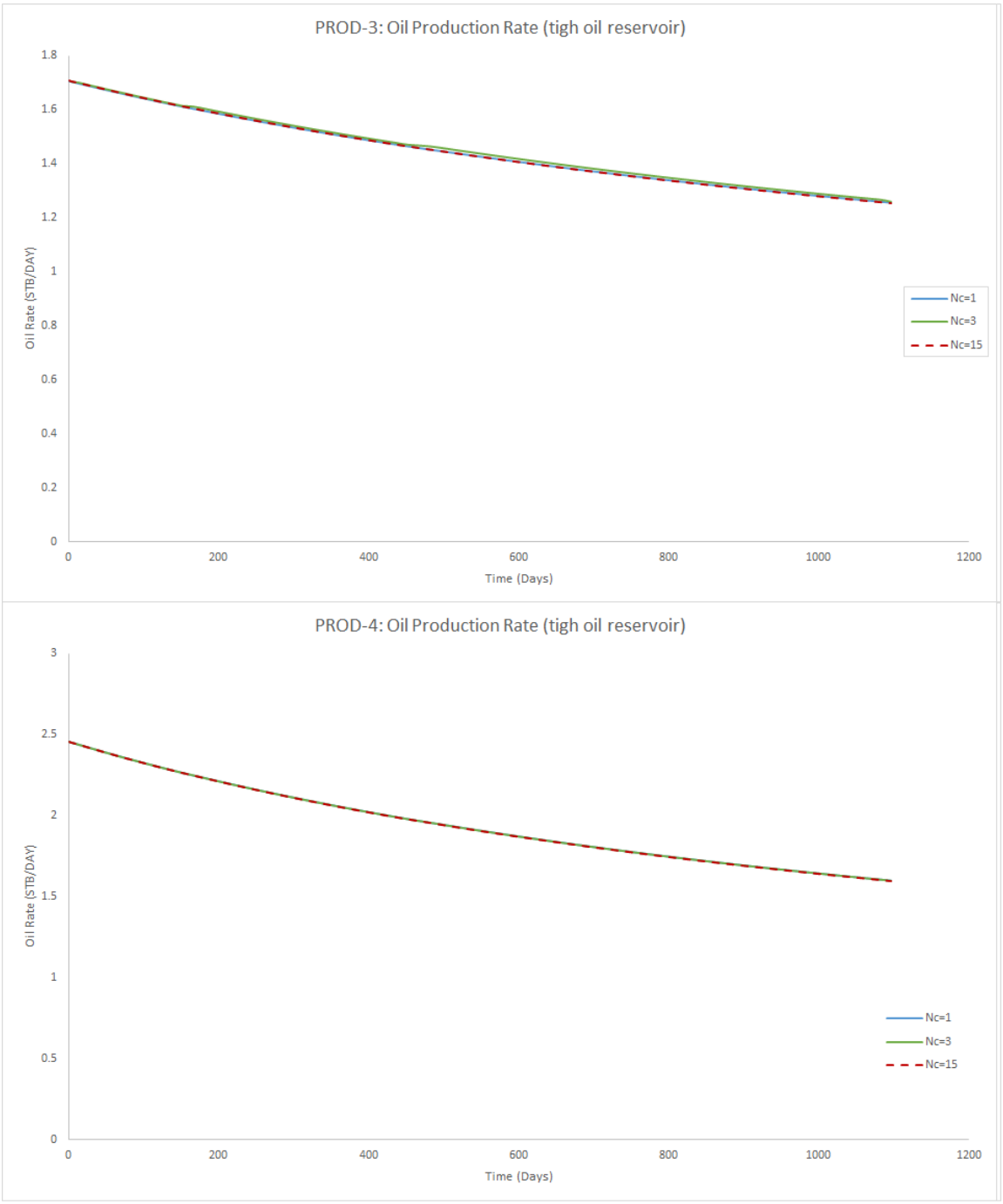

Figure 4.16: Oil production for Scn-4 (PROD-3 and PROD-4)

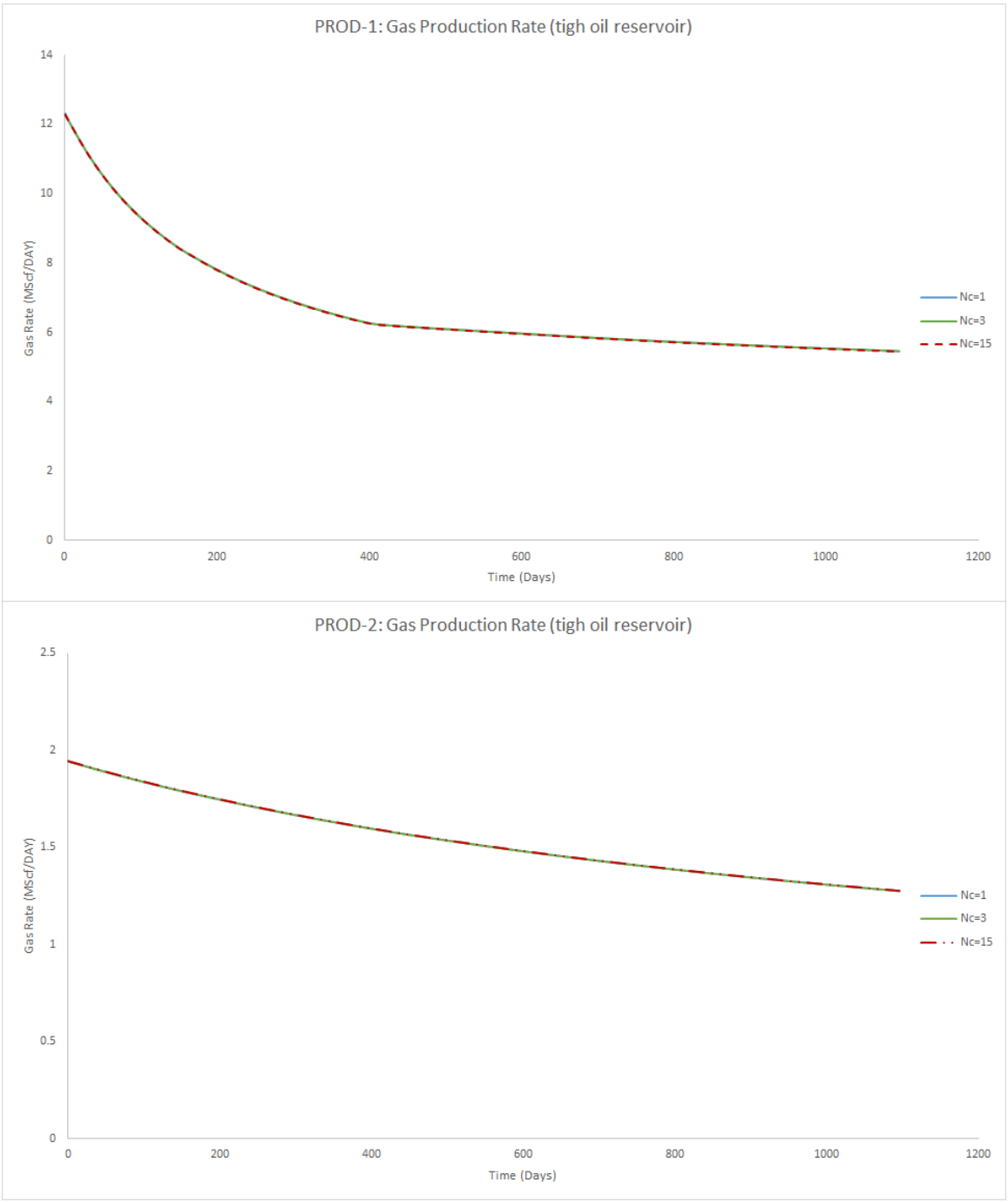

Figure 4.17: Gas production for Scn-4 (PROD-1 and PROD-2)

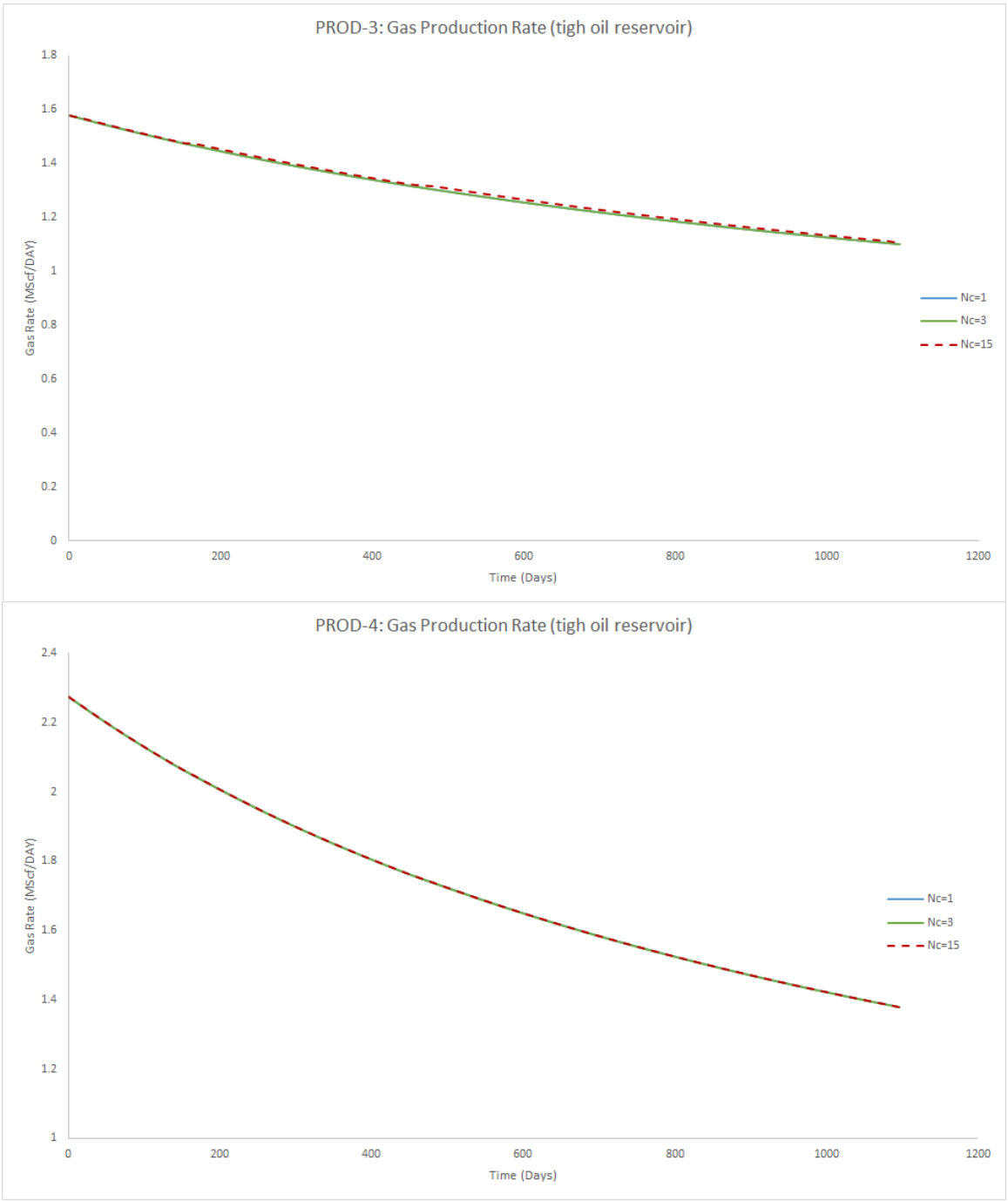

Figure 4.18: Gas production for Scn-4 (PROD-3 and PROD-4)

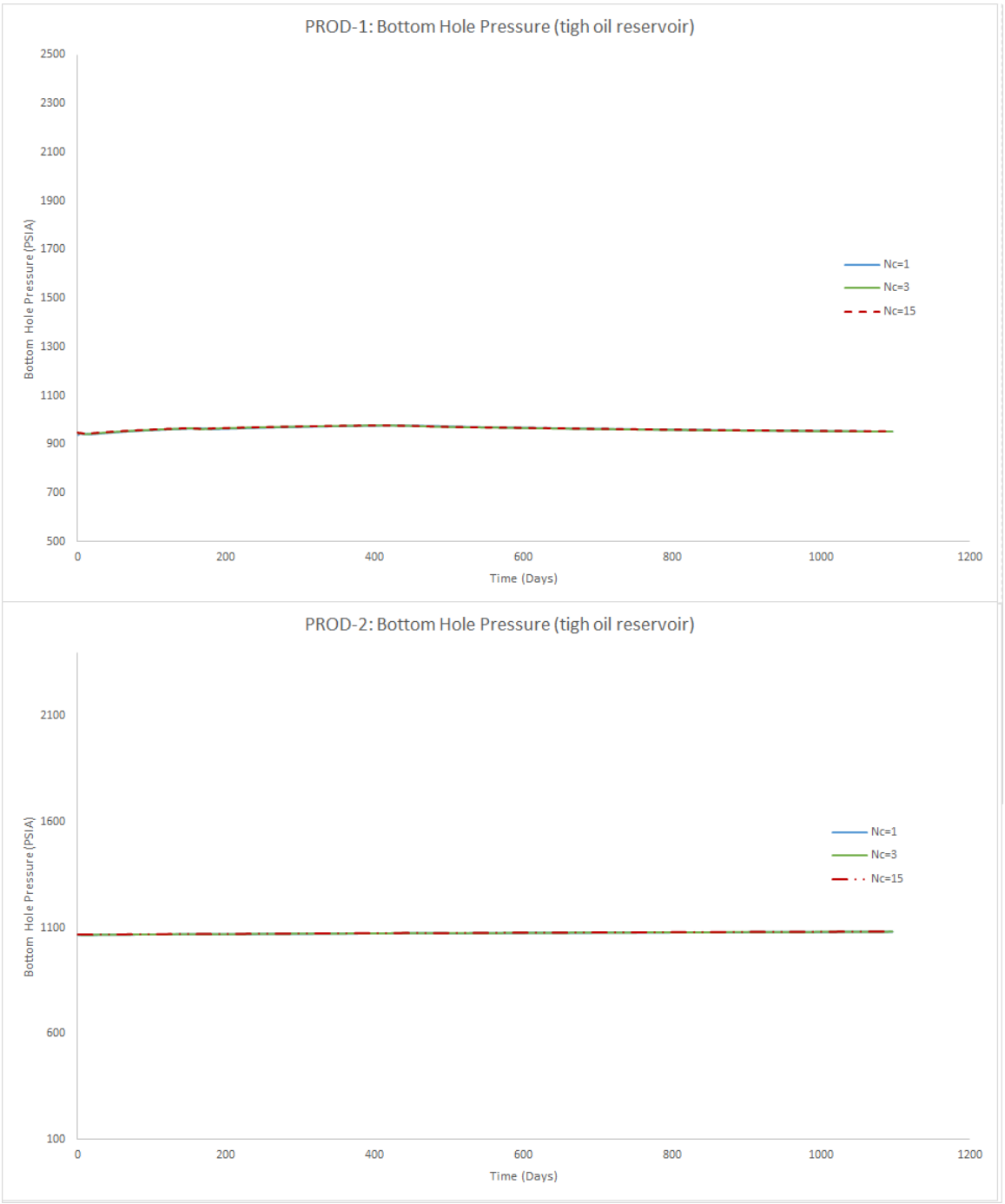

Figure 4.19: Bottom hole pressure for Scn-4 (PROD-1 and PROD-2)

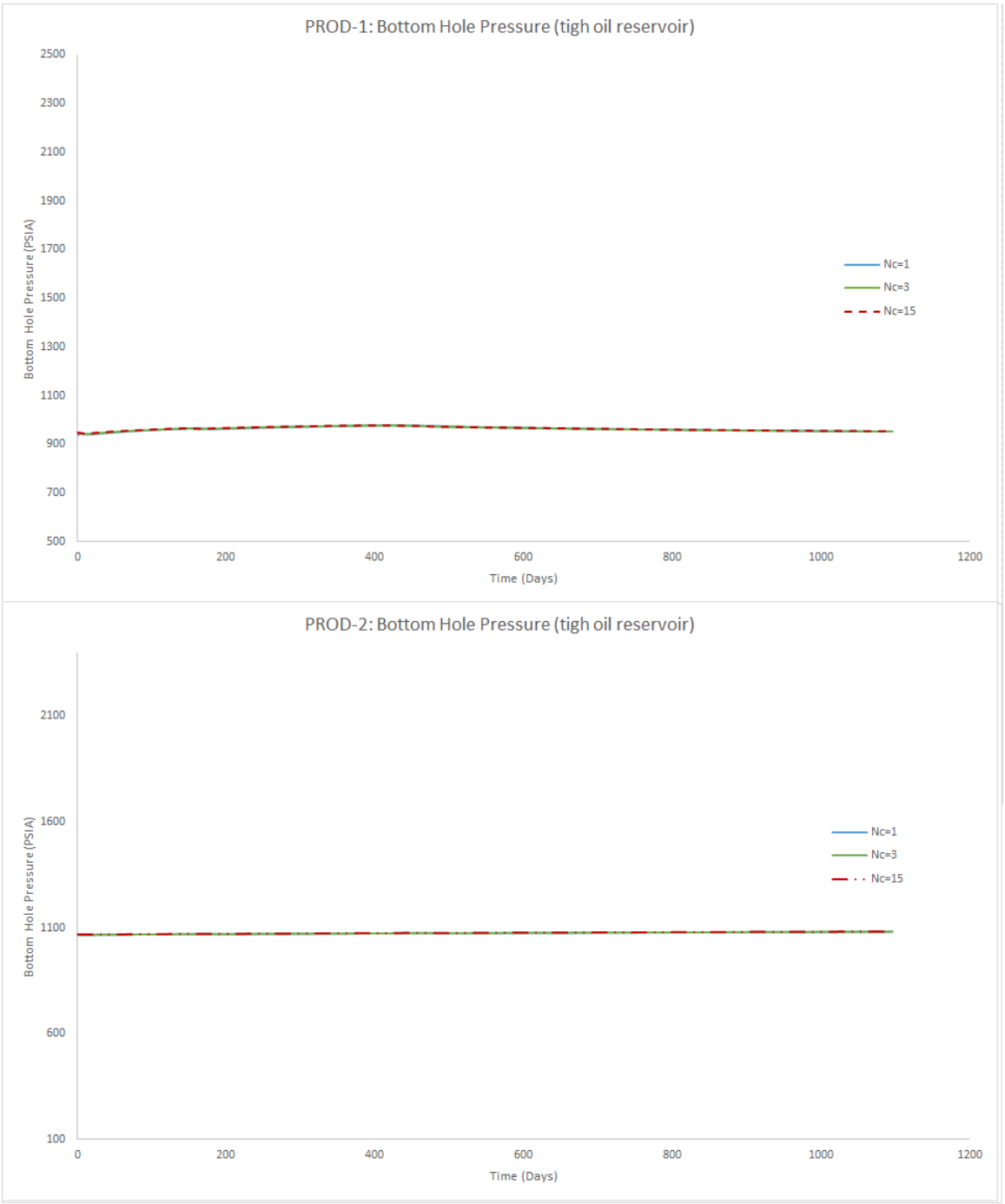

Figure 4.20: Bottom hole pressure for Scn-4 (PROD-3 and PROD-4)

Referring to the results shown above, it can be seen that the oil/gas production rates from tight oil reservoir is very low, and there is no obvious drop in production rate. This can imply that the reservoir pressure is kept almost constant during the production. Since there is no significant variations of production profiles in time, the Filed-Management needed low coupling frequency to complete the coupling/balance action. Therefore, the differences in production profiles under different coupling frequency are not obvious. It can be concluded that the tight oil reservoir is not sensitive to the coupling frequency.

4.4 Sensitivity Study and Summary

In this section, we investigated the impacts of various coupling frequencies on the production profiles under different descriptions of reservoir models. The quantified change in cumulative production due to various coupling frequency is analyzed in this section.

Since the total production differs for different descriptions of reservoir model, it is difficult to compare the their changes directly. Therefore, we used the Dimensionless recovery (N_{DP}) to observe the changes of production for different coupling frequency and different reservoir model. The Dimensionless recovery is defined as the ratio of total production of all phases obtained with different coupling frequencies to the total recovery obtained with the coupling frequency of 15 in percentage form:

$$N_{Dp} = \frac{N_{p_i}}{N_{p15}} \tag{4.1}$$

where, the subscript i indicates the coupling frequency (Nc), which equals to 1, 3 and 15 in this study.

Figure 4.17-4.20 show the Dimensionless Recovery (N_{Dp}) in different scenarios.

The x-axis represents the different coupling frequency. The green and red color represent oil and gas phase, respectively. Referring to the equation (4.1), the dimensionless recovery of Nc=15 equals to 1, and a larger difference shown in certain phase indicates that this phase is more sensitive to the change of coupling frequency.

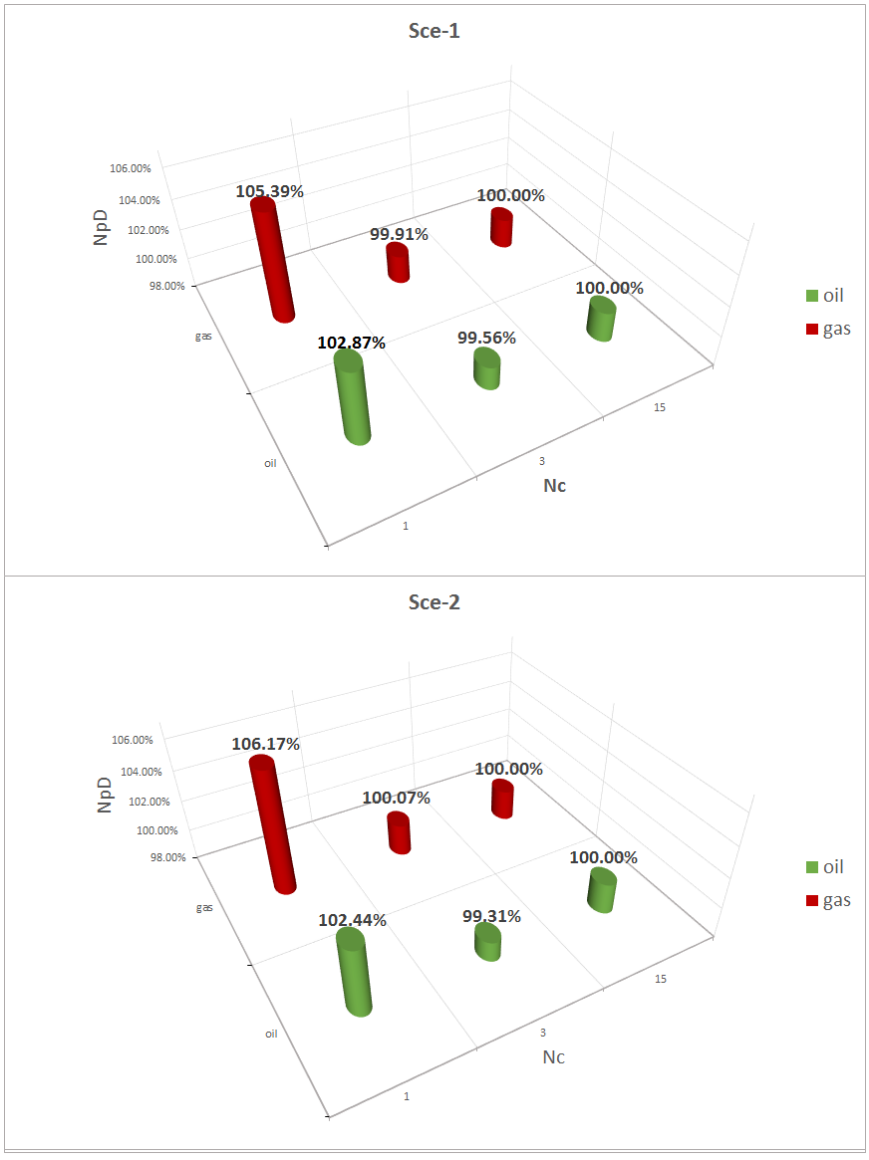

Figure 4.21: N_{Dp} of oil and gas for Scn-1 and Scn-2

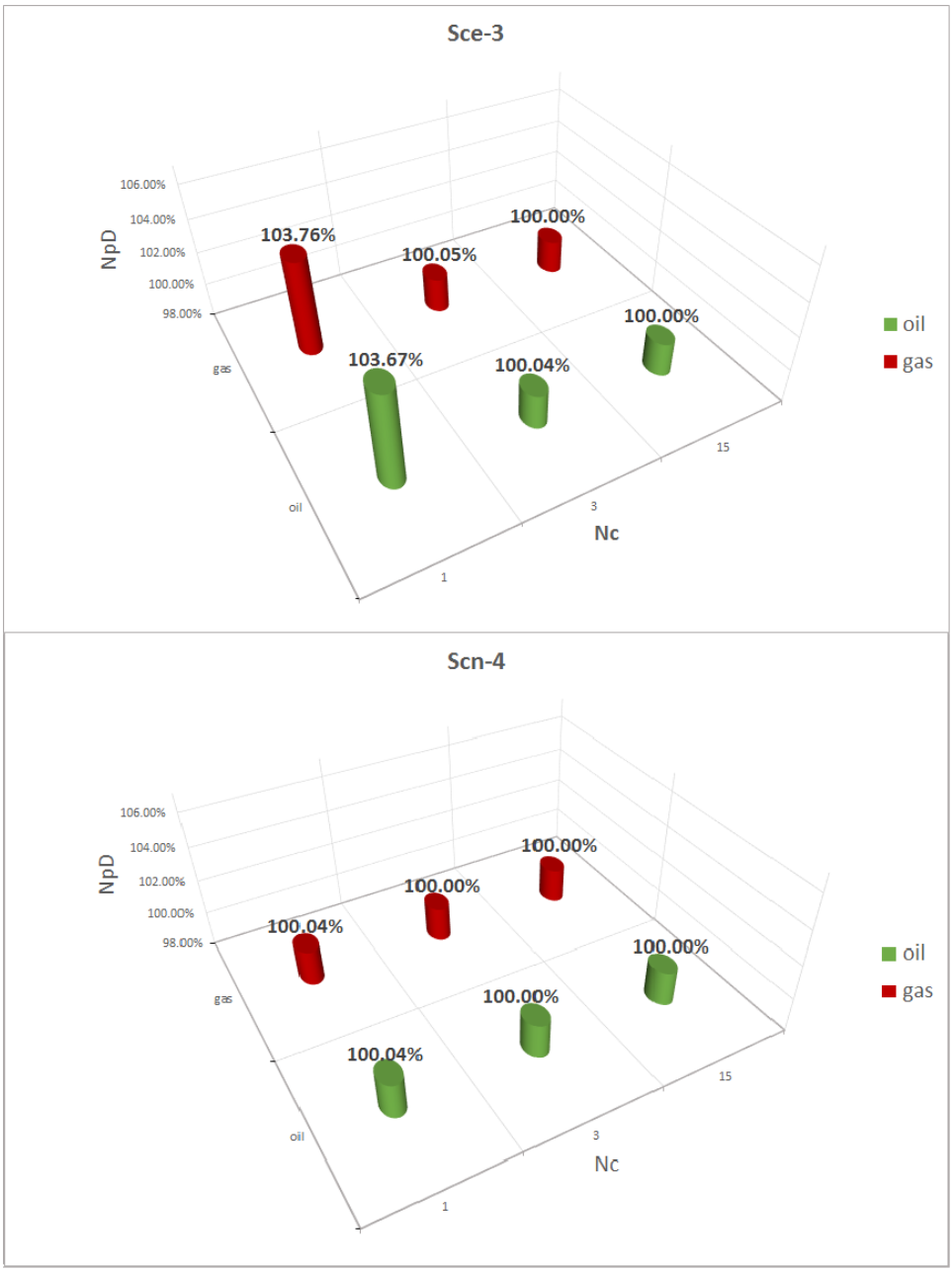

Figure 4.22: N_{Dp} of oil and gas for Scn-3 and Scn-4

Based on the sensitivity study above, we come up to the following summary:

- When the partially implicit coupling frequency is set to 3 and 15, the difference

in production profile due the the change of coupling frequency is less obvious, implying that the surface and subsurface models can be balanced completely within the first 3 Newton iterations of simulation timestep. That is why there is no significant difference when using $N_c = 3$ or 15. Therefore, it can be concluded that the results from $N_c = 3$ and 15 are accurate.

- When comparing the results from low and high homogeneous permeability reservoir, it showed that the coupling frequency has more effects on the production profiles in high homogeneous permeability reservoir due to the high mobility ratios of phases.

- By comparing Scn-3 to Scn-1 and Scn-2. it can be seen that the heterogeneous permeability reservoir is more sensitive to the coupling frequency than homogeneous permeability reservoir.

- From the study of Scn-4, we found that the variation of production behavior in time is not obvious in unconventional reservoir, therefore the coupling/balance can be accomplished by using low coupling frequency. It can be concluded that the production performance from tight oil reservoir is less sensitive to the coupling frequency, comparing to other types of reservoirs.

5. EFFECT OF THE SURFACE NETWORK ELEMENTS ON PRODUCTION PERFORMANCE

in previous chapter, the surface and subsurface model are coupled with the INTERSECT Field Management tool. However, the assessment with the commercial tool showed some of the drawbacks of the partial coupling method: the accuracy of the coupled model highly depends on the implicit coupling frequency; Also, the injection network is not supported in the Field Management system, these drawbacks makes it fail to investigate the effect of the entire surface facilities. In order to overcome these issues, in this work we will develop a fully coupled model by modifying an open source reservoir simulator called MRST, which is developed by Lie, et al.[26]. In this chapter, the modifications made in MRST will be explained; and the effect of the coupled surface network on production performance will be investigated with modified fully implicit coupled model.

5.1 Modification of MATLAB® Reservoir Simulation Toolbox (MRST)

In this project, the MATLAB® Reservoir Simulation Toolbox (MRST) is modified in order to construct the fully coupled model. MRST is an open source simulator within the MATLAB environment, which is based on advanced coding language for numerical computing. MRST toolbox consists of two main parts: a core offering basic functionality (i.e. pressure and transport solver for single and two-phase flow, etc.) and a set of add-on modules (fully implicit black-oil solver, the implicit pressure and explicit saturation solver, etc).

Since the reservoir model used in this study is a black-oil model, the fully implicit black-oil solver module of MRST is modified in our study. As discussed in

previous chapter, the governing equations of the fully coupled model are non-linear, which requires the Newton Raphson method to linearize the residuals of the governing equations and generate the Jacobian matrix. Usually, the Jacobian matrix of residuals is calculated with finite difference approximation, this approach is the prone to unstable solution and oscillation. In this case, the functionality of automatic differentiation implementation (ADI) is employed in our fully implicit solver routines.

5.1.1 Modification of MRST for fully implicit coupling

The main tasks of routines in MRST can be classified in three broad classes: (1) routines for reading and pre-processing ECLIPSE input *data*. file; (2) fully implicit solver routines; (3) routines for process the solutions from simulation run, Figure 5.1 shows the procedure of the original MRST simulation work. The modification for fully coupling mainly focuses on the first two parts, which enables the MRST black-oil fully implicit solver to read the surface network input file and solve the coupled surface and subsurface system equations. Figure 5.2 shows the procedure of the modified MRST fully implicit solver; the orange color indicates the routines where the modifications are developed.

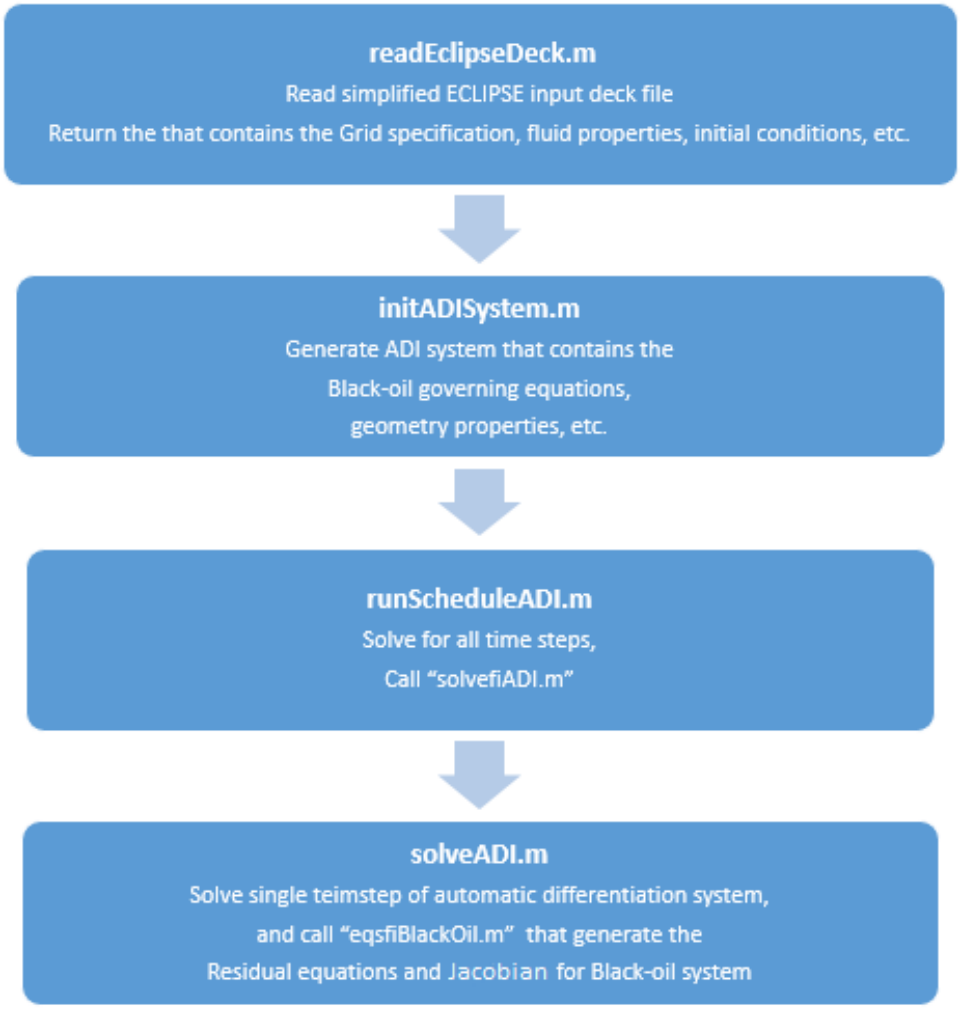

Figure 5.1: General procedure of MRST fully implicit black-oil solver

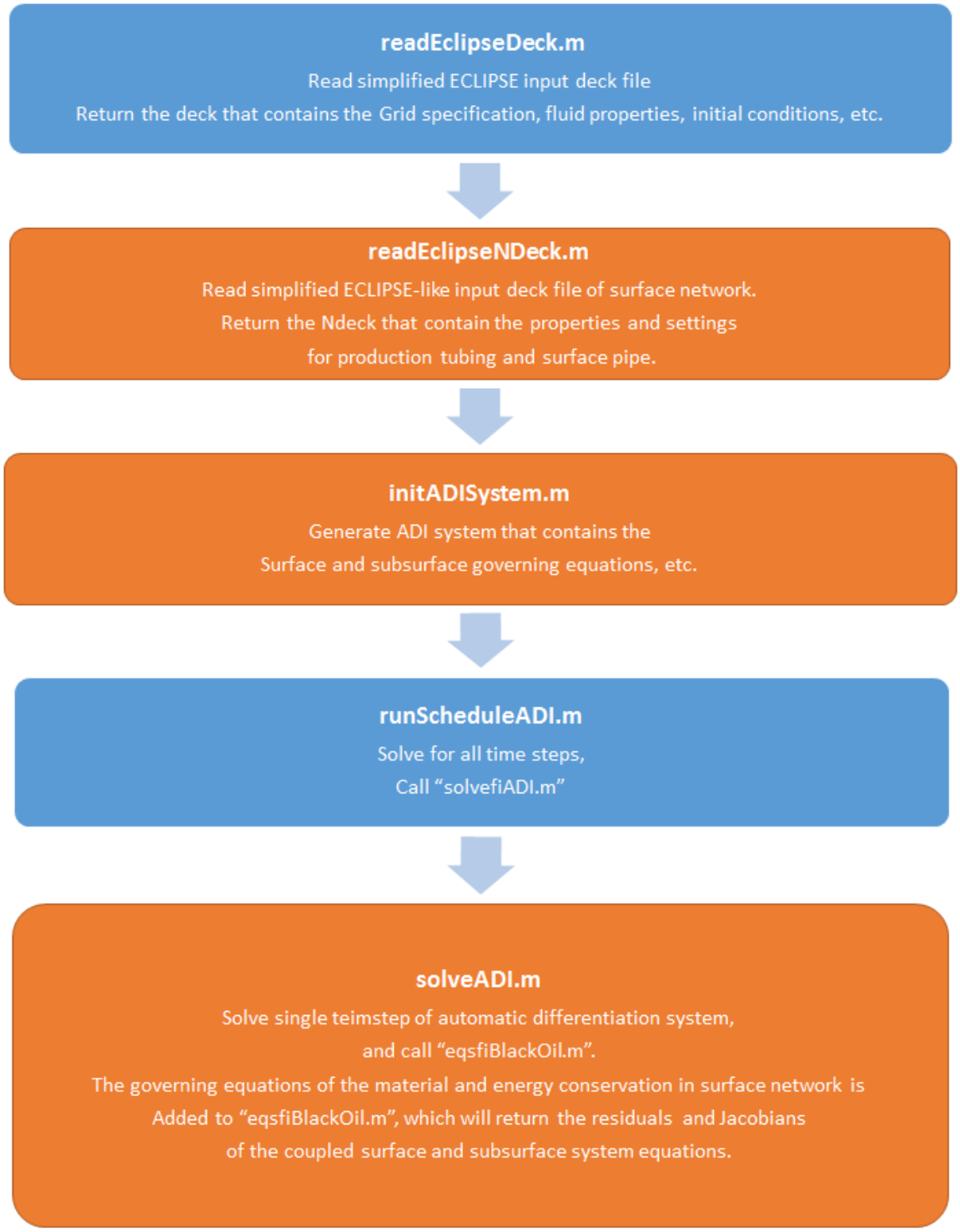

Figure 5.2: General procedure of modified MRST fully implicit solver for coupled model

The main task of the modification is to add the governing equations of the surface system to the "eqsfiBlackOil.m" routine, where the residual ($R(U)$, U is the unknown vectors) and Jacobian matrix, J (see Figure 5.3) of coupled surface/subsurface equations are calculated based on the Eqs 3.1-3.16. The solution of the coupled equations can be calculated by using Newton-Raphson method. In our simulator, the solution will be obtained when

$$R(U) = 0$$

Referring to Section 3.2.2, we have

$$J\delta = -R,$$
$$\delta = J^{-1}(-R)$$

In our simulator, the δ is solved by using "\" in MATLAB, which represents a direct solver. The Jacobian matrix is calculated with *Automatic Differential* (AD). In the conventional approach, the Jacobian is calculated with finite difference method, which will result in inaccuracy or truncation errors if inappropriate perturbation is applied; These issues can be overcome by using the AD method, since the AD is able to calculate the exact Jacobian through a semi-analogical approach.

The updated unknown vector (U_{n+1}) can be calculated with:

$$U_{n+1} = U_n + \delta$$

This fashion will be repeated until the norms of all the residual equations smaller than the toleration.

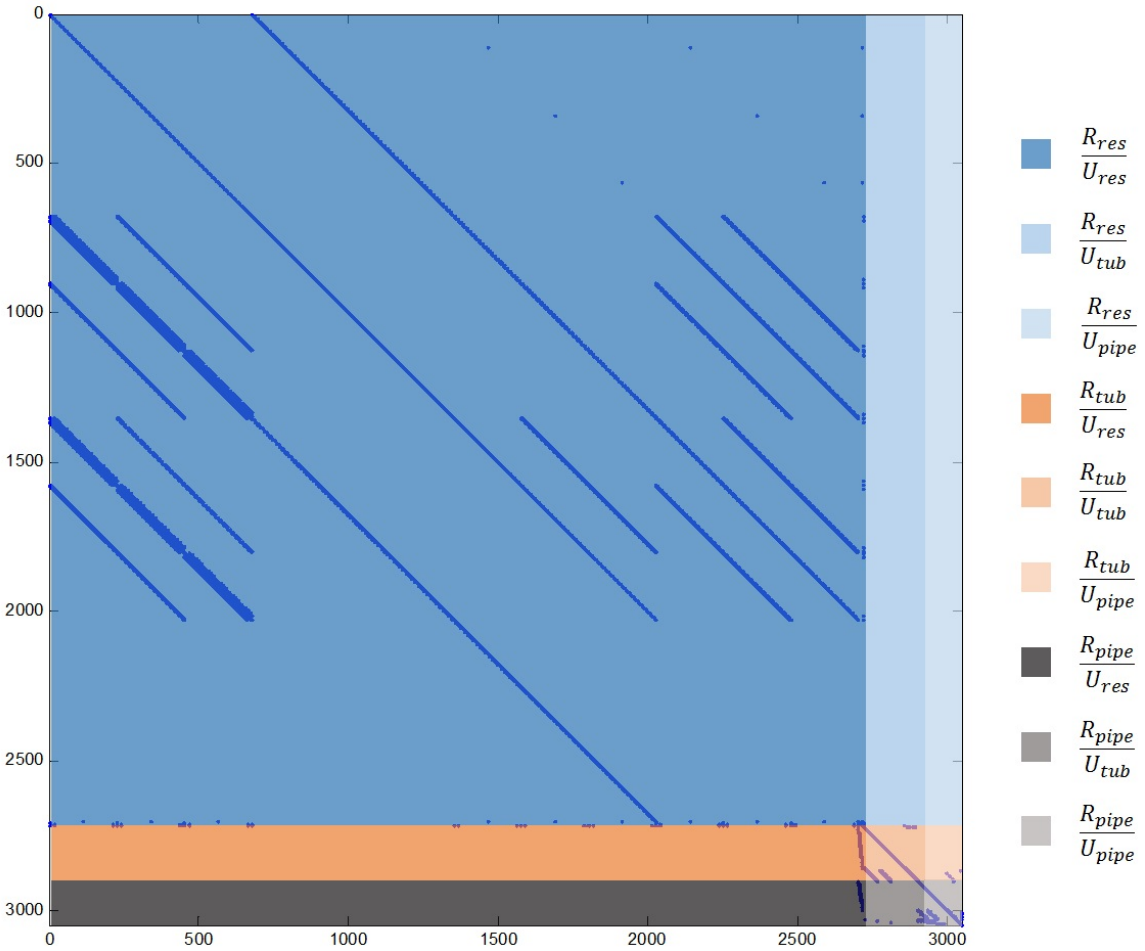

Figure 5.3: Jacobian matrix of fully coupled model

5.2 Validation Test of the Modified MRST Fully Coupled Model

Prior to the investigation with fully implicit model, the validation of the fully coupled model is tested. This section focuses on checking the consistencies between the modified MRST and INTERSECT Field Management (IX). Since the injection network is currently not supported within INTERSECT Field Management, the injection system is decoupled in the modified MRST fully coupled model for comparison. Both commercial and our coupled models are performed under the same

reservoir conditions and production strategy. The coupled model used for validation test is the Scenario-3, which is used in the chapter 4.

The comparison of the production results from modified MRST fully coupled model and INTERSECT Field Management system is shown Figure 5.4-5.7. The 5-spot water-flooding pattern is used in study case. Since the PROD-1 has higher production rate, the results of PROD-1 is separated from the results of other producers. The dash lines represent the results obtain from INTERSECT Field Management, where the coupling frequency (N_c) is set to 15; while the solid lines represent the results from modified MRST fully implicit coupled model.

Referring to the compared results displayed, the bottom hole pressure profiles show a difference after the water is produced. This can be explained as that emulsion effect is considered for oil-water mixture in PIPESIM, which will result in a higher viscosity when water cut ranges between 30% and 50%. Therefore, the pressure loss due to the friction is higher when consider emulsion effect.

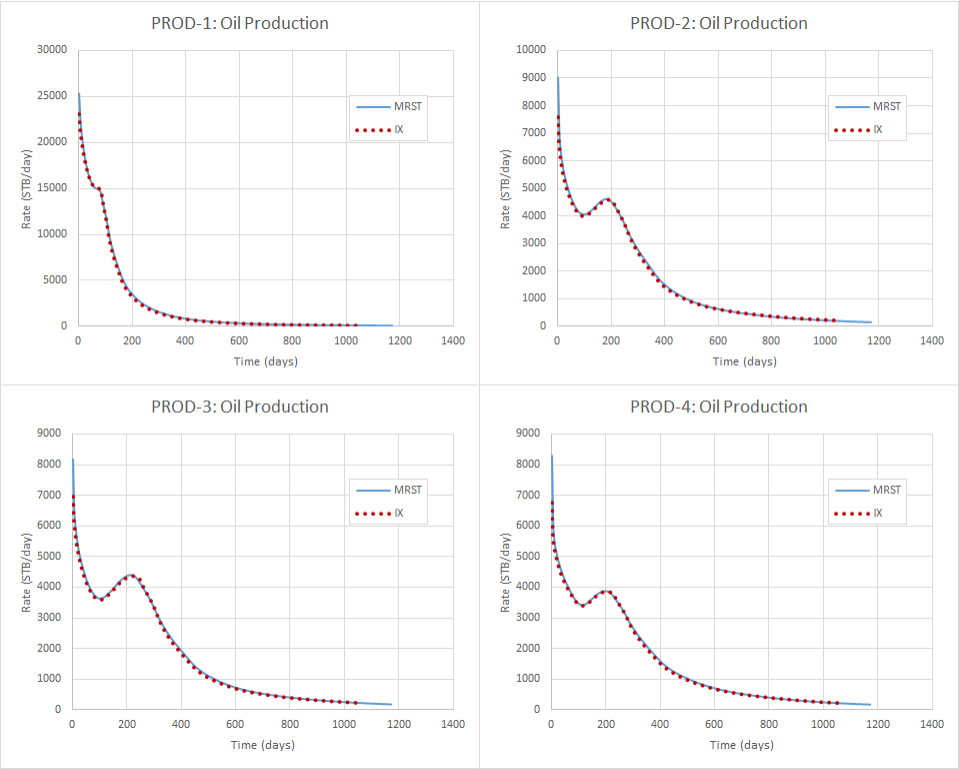

Figure 5.4: Comparison of oil production rates from modified MRST and INTERSECT field management

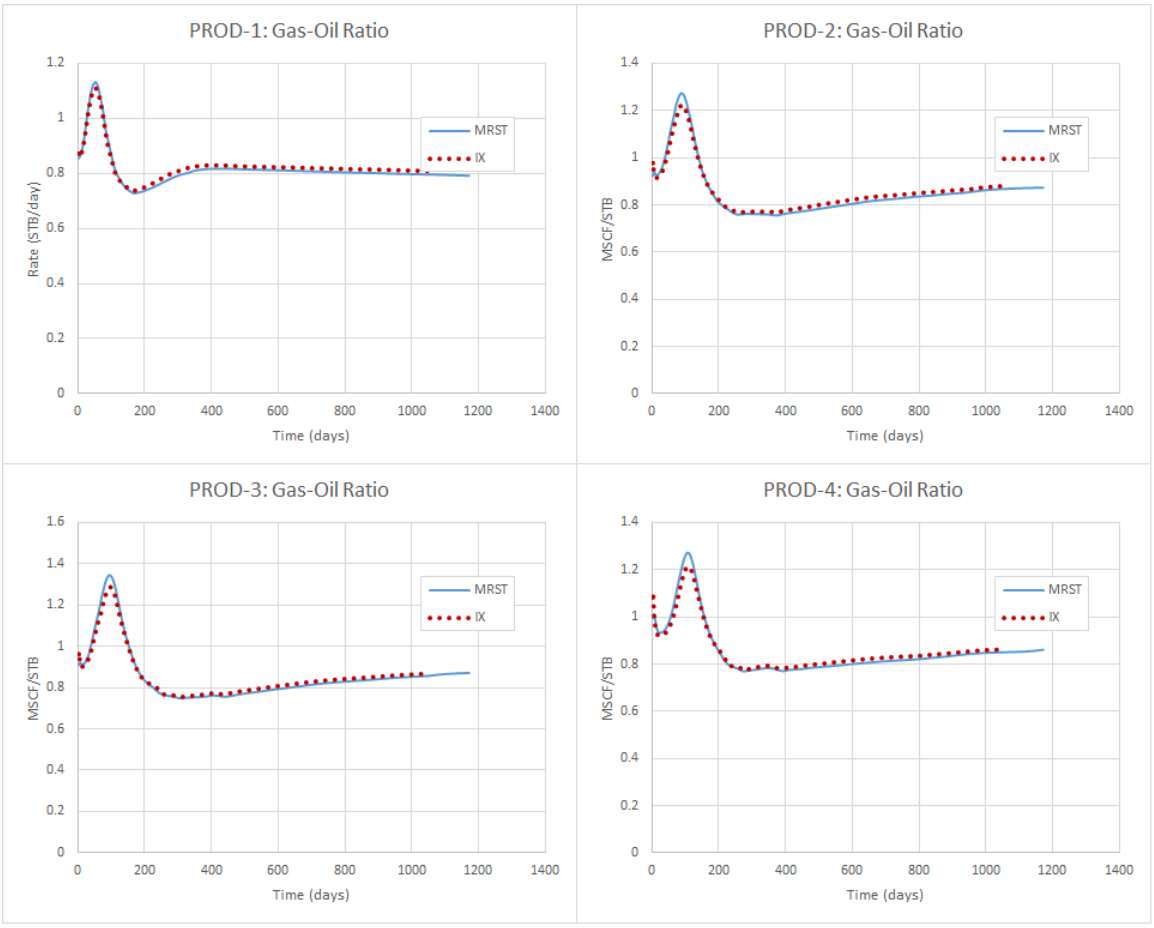

Figure 5.5: Comparison of gas-oil ratio from modified MRST and INTERSECT field management

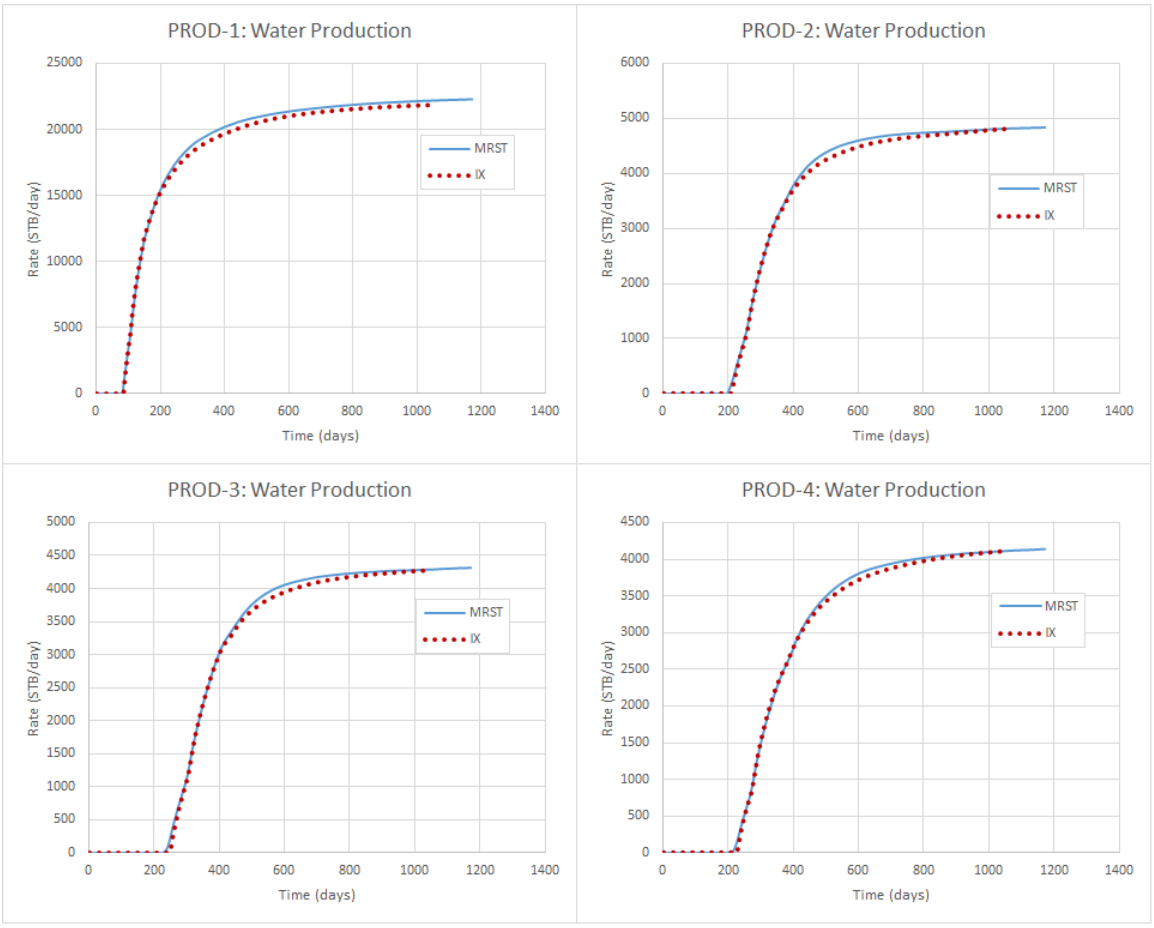

Figure 5.6: Comparison of water production rates from modified MRST and INTERSECT field management

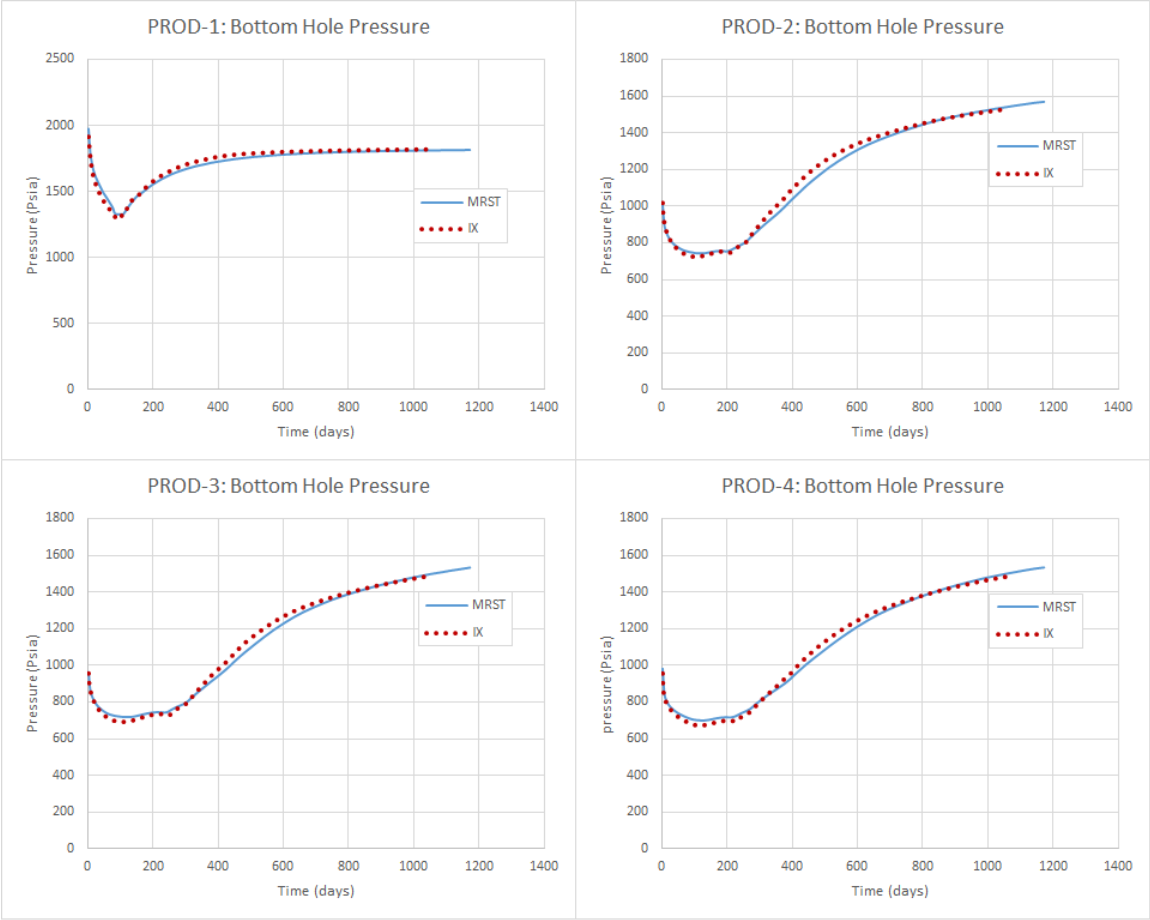

Figure 5.7: Comparison of bottom hole pressure from modified MRST and INTERSECT field management

By observing the Gas-oil ratio (GOR) and BHP profiles, it can be found that the BHP of producers decreases while GOR is increasing, this is because that the increasing GOR indicates the existence of free gas within reservoir and tubings, and the free gas will reduce the average density of the mixture within the tubing, and consequently reduce pressure loss caused by potential energy. Thus, the decreasing BHP can be observed when GOR is increasing. When water breakthrough occurred, the invasion water will again increase the wellbore fluid density,and consequently

increase BHP can be observed after water breakthrough.

5.3 The Effect of Coupled Surface Model on Production Performance

This section aims on investigating the impacts of different settings within the surface network on production performance. The discussion of the impacts can be used to improve the field management and operation strategies.

In this section, the reservoir model of Scenario-3 will be used. The surface network model includes one injection well and four production wells. For injection system, the boundary is located at the wellhead, while the production system is terminated at separator. The production strategy and properties of the base surface network model are displayed in Table 5.1.

Table 5.1: Production strategy and properties of the surface network model

Production/injection system settings	Value	Unit
Production/injection Tubing ID	3	in
production/injection Tubing Length	3005	ft
Production Pipe ID	3	in
Production Pipe Length	1000	ft
Downstream pressure	300	psia
Upstream pressure (at bottom hole)	2700	psia
Roughness	0.001	

5.3.1 Effects of tubing size

This study will discuss the effect of tubing size on pressure loss and production performance. Four cases are performed in this study, different production tubing/pipe sizes are used. The are 1.5", 2", 2.5" and 3" respectively. The Injection and production profiles are displayed in Figure 5.8-5.16, each color represent the result obtained with each tubing size.

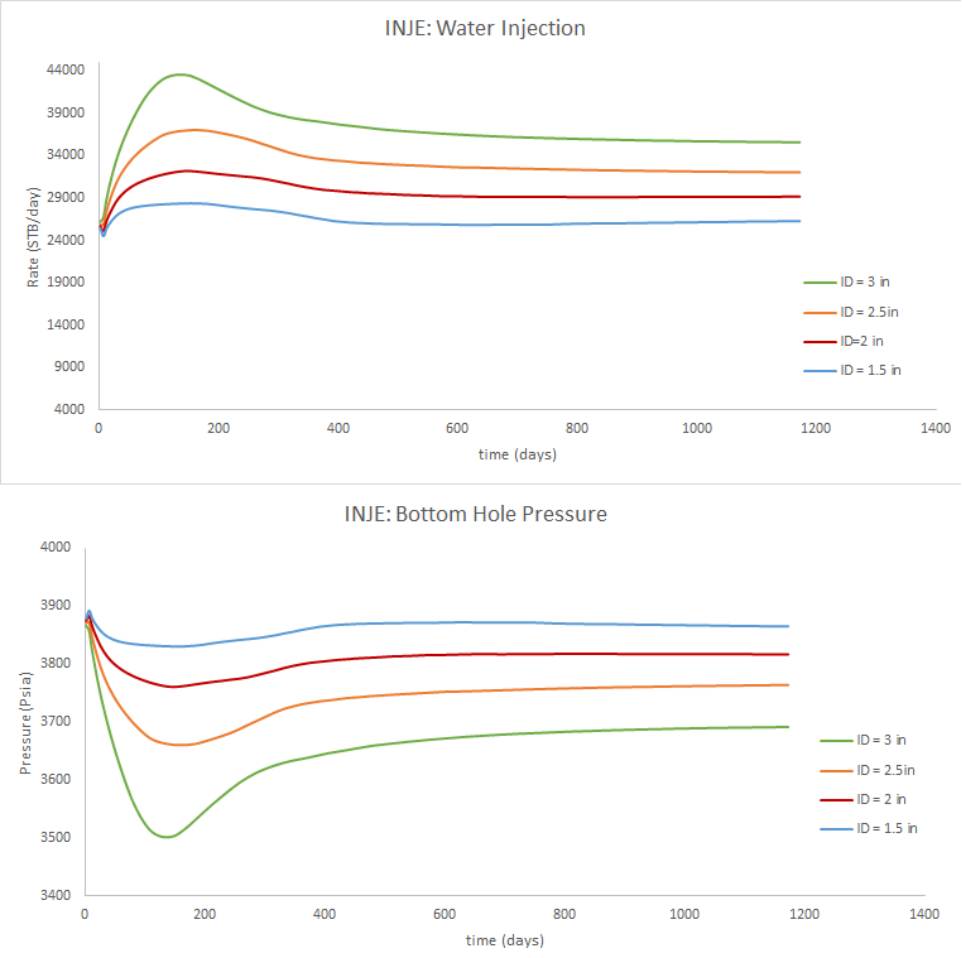

Figure 5.8: Injection profiles for investigating the effects of tubing size

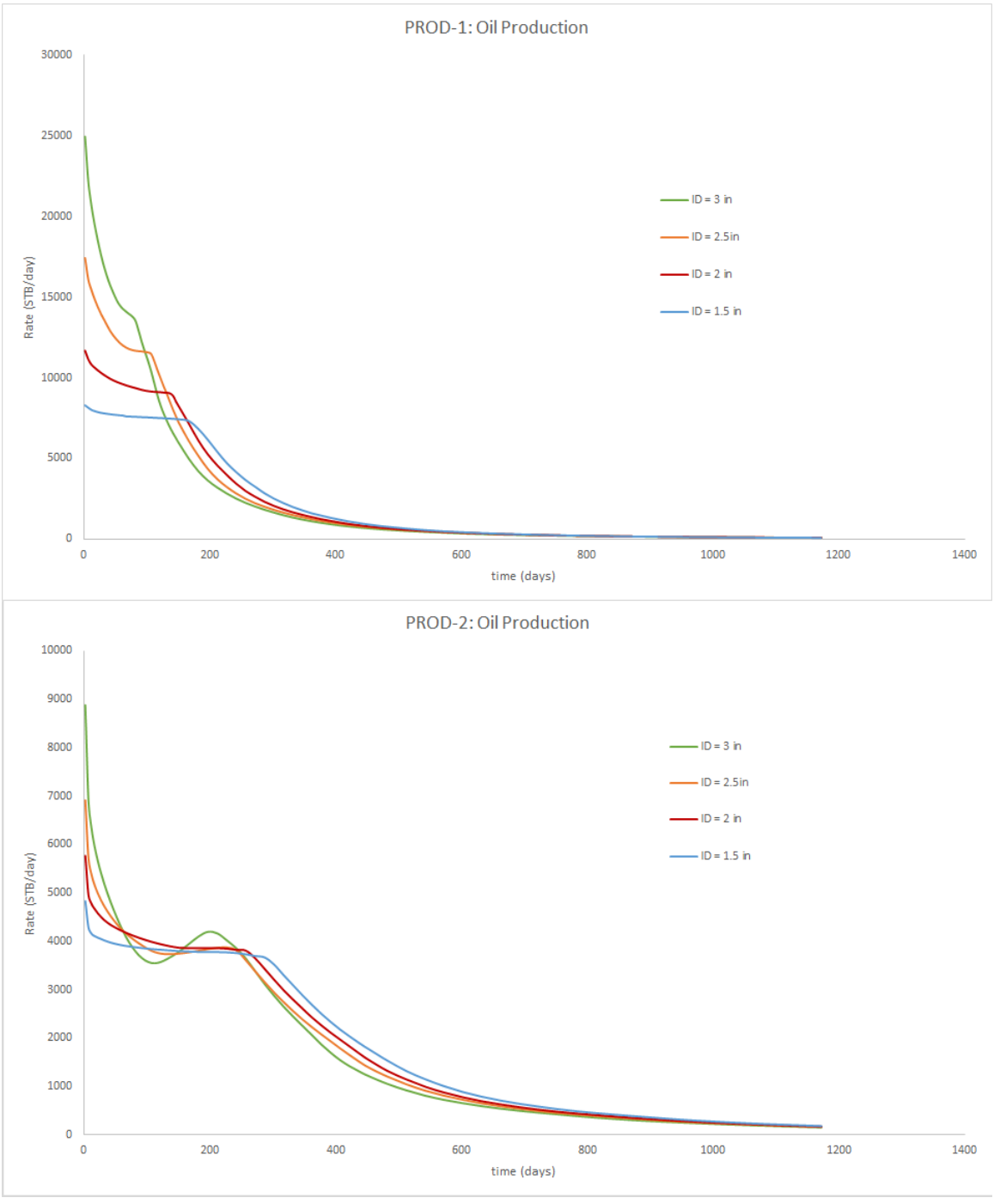

Figure 5.9: Oil production rates for investigating the effect of tubing size (PROD-1 and PROD-2)

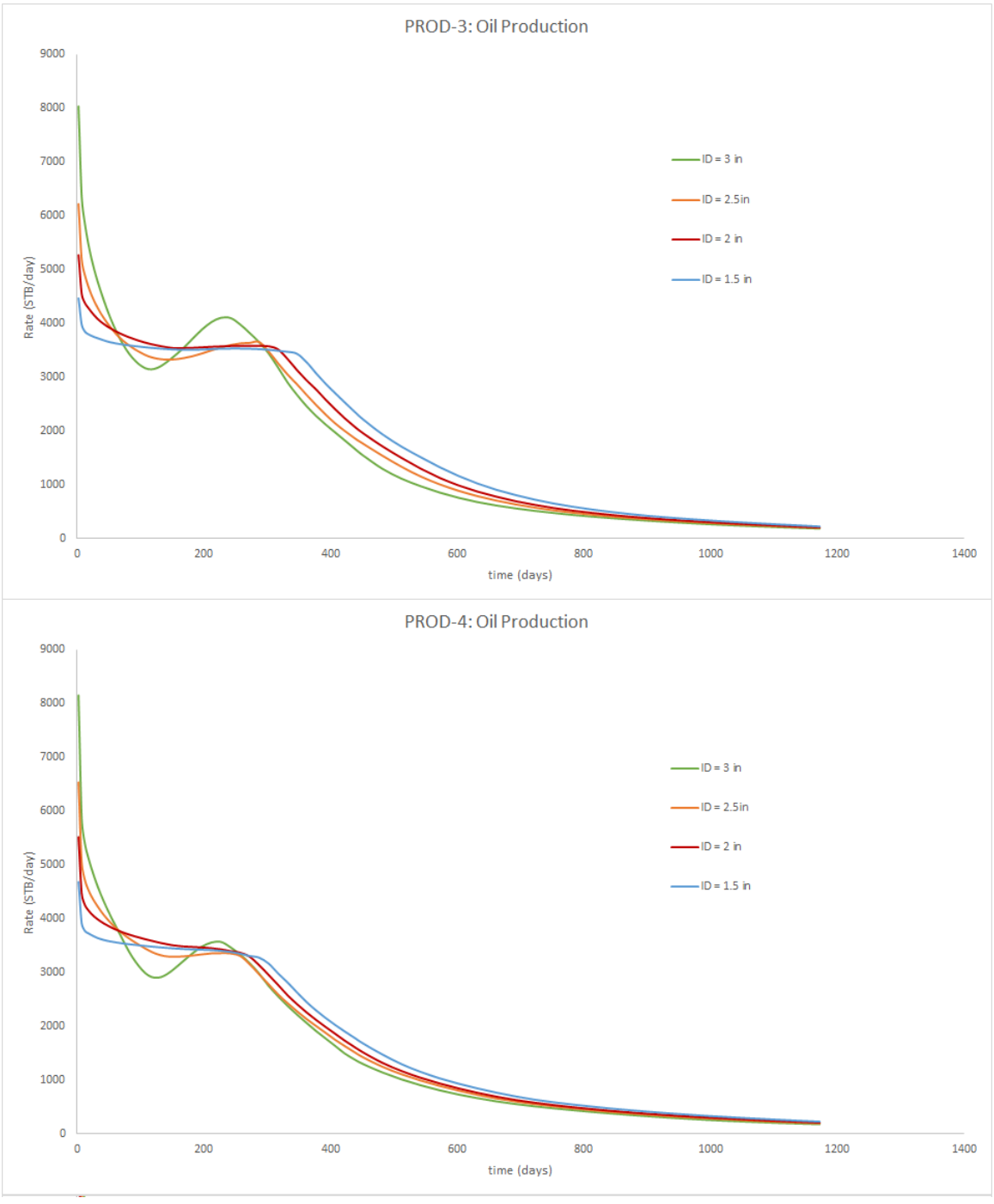

Figure 5.10: Oil production rates for investigating the effect of tubing size (PROD-3 and PROD-4)

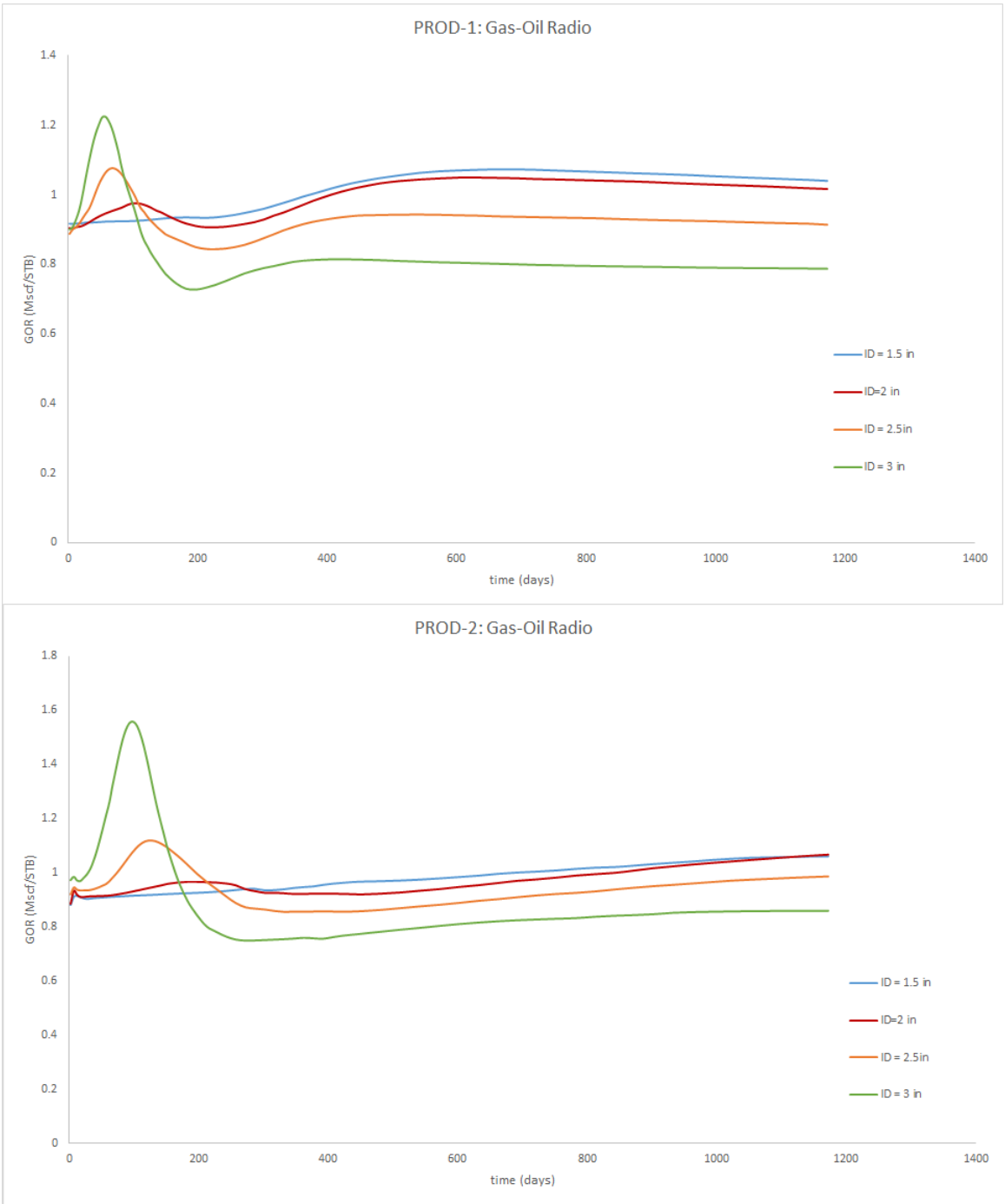

Figure 5.11: Gas-oil ratio for investigating the effect of tubing size (PROD-1 and PROD-2)

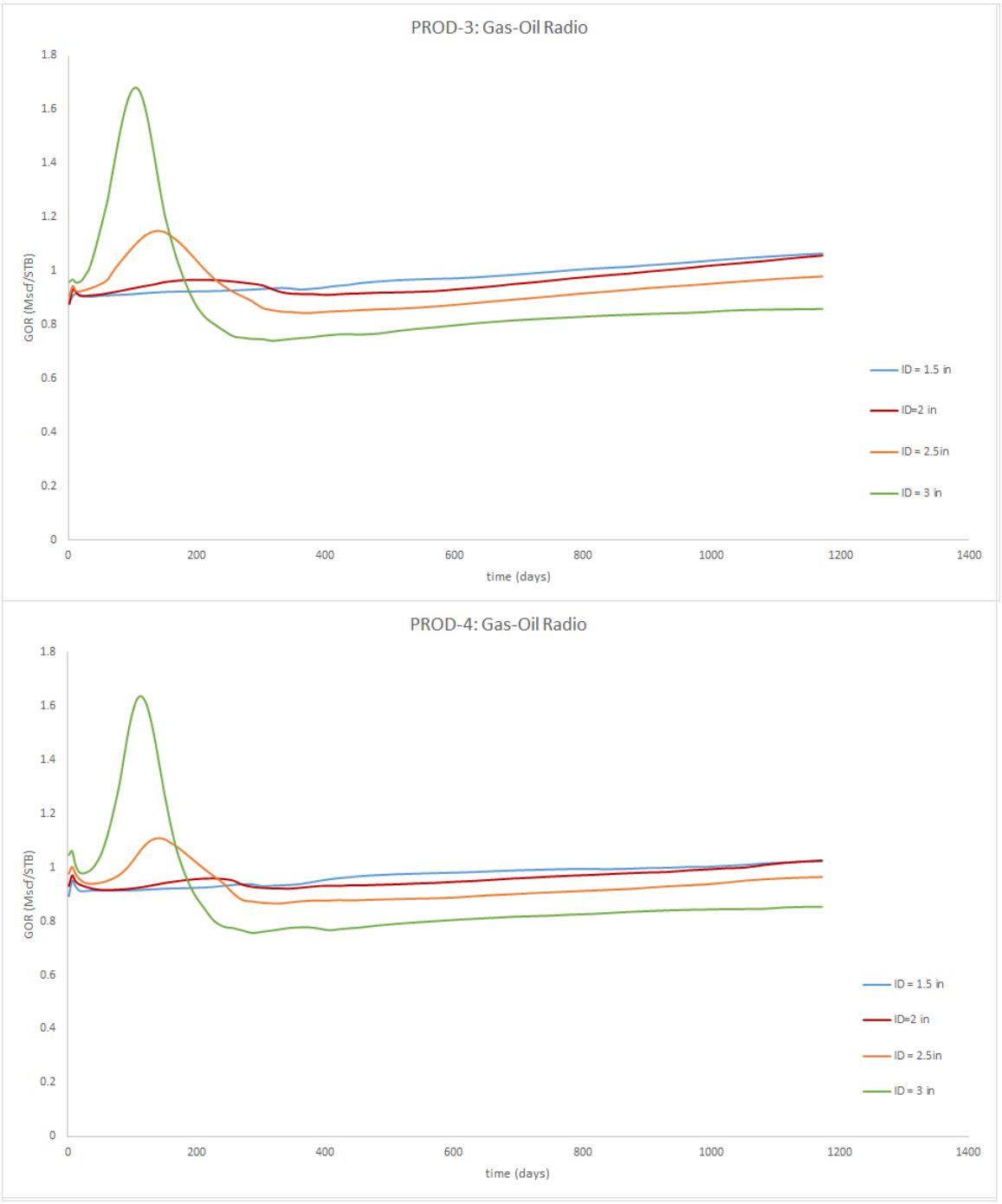

Figure 5.12: Gas-oil ratio for investigating the effect of tubing size (PROD-3 and PROD-4)

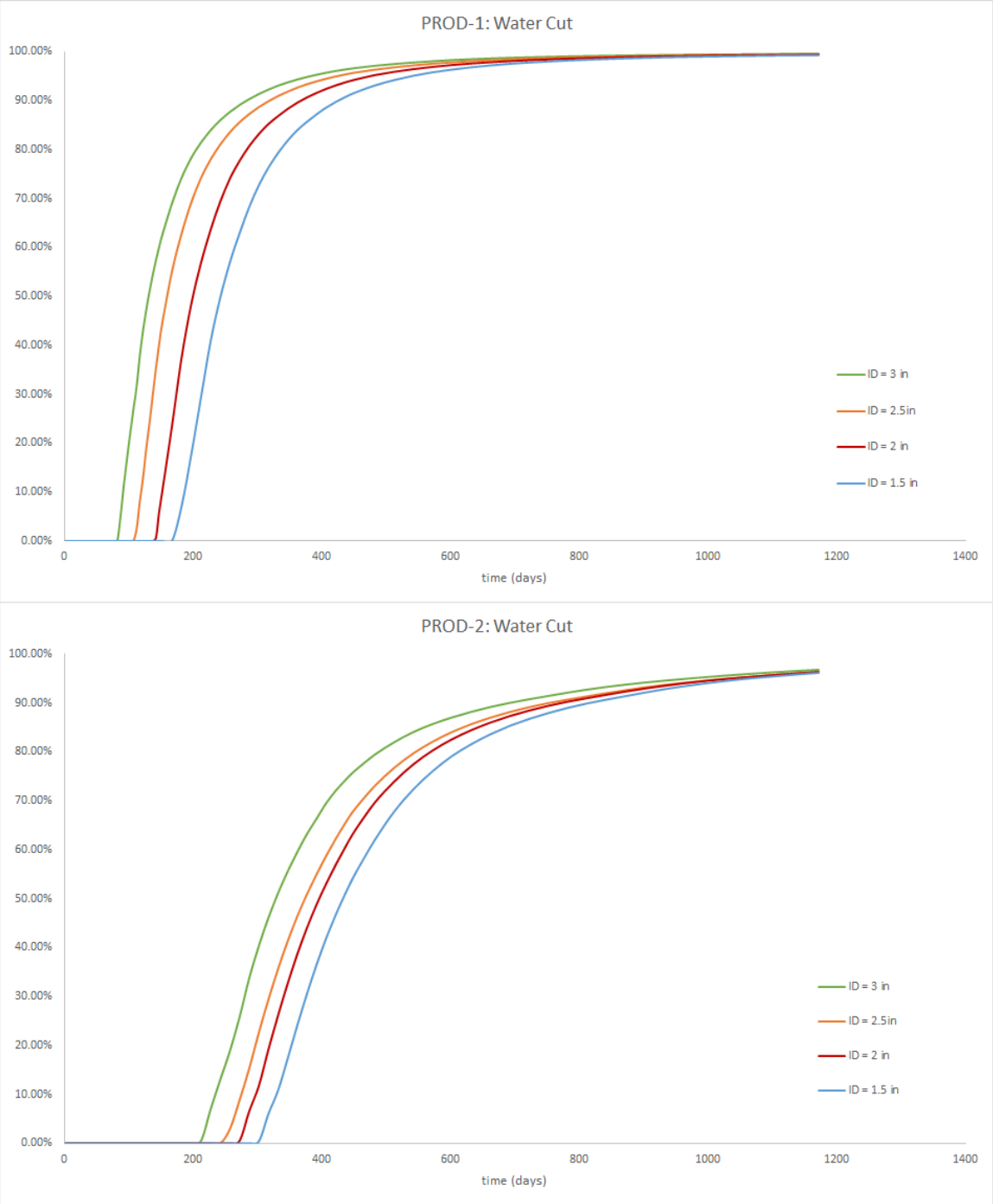

Figure 5.13: Water production for investigating the effect of tubing size (PROD-1 and PROD-2)

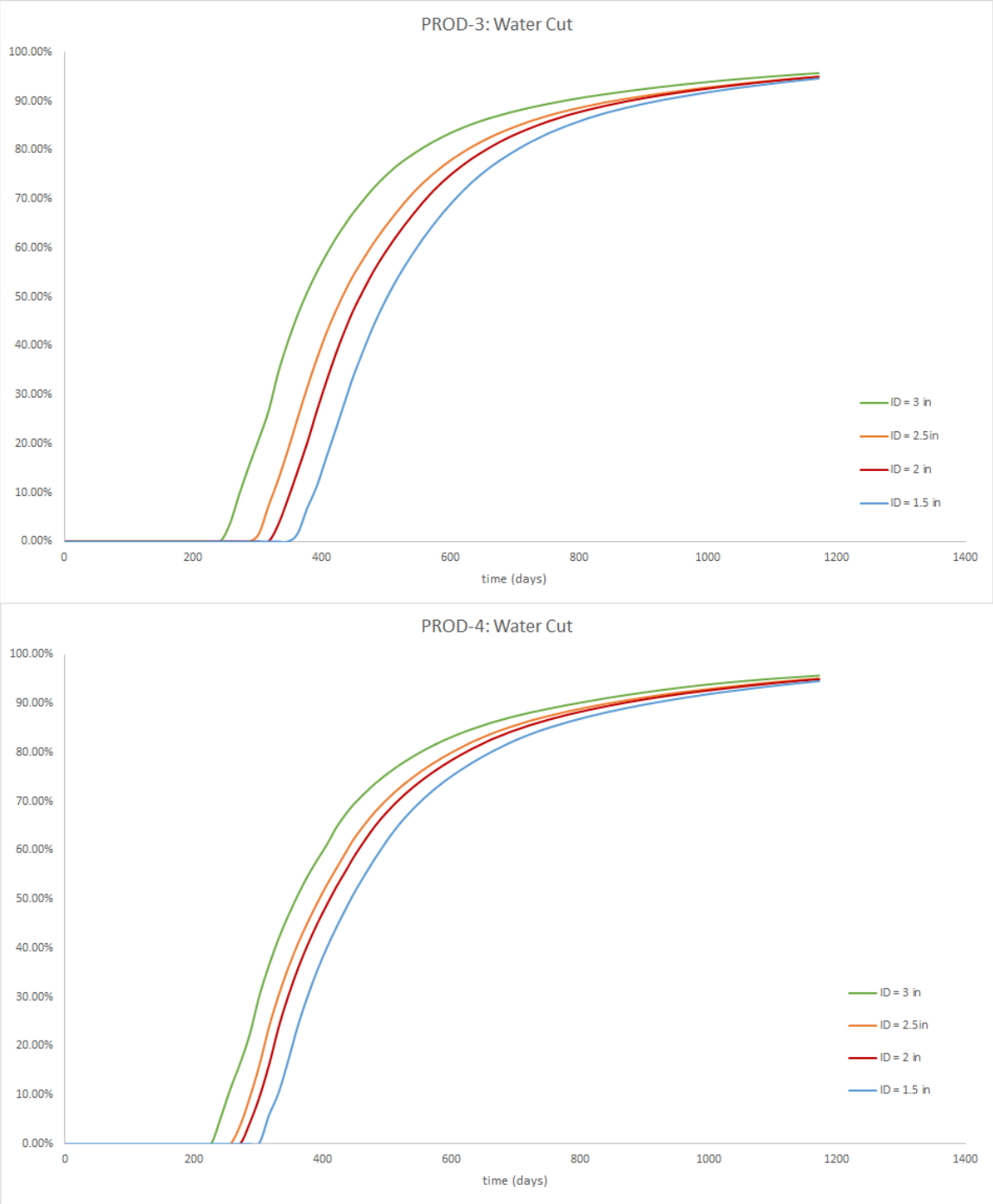

Figure 5.14: Water production for investigating the effect of tubing size (PROD-3 and PROD-4)

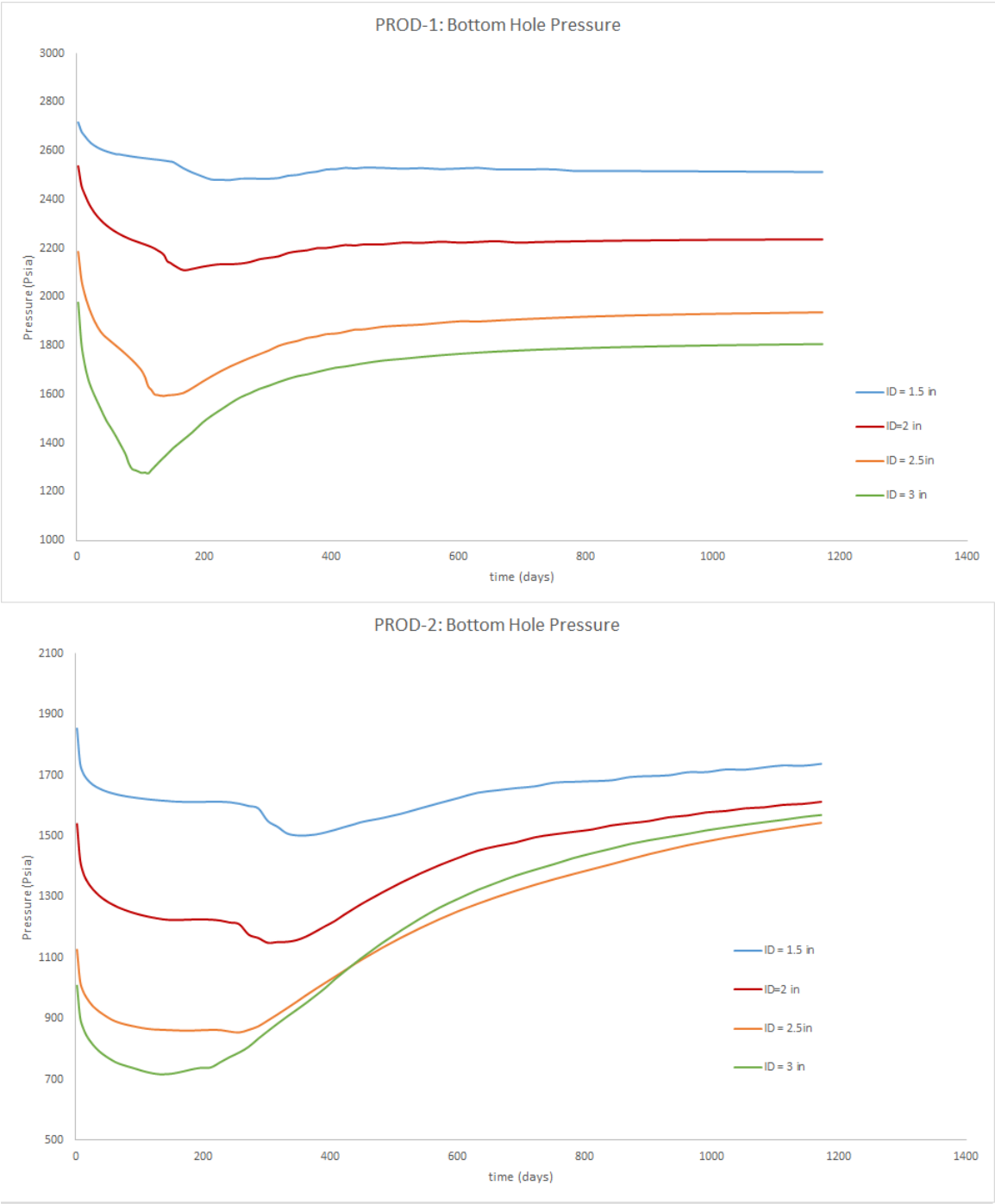

Figure 5.15: Bottom hole pressure of producers for investigating the effect of tubing size (PROD-1 and PROD-2)

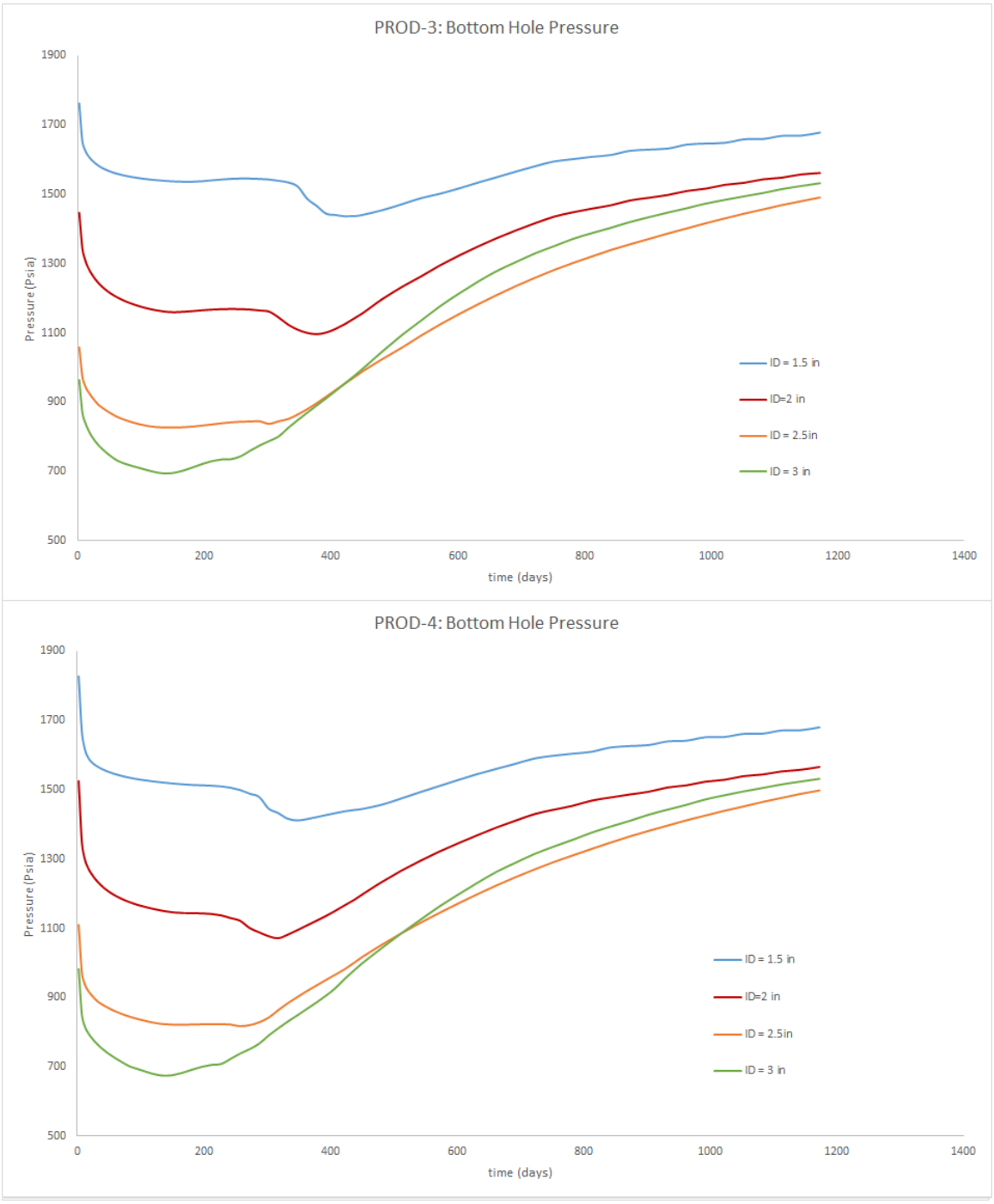

Figure 5.16: Bottom hole pressure of producers for investigating the effect of tubing size (PROD-3 and PROD-4)

Referring to Figure 5.7 and Figure 5.11, it can be observed that all producers with a smaller tubing size have a higher BHP profiles. Thus, it can be concluded that the tubing with smaller diameter has more restriction (due to friction) to the fluid flow, and consequently result in a larger pressure loss through the tubing. By observing oil production profiles, it is found that the oil production rate is relative high when using larger tubing size, this is due to the lower BHP of producers and higher water injection. From Figure 5.11-5.12, it can seen that the case of large tubing size will lead to more free gas existing within the reservoir, which indicates that the reservoir pressures drop faster. This can be explained as that when using large tubing, the oil production rate is too high and the water injection rate is hard to maintain energy within the formation, therefore we can observe more free gas produced from production wells. From the discussion above, it can be conclude that using large production tubing could result a high oil production rates at the beginning. However, oil production will drop rapidly and the reservoir energy is hard to be maintained by using large tubing producers, thus it is recommended to use relative small tubing size for production, in order to maintain the energy within the reservoir.

5.3.2 Effects of adding a choke

At the early time of oil production, the production rate is very high without restriction. Generally, it is necessary to restrict the flow rate in order to prevent sand production and gas coning in the oil reservoir. However, using a high downstream pressure (i.e. separator pressure) to restrict production rate is not applicable in the field. Therefore, the choke is required for restricting production rate as well as keeping the downstream pressure at standard conditions.

In order to study the effect of choke on production performance, we need to

perform the choked model and our base coupled model. For the choked model, a choke size of 32/64 inch is placed at the wellhead of each producer, keeping properties of production settings exactly the same as the one used in last section, and the tubing/pipe size is set to 3". Another production strategy is that the production will be ceased once the field water-cut exceeds 0.95. Figure 5.17 shows the field water-cut from running base and choked model.

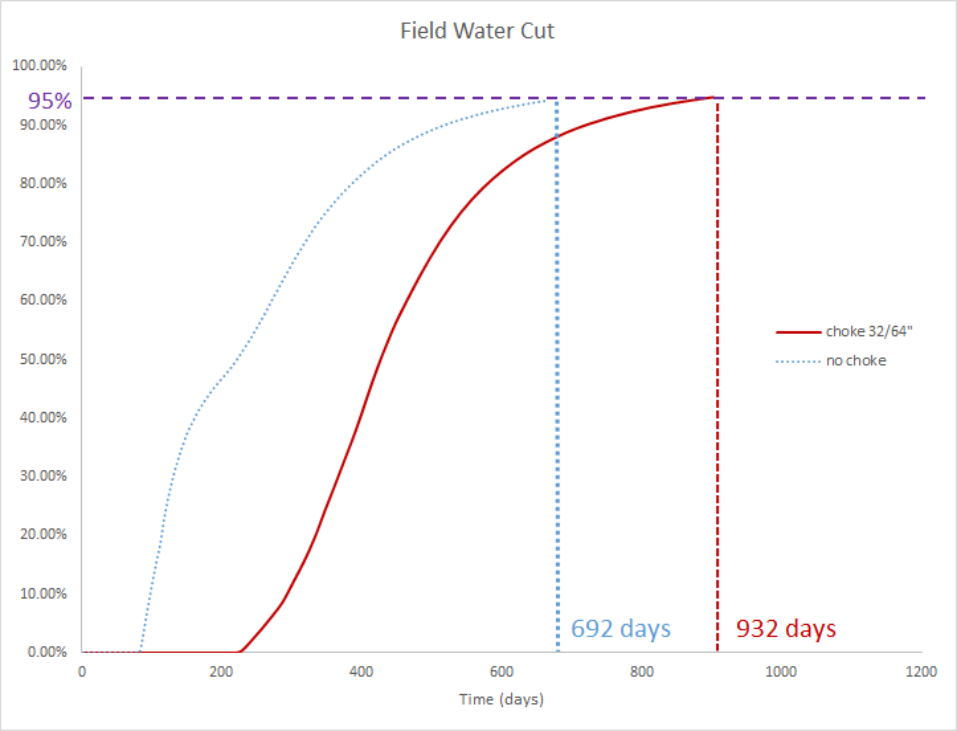

Figure 5.17: Field water cuts of choked and base models

Referring to the Figure 5.14, it can be seen that the adding choke could delay the water breakthrough and extend the production time. Therefore, the total production times for base and choked case are 692 and 932 days, respectively. The injection and

production profiles are shown in Figure 5.15-5.20, where the blue curves represent the results from base model, and the red curves represent the results from choked model.

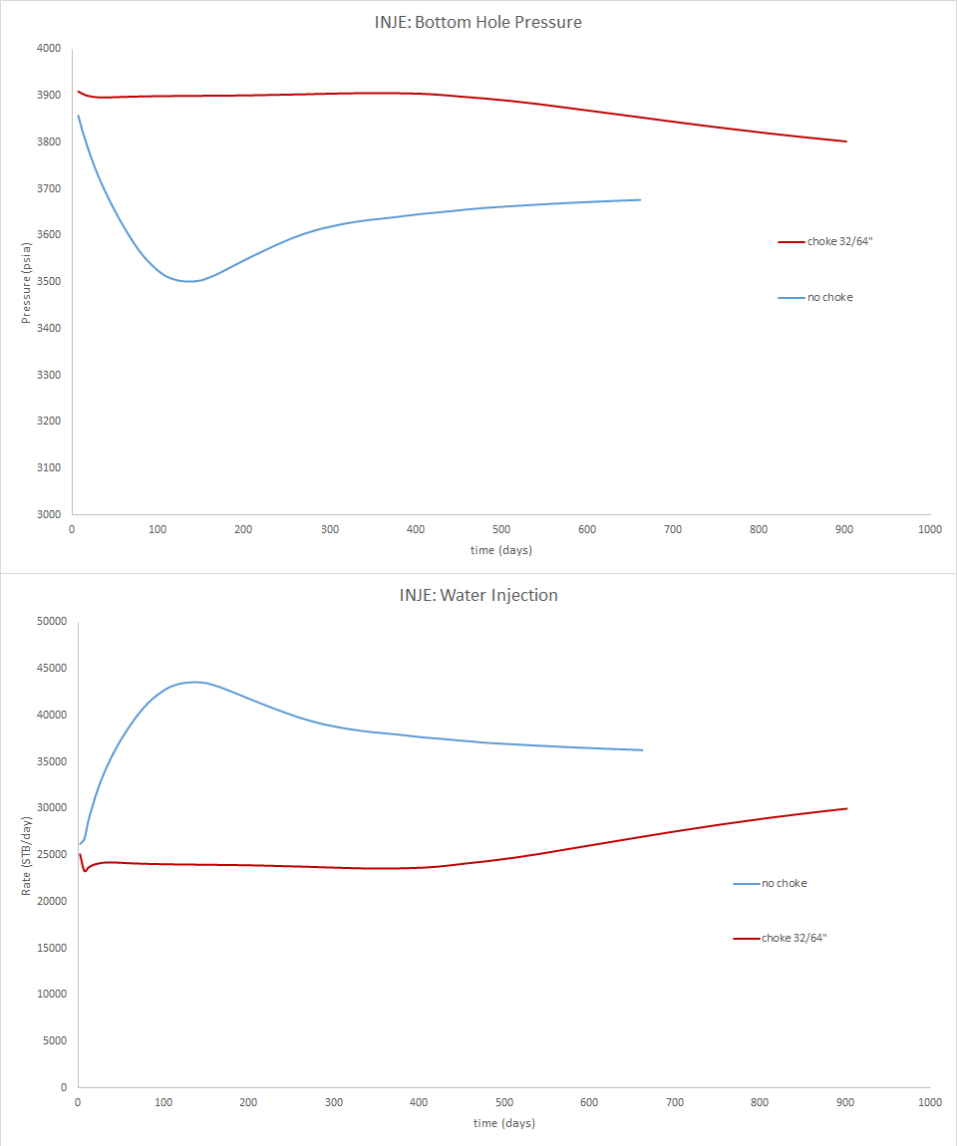

Figure 5.18: Injection profiles for comparing base and choked case

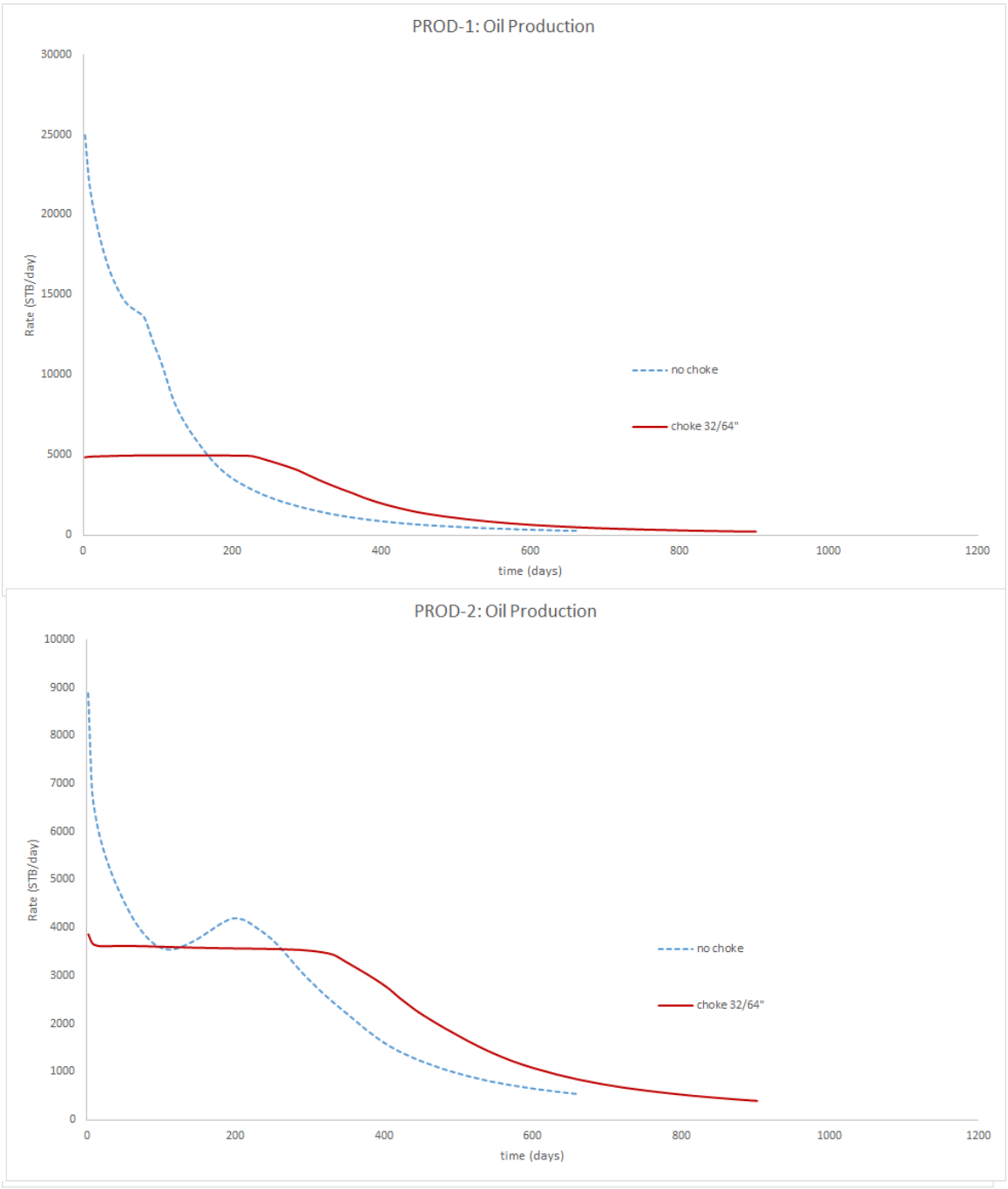

Figure 5.19: Oil production for comparing base and choked case (PROD-1 and PROD-2)

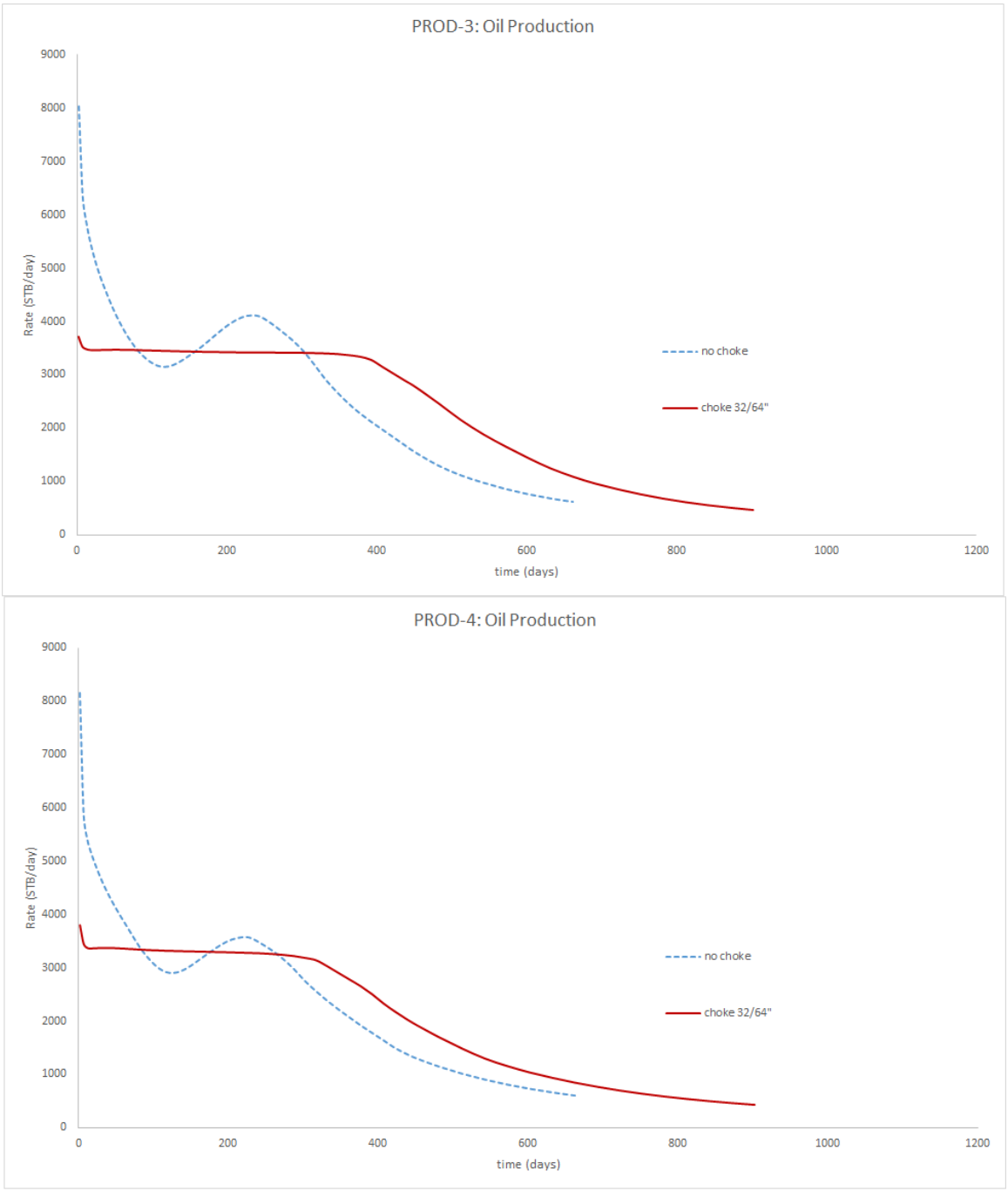

Figure 5.20: Oil production for comparing base and choked case (PROD-3 and PROD-4)

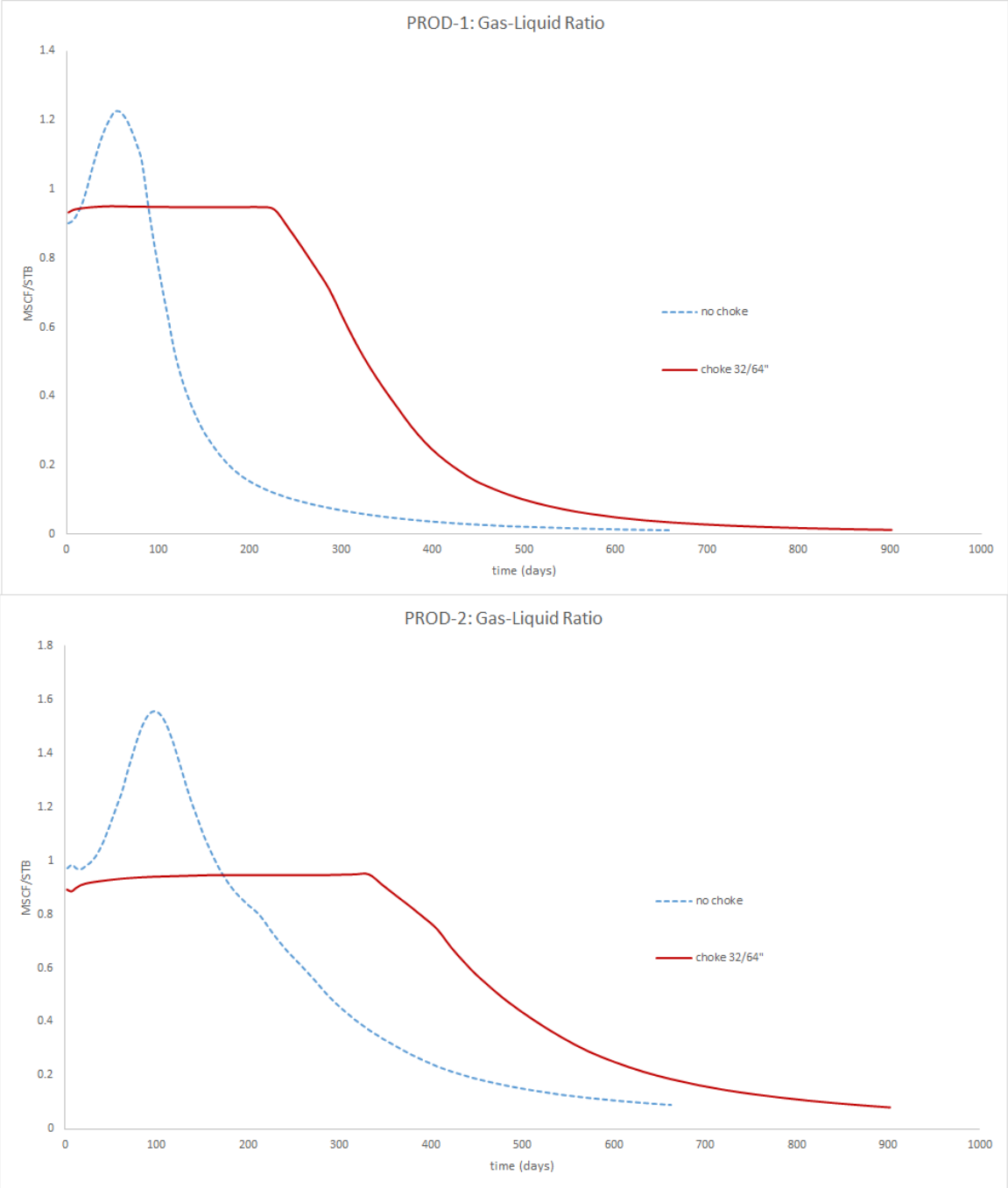

Figure 5.21: Gas liquid ratio for comparing base and choke case (PROD-1 and PROD-2)

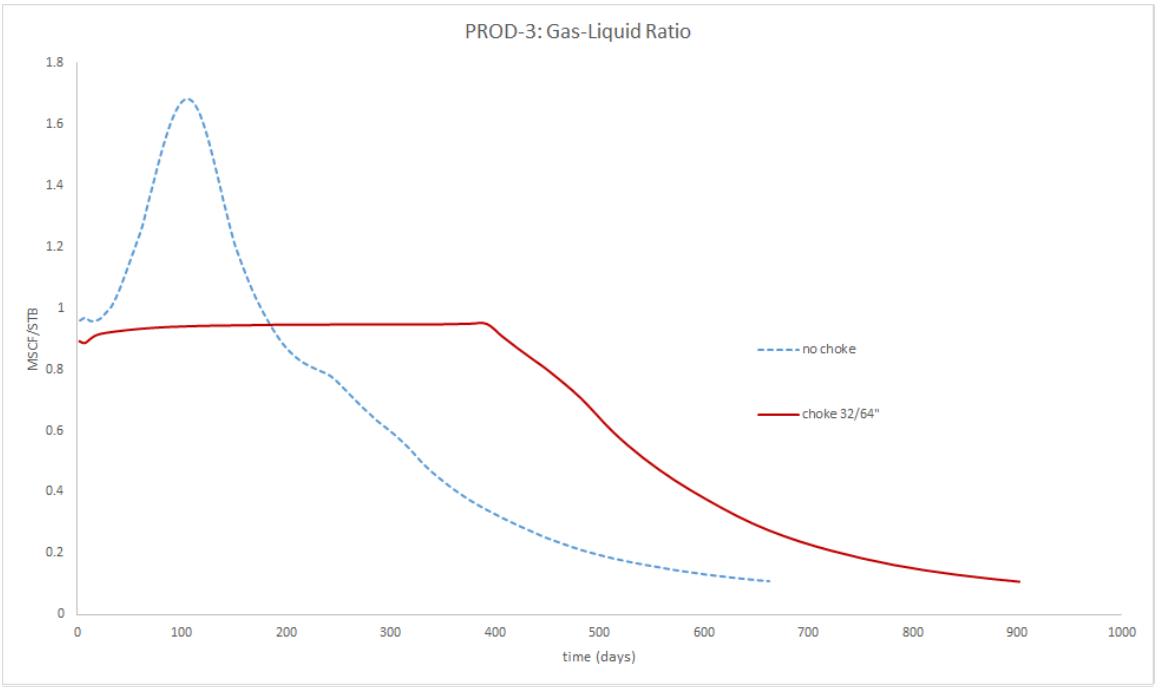

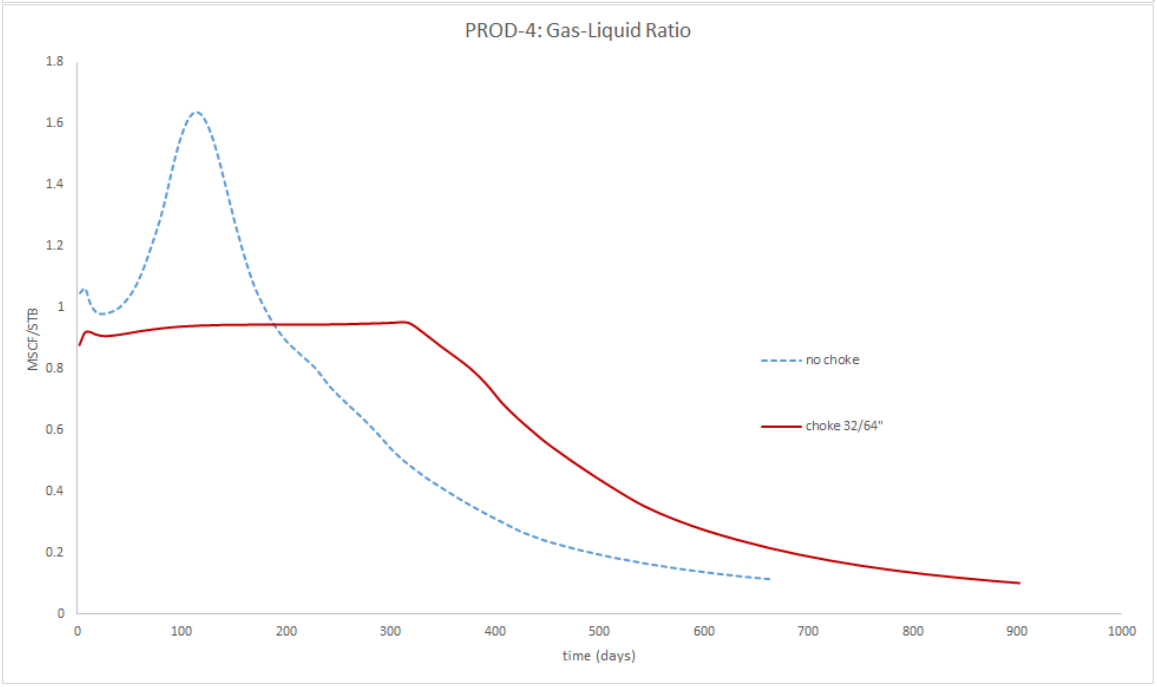

Figure 5.22: Gas liquid ratio for comparing base and choke case (PROD-3 and PROD-4)

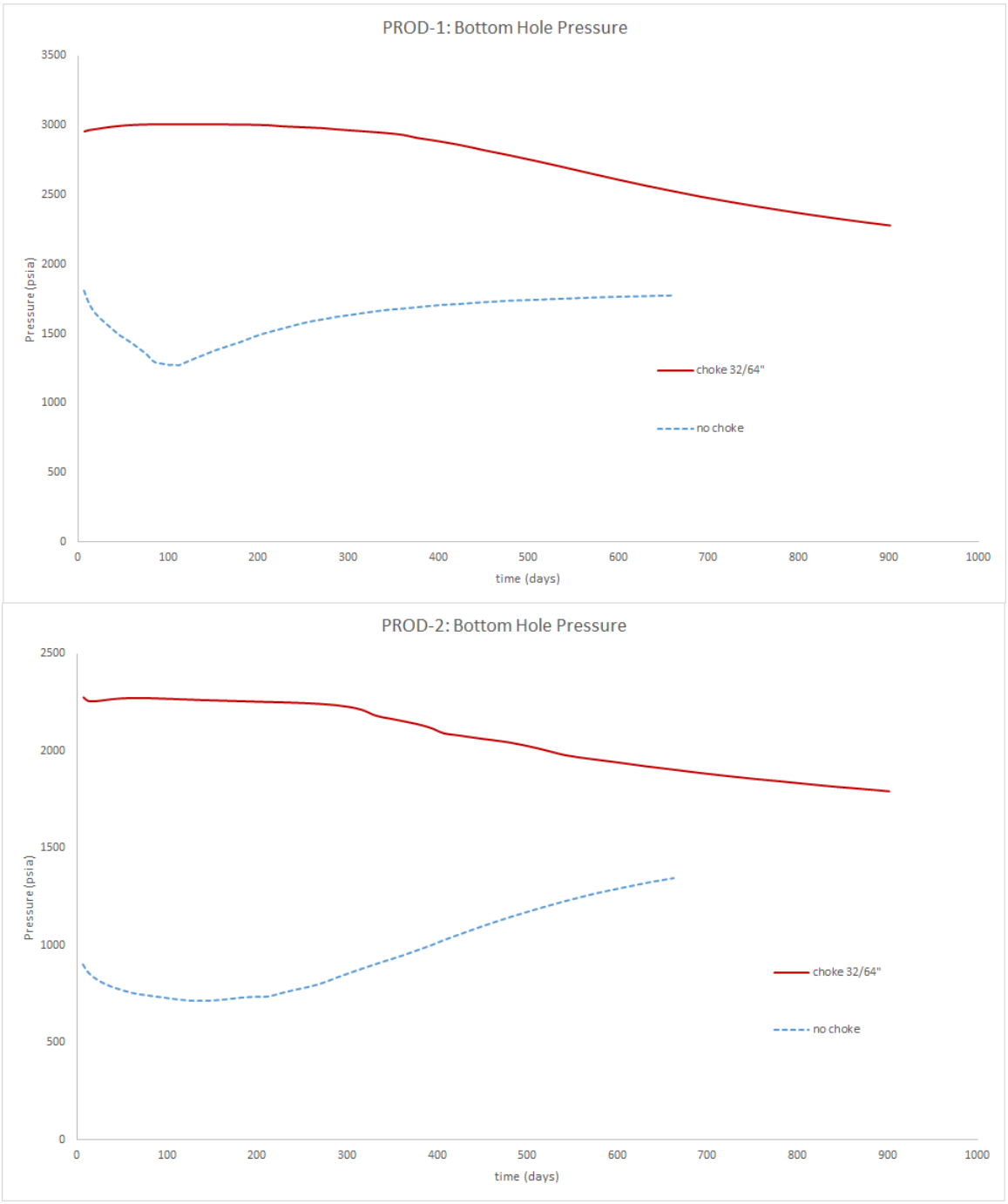

Figure 5.23: Bottom hole pressure for comparing base and choke case (PROD-1 and PROD-2)

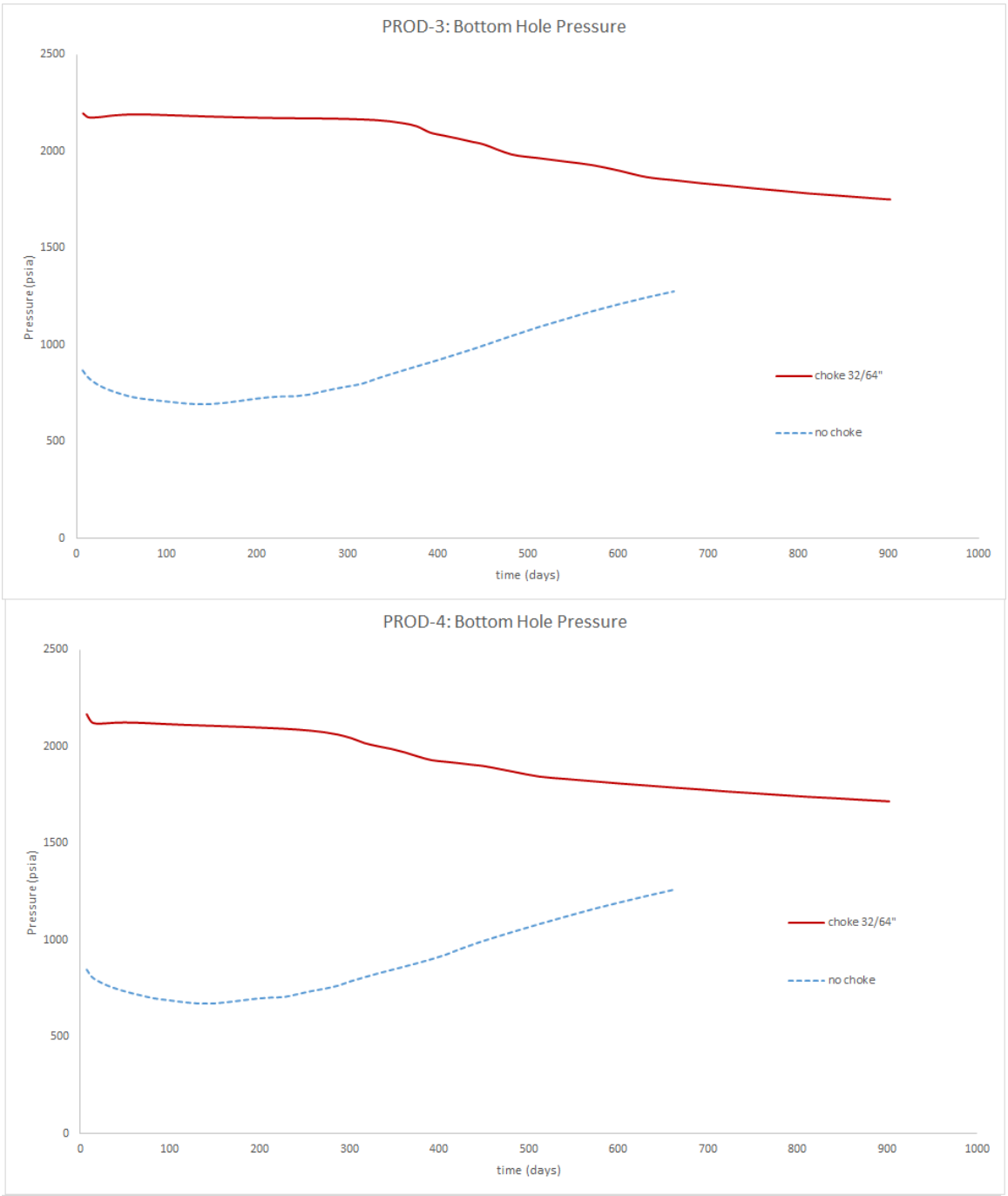

Figure 5.24: Bottom hole pressure for comparing base and choke case (PROD-3 and PROD-4)

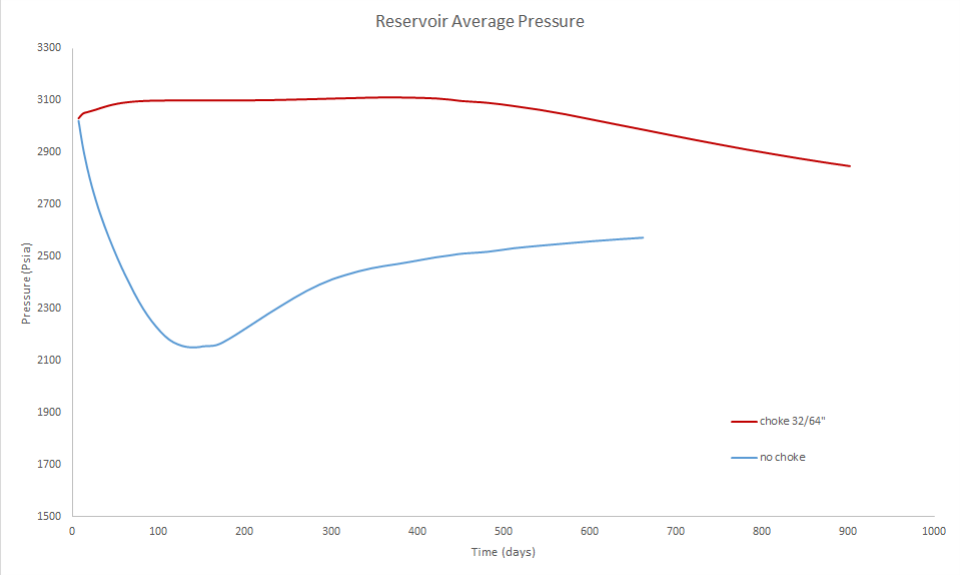

Figure 5.25: Reservoir pressure for comparing base and choke case

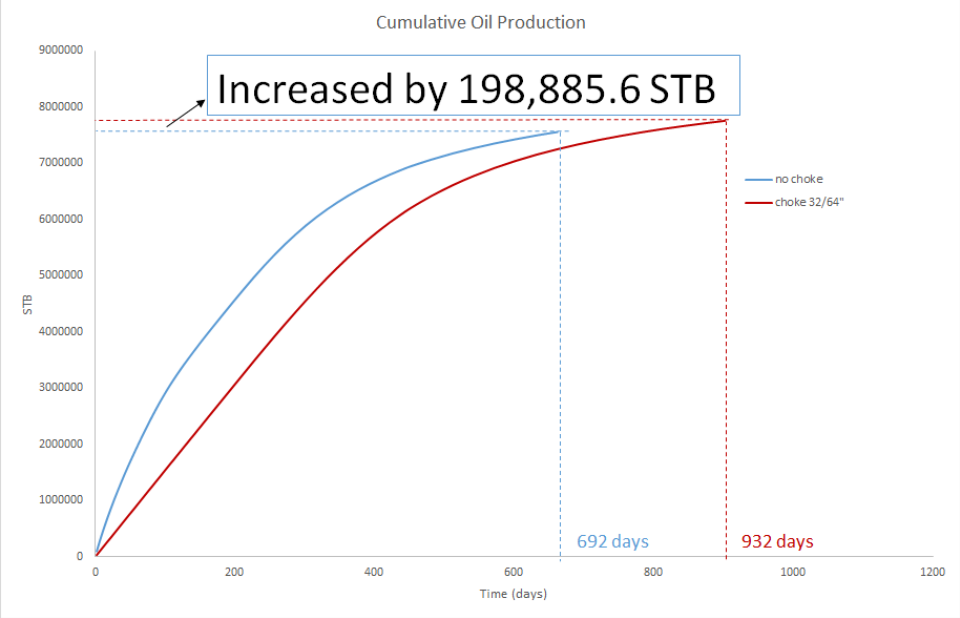

Figure 5.26: Cumulative oil production for comparing base and choked case

By observing injection profiles, a higher BHP and lower injection rate can be found in the choked case, this indicates a high reservoir pressure around the injection well. From the oil production profile, it can be seen that the oil production rate is restricted by the choke within the desired range; also the time for constant oil production is extended due the placed choke. Although the cumulative production of the choked case increases slower than that of base case, the final oil recovery is increased by 198885 STB in the choked case, due to the longer production time. Referring to the Figure 5.18 and 5.19, it is found that the producers' BHPs start to decline after water breakthrough, this can be explained as that the Gas-Liquid Ratio (GLR) will be reduced when well starts to produce water, and smaller GLR will results in a smaller upstream pressure at choke, consequently results in a lower BHP. Therefore, the decline in producers' BHP can be observed when water enter the production tubing.

5.4 Performing Fully Coupled Simulator with Realistic Scenario

In this section, we tested the stability of our in-house simulator to more realistic scenario. The coupled and non-coupled model will be compared, in order to investigate the effect of surface network elements on the production performance. The reservoir model that used in this study is the SPE-10 benchmark[25].

5.4.1 Description of reservoir model and properties of fluid

In general, our simulator is able to apply the couplings to a black-oil 3D model. However, since there are over one million grid blocks within the SPE-10 benchmark, we only modeled the first layer of SPE-10 in this study, in order to save on the computational cost. The description of SEP-10 reservoir model is summarized in Table 5.2.

Table 5.2: Descriptions of SPE-10 reservoir model

Reservoir Conditions	Value	Unit
$N_x : N_y : N_z$	60:220:1	ft
$\Delta x \times \Delta y \times \Delta z$	6×3×2	
permeability	Heterogeneous (refer to Fig 5.21)	mD
Porosity	Heterogeneous (refer to Fig 5.21)	%
Reservoir Initial Pressure	6000	Psia
Initial Water Saturation	0	%
Initial Oil Saturation	100	%
Reservoir Top Depth	12000	ft
Production Scenario	5-spot water flooding	

Both the permeability and porosity of SPE-10 reservoir model are heterogeneous, and the permeability ranges from 0 to 4650 mD, while the porosity is between 0 and 0.45, Their maps are shown in Figure 5.27.

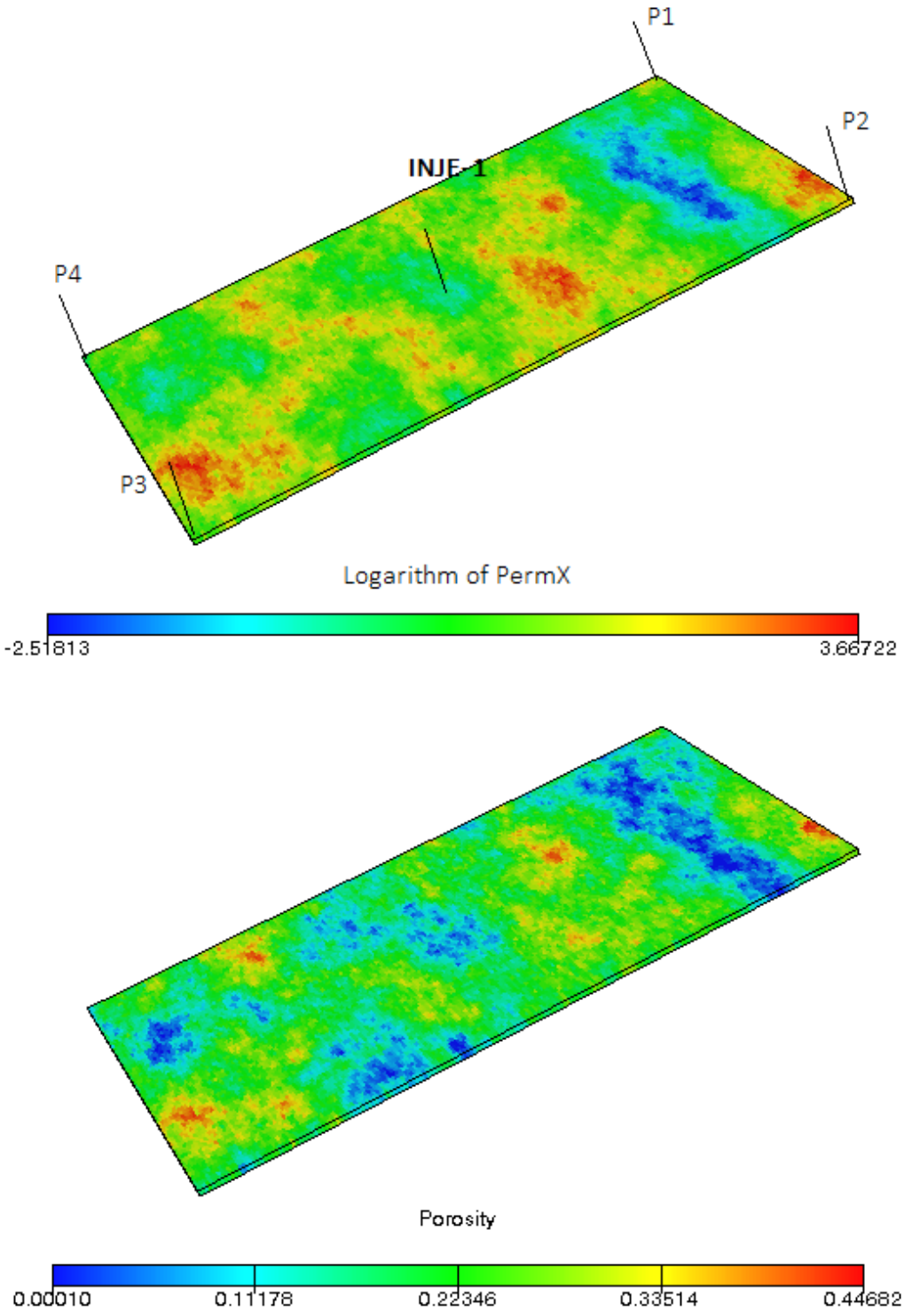

Figure 5.27: Permeability and porosity map of SPE-10 benchmark

Referring to Figure 5.27, it can be seen that the production scenario is a 5-spot water flooding pattern, where the injection well is placed at the center of reservoir that has low porosity and permeability.The four producers are placed at four corners of the reservoir respectively; the PROD-3 and PROD-4 are located at the high permeability zones.

5.4.2 Production strategy and facilities' properties

The production strategy and facility properties of coupled case is shown in Table 5.3. For the non-coupled case, only the production strategy is shown in Table 5.4.

Table 5.3: Production strategy and facility properties used for coupled case

Production strategy & facility properties	Value	Unit
Production Tubing ID	2	in
production Tubing Length	12000	ft
Surface Pipe ID	2	in
Surface Pipe Length	1000	ft
Downstream production pressure	200	psia
Upstream injection pressure	2000	psia
Roughness	0.001	
Choke size	3/64	inch

Table 5.4: Production strategy used for non-coupled case

Production strategy	Value	Unit
Downstream production pressure	3650	psia
Upstream injection pressure	7460	psia

5.4.3 Results and discussions

The results of comparing coupled and non-coupled cases are shown in Figure 5.28-5.32, where the red curves represent the results from performing coupled model, while the blue curves represent the results from non-coupled case. Since the difference between coupled and non-coupled case is not obvious for PROD-1, PROD-2 and PROD-4, only the production profiles of PROD-3 are shown.

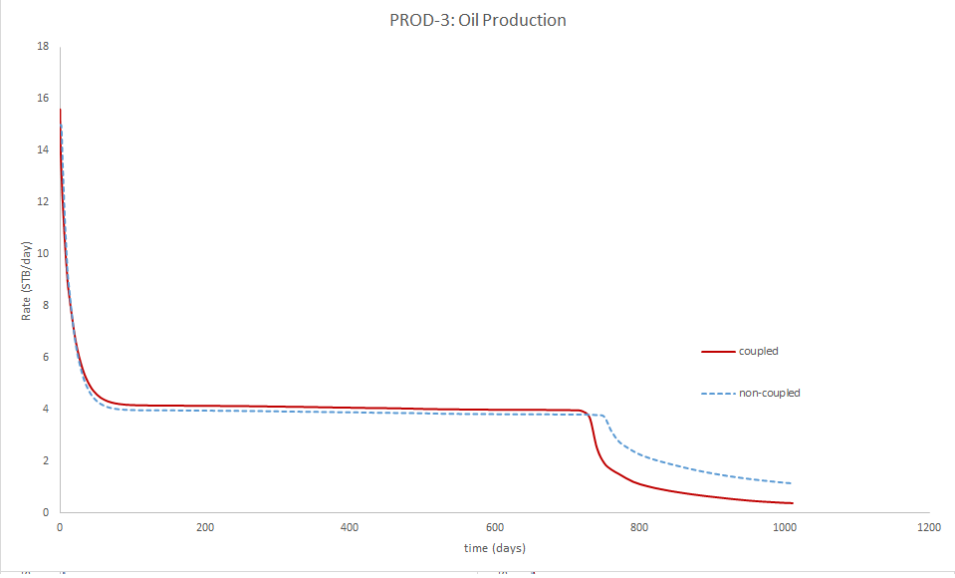

Figure 5.28: Oil production for comparing coupled and non-coupled with SPE-10 case

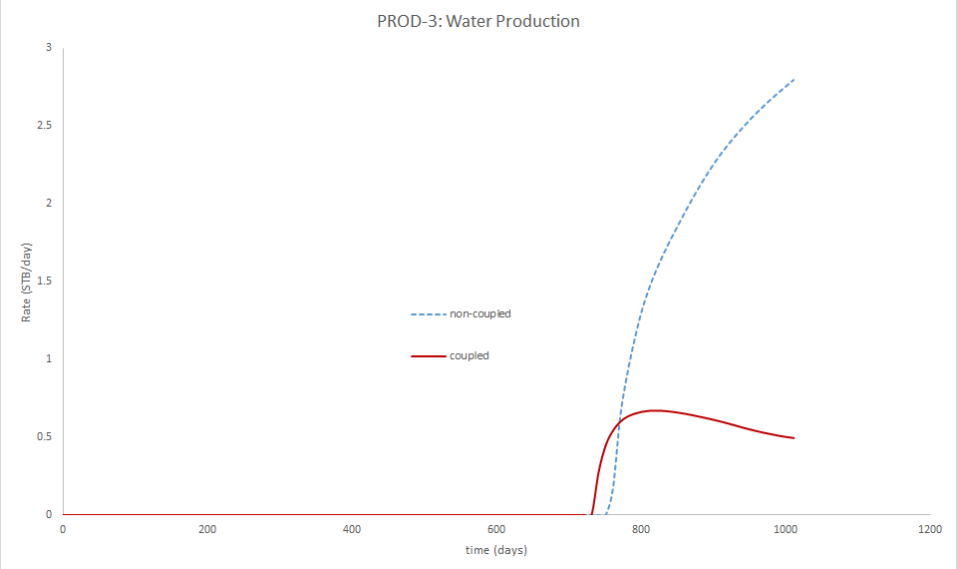

Figure 5.29: Water production for comparing coupled and non-coupled SPE-10 case

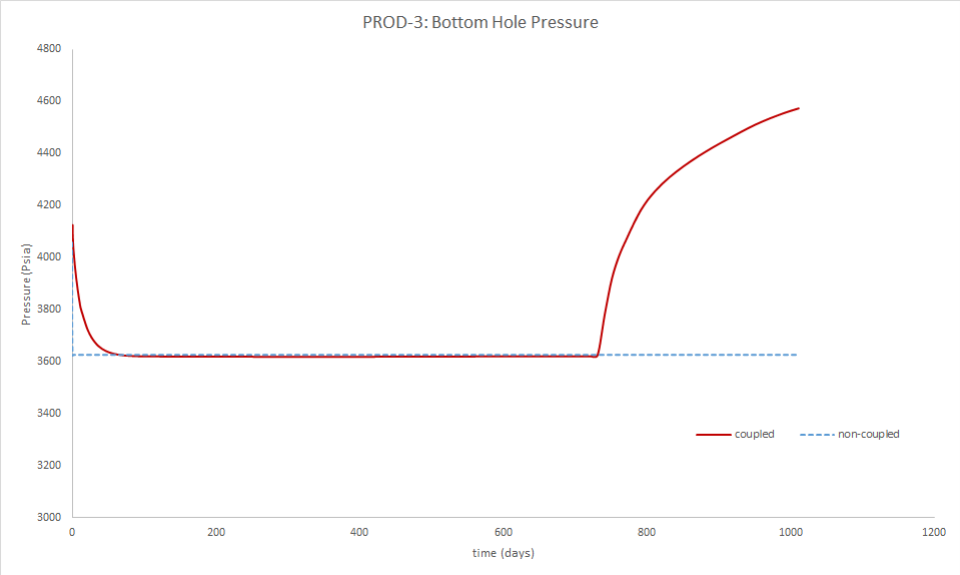

Figure 5.30: Bottom hole pressure for comparing coupled and non-coupled SPE-10 case

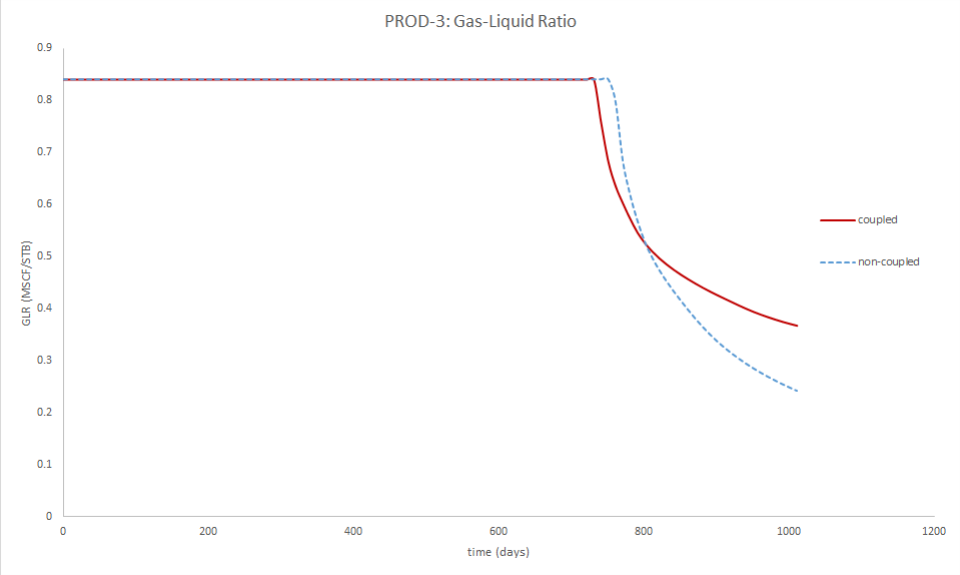

Figure 5.31: Gas-liquid ratio for comparing coupled and non-coupled SPE-10 case

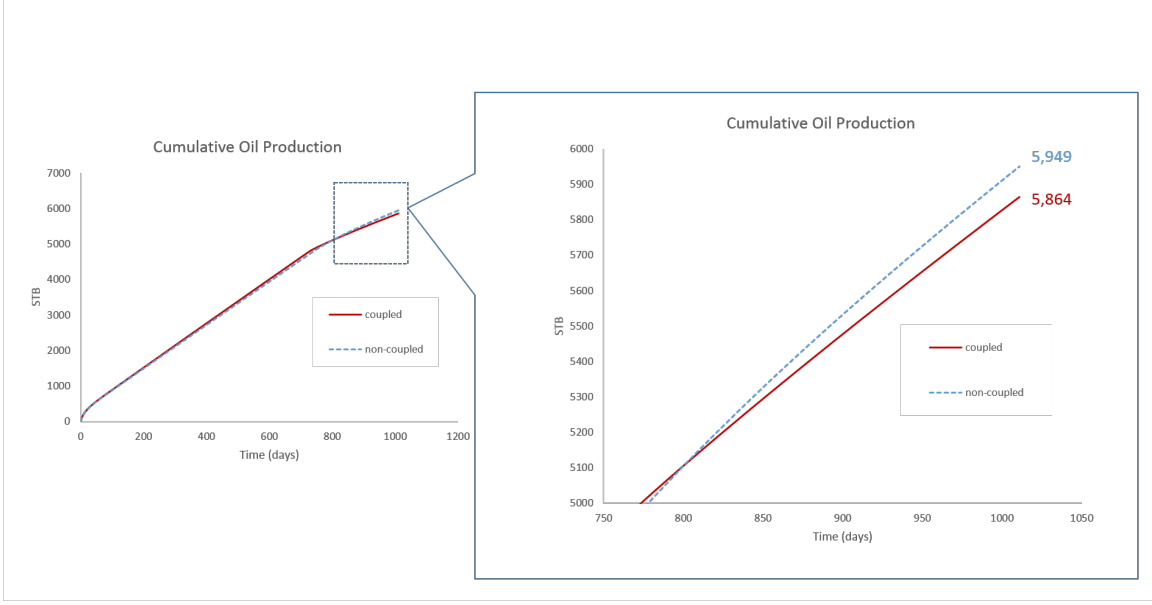

Figure 5.32: Total cumulative oil production

By observing the water production profile, we find that the water breakthrough only occurred in PROD-3. Since the gas-oil ratio kept constant during the production, it is inferred that there is no free gas entered the production tubing, and therefore, the bottom hole pressure kept is constant before the breakthrough. For PROD-3, an increase of bottom hole pressure can be observed after water breakthrough, this is differs from what concluded in last chapter that the decreased GLR will reduce the bottom hole pressure for choked model, this implies that the bottom hole pressure is affected by both the GLR and mixture density in the tubing, when the flow rate is small, the change of pressure caused by change of GLR will be small, therefore, the mixture density will be the dominating factor that impacts the bottom hole pressure of producers.

By comparing the coupled and non-coupled cases, it is found that the non-coupled failed to predict the bottom behavior after water breakthrough, which will results in overestimation of water production and oil recovery.

The total iterations of running coupled and non-coupled cases are summarized in Table 5.5. It is found that fully coupling will increase both the iterations and simulation time. Referring to the Newton-Raphson, we counted the Newton iterations for all the timesteps. The iterations of each timestep for the two cases are shown in Figure 5.33. It can be seen that the coupled model used more Newton iterations at the beginning of production. Also, it is concluded that the CPU time of coupled model is 2.95 times of the non-coupled case. However, the difference in total recovery from coupled and non-coupled cases are not obvious. Therefore, in order to save computation time, it is recommended to use non-coupled model when perform the SPE-10 scenario.

Table 5.5: Summary of iterations and elapsed time

model type	iterations	Elapsed time (s)
coupled	718	1621.79
non-coupled	671	510.5

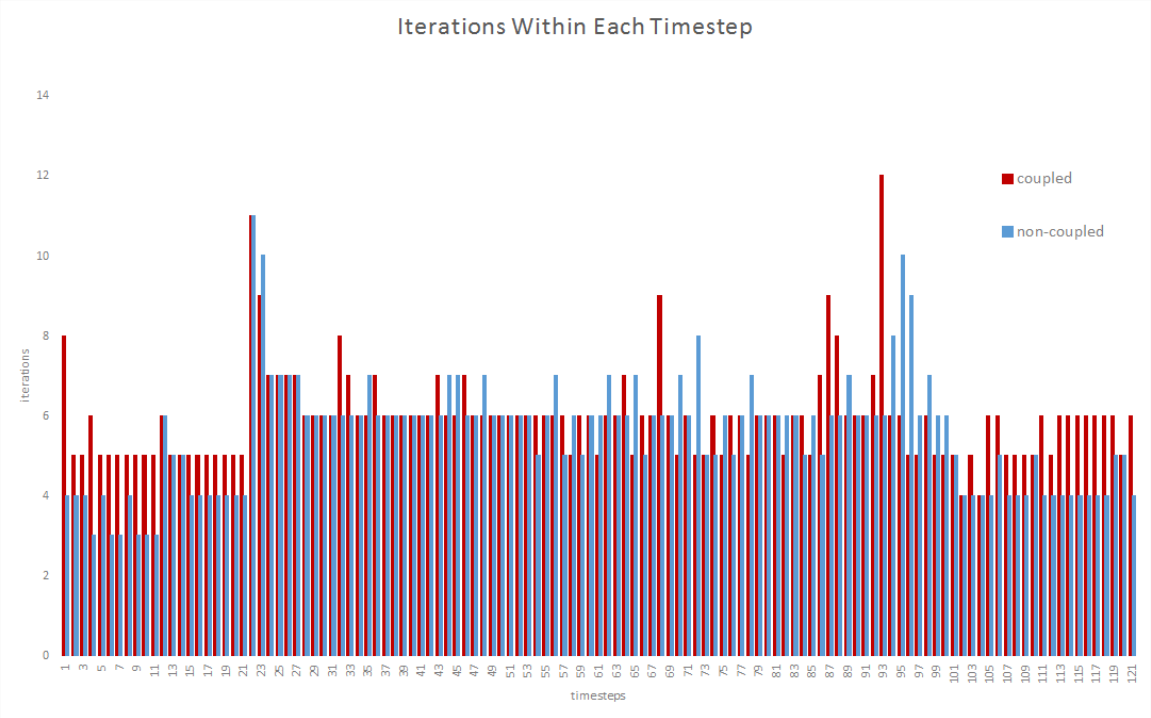

Figure 5.33: Iterations of each timestep for comparing the coupled and non-coupled model

6. CONCLUSIONS AND RECOMMENDATION

6.1 Summary and Conclusions

We have investigated the fluid flow characteristics within the porous media and the surface network; and studied the mechanism of different coupling approaches. Four scenario were constructed and through a sensitivity study we assessed the impact of coupling frequency on production performance under different scenario.

The construction of a fully coupled model that includes both the production system and injection system realized the production prediction considering the entire surface facilities. In addition, the flexible code implementation allows incorporation of additional physics in the simulator. With the in-house fully coupled model, we have investigated the effect of network settings on production performance.

Based on the completed tasks, we conclude:

- For the partially implicit coupling, the coupling frequency has impact on the simulation efficiency and production performance. It is found that using low coupling frequency could reduce the computational time. However, low coupling frequency may fail to accurately predict the production, since the incomplete balance action cannot predict the state of bottom at the end of each timestep;

- The high permeability reservoir shows more sensitivity to coupling frequency than low permeability reservoir in terms oil and gas recovery;

- The oil/gas production forecast of heterogeneous permeability reservoir is more sensitive to coupling frequency than that of homogeneous permeability reservoir;

- When partially coupling performed under unconventional reservoir, the impacts of coupling frequency on simulation results is insignificant, because the production states keep constant during the production, and a complete balance of reservoir/network can be achieved by using low coupling frequency.

- At early time of production, the gas-oil ratio is the dominating factor that impacts the bottom hole pressure of producers. It is found that the increased gas-oil ratio will reduce the bottom hole pressure of producers. When the water breakthrough occurred, the bottom hole pressure is mainly dependent on the fraction of water within the tubing; it is found that the pressure will increase with the increasing water production rate;

- The production tubing size has impact on well boundary conditions, it is found that for producers, the small tubing size will restrict the flow rate, and increase the flowing pressure at bottom hole.

- For the model with choke restricted, the bottom hole pressures of producers are mainly determined by both the gas-liquid ratio and mixture density within the tubing. When flow rate is high, the GLR will be the dominating factor that determines the bottom hole pressure of producers;

- By placing the choke at the wellhead, the oil production rate can be constrained within the desired pressure limit; also the improve the voidage replacement;

- By performing different experiments with several coupling methods, including partially coupled, fully coupled and non-coupled model, we concluded that the selection of coupling method depends on the particular reservoir. When performing the simulations under unconventional reservoir (e.g. tight-oil reservoir), where the variation of production behavior and well boundary condition

in time is insignificant, the non-coupled simulator is recommended in order to save computation time. When the simulation is performed under conventional reservoir, where significant variations of production states and well boundary conditions in time may occur, then the fully coupling and high coupling frequency partially coupling is recommended. The advantages of partially coupling is that by well tuned coupling frequencies, one can couple two individuals external commercial software with great computational saving. However, when using partially coupling method, one has to be careful with oscillations into the solution, therefore, the fully coupling method is recommended with the considerations of stable solutions and fast convergence.

6.2 Future Work

Based on our research studies, a suggestions will be given regarding the future work of this project.

In real production field, the production operation strategy is more complicated. In our research, only one water flood pattern is considered. However, in the realistic scenario, the production field could consist of multiple unit of water flooding pattern. Another assumption made in our project is that all the production wells is simplified vertical wellbore model, thus the coupled model can further consider more complicated wellbore models, such as horizontal or multilayers wellbore model. The research study can be further developed by considering the transient flow within each timestep. As mentioned in chapter 2, we assumed that the tubing/pipe flow is in steady state, which could result in inaccuracy of the pressure loss calculation. Thus, it is necessary to consider the transient flow in the more complicated models. By implementing these suggestions into the future studies, a more comprehensive conclusion of surface/subsurface coupling would be achieved.

REFERENCES

1. Holmes, J.A.: "Enhancements to the Strongly Coupled, Fully Implicit Well Model: Wellbore Crossflow Modeling and Collective Well Control," paper SPE 00012259 presented at the 1983 SPE Reservoir Simulation Symposium.

2. Holmes, J.A., Barkve, T. and Lund, O.: "Application of a Multisegment Well Model to Simulate Flow in Advanced Wells," paper SPE 50646 presented at the 1988 SPE European Petroleum Conference. Hague, 20-22 October.

3. Stone, T.W. *et al.*: "Thermal Simulation with Multisegment Wells," paper SPE 66373 presented at the 2001 SPE Reservoir Simulation Symposium, Houston, 11-14 February.

4. Dempsey, J.R. *et al.*: "An Efficient Method for Evaluating Gas Field Gathering System Design," *JPT* (September 1971) 1067.

5. Beggs, H.D.: "An Experimental Study of Two-Phase Flow in Inclined Pipes," PhD dissertation, U. of Tulsa (1972).

6. Startzman, R.A. *et al.*: "Computer Cobines Offshore Facilities and Reservoir Forecast," *Petroleum Engineer* (May 1977) 65.

7. Feng, W.Y. and Lom K.K.: "A Generalized Well Management Scheme for Reservoir Simulation," *SPE Reservoir Engineering* (May 1996) 116-120.

8. Wijestinghe, A.M.: "A Comprehensive Well Management Program for Black Oil Reservoir Simulation," paper SPE 12260 presented at the 1983 SPE Symposium on Reservoir Simulation, San Francisco, Nov. 15-18.

9. Schiozer, D.J. and Aziz, K.: "Use of Domain Decomposition for Simultaneous Simulation of Reservoir and Surface Facilities," paper SPE 27876 presented at the 1994 SPE Western Regional Meeting, Long Beach, California, 23-25 March.

10. Byer, T.J., Edwards, M.G. and Aziz, K.: "Preconditioned Newton Methods for Fully Coupled Reservoir and Surface Facility Models," paper SPE 49001 presented at the 1988 SPE Annual Technical Conference and Exhibition, New Orleans, 27-30 September.

11. Coats, B.K., Fleming, G.C., Watts J.W., Rame, M. and Shiralkar, G.S.: "A Generalized Wellbore and Surface Facility Model, Fully Coupled to a Reservoir Simulator," *Reservoir Evaluation and Engineering* (April 2004) 132.

12. Guyaguler, B. *et al.*: "Near-Well Subdomain Simulations for Accurate Inflow Performance Relationship Calculation to Improve Stability of Reservoir-Network Coupling," paper SPE 141207 presented at 2011 SPE Reservoir Simulation Symposium, Woodlands, 21-23 February.

13. Hayder, E.M., Dahan, M. and Dossary, M.N.: "Production Optimization through Coupled Facility/Reservoir Simulation," paper SPE 100027 presented at the 2006 Intelligent Energy Conference and Exhibition.

14. Ursini, F., Rossi, R. and Pagliari, F.: "Forecasting Reservoir Management through Integrated Asset Modeling," paper SPE 128165 presented at the 2010 North Africa Technical Conference and Exhibition.

15. Gonzalez, F.E. *et al.*: "A Fully Compositional Integrated Asset Model for a Gas-Condensate Field," paper SPE 134141 presented at the 2010 SPE Annual Technical Conference and Exhibition.

16. Ghorayeb, K. *et al.*: "A General Purpose Controller for Coupling Multiple Reservoir Simulations and Surface Facility Networks," paper SPE 79702 presented at the 2003 SPE Reservoir Simulation Symposium, Houston, Texas, USA (February 3-5, 2003).

17. Hepguler, G., Barua, S. and Bard, W.: "Integration of Field Surface and Production Network with a Reservoir Simulator," *SPECA* (June 1997) 88.

18. Guyaguler, B. and Ghorayeb, K.: "Integrated Optimization of Field Development, Planning, and Operation," paper SPE 102557 presented at 2006 SPE Annual Technical Conference and Exhibition, San Antonio, 24-27 September.

19. *INTERSECT Version 2013.1 Reference Manual*, Schlumberger Information Systems.

20. Ertekin, T., Abou-Kassem, J.H., King, G.R., *Basic Applied Reservoir Simulation* (1993), Richardson, Texas: Textbook Series, SPE

21. Economides, M.J., Hill, A.D., Ehlig-Economides, C. and Zhu, D., *Petroleum Production Systems* (January 2013), Upper Saddle River: Prentice Hall.

22. Hagedorn, A.R. and Brown, K.E.: "Experimental Study of Pressure Gradiants Occurring During Continuous Two-Phase Flow in Small-Diameter Vertical Conduits," *J. Pet. Tech.* (April 1965) 475-484.

23. *PIPESIM Version 2013.1 User's Guide*, Schlumberger Information Systems.

24. Trick, M.D.: "A Different Approach to Coupling a Reservoir Simulator with a Surface Facility Model," paper SPE 00040001 presented at the 1998 SPE Gas Technology Symposium.

25. Christie, M. and Blunt, M.: "SPE Comparative Solution Project," retrieved July 15, 2014, from http://www.spe.org/web/csp//

26. Lie, K.-A., Krogstad, S., Ligaarden, I. S., Natvig, J. R., Nilsen, H. M., and Skaflestad, B.: "Open source MATLAB implementation of consistent discretisations on complex grids," retrieved August 10, 2014, from http://www.sintef.com/Projectweb/MRST/